Mud volcanoes: Indicators of stress orientation and tectonic controls

Marco Bonini *

Consiglio Nazionale delle Ricerche, Istituto di Geoscienze e Georisorse, Via G. La Pira 4, I-50121 Florence, Italy

ABSTRACT

This study examines the use of specific mud volcano features (i.e., elongated calderas, aligned vents and elongated volcanoes) as potential indicators of tectonic stress orientation. The stress indicator principles, widely recognised for magmatic systems, have been discussed and applied to mud volcano settings such as in the Northern Apennines and the Azerbaijan Greater Caucasus, as well as in other instances where the analysis was fully based on a remote sensing study. The results of these applications are promising, the obtained maximum horizontal stress (S_H) directions generally showing a good correlation with those determined in the upper crust by classical methods (i.e., earthquake focal mechanism solutions, well bore breakouts). Therefore, stress information from mud volcanoes could be used as a proxy for stress orientation (1) where stress data is lacking, (2) where settings are inaccessible (i.e., underwater or the surface of planets), or simply (3) as supplementary stress indicators. This study also pays special attention to structural elements that may control fluid expulsion at various length scales, and pathways that should have spawned the mud volcanoes and controlled their paroxysmal events and eruptions. Different types of sub-planar brittle elements have been found to focus fluid flow rising up-through fold cores, where the vertical zonation of stresses may take part in this process by creating distinctive feeder fracture/fault sets. On a regional scale, mud volcanoes in active fold-and-thrust belts may occur over wider areas, such as the prolific mud volcanism in Azerbaijan, or may cluster along discrete structures like the steep Pede-Apennine thrust in the Northern Apennines, where the generation of overpressures is expected to establish a positive feedback loop allowing for fault movement and mud volcanism.

© 2012 Elsevier B.V. All rights reserved.

Contents

* Tel.: +39 055 2757528; fax: +39 055 290312.
  E-mail addresses: marco.bonini@igg.cnr.it, mbonini@geo.unifi.it.

1. An introduction to mud volcanism and aims of the study

Mud or *sedimentary volcanism* is a process that drives the extrusion to the topographic surface of material which originated from deeply buried sediments, such as mud, fragments or blocks of country rock, saline waters and gases of which methane often represents the dominant fraction. This mechanism is typically linked to in-depth hydrocarbon traps (Higgins and Saunders, 1974), and it builds up a variety of scenic features the most typical of which being the steep-sided conical edifices that are usually crowned by a shallow crater lake. These conical edifices vary in size from centimetre-scale to large mud volcanoes of up to a few hundred metres high and some kilometres across (Fig. 1a, b). Conventional nomenclature (e.g., Planke et al., 2003) refers to *salses* as water-dominated pools (or *mud pots*) with gas seeps, and subdivides the sub-conical extrusive edifices in *gryphons* (≤3 m high), *mud cones* (3 to 10 m high), and *mud volcanoes* for the largest edifices, up to ~400 m tall in Azerbaijan (Fig. 1a). Thousands of mud volcanoes occur globally predominantly underwater. Mud volcanoes are described in various tectonic scenarios, but the majority occur in fold-and-thrust belts and submerged accretionary prisms, and develop at convergent plate margins (Higgins and Saunders, 1974; Henry et al., 1990; Milkov, 2000; Kholodov, 2002a; Kopf, 2002).

1.1. Mud volcano processes

Once a mere natural curiosity, mud volcanoes have been regarded as features interrelated to many relevant aspects (see Mazzini, 2009), spanning from their role in (1) predicting petroleum reservoirs (e.g., Devlin et al., 1999; Feyzullayev and Lerche, 2009), to (2) the environmental implications related to their input of fossil methane into the atmosphere (e.g., Hovland et al., 1997; Kopf, 2003; Milkov, 2004; Kvenvolden and Rogers, 2005), and (3) their hints into how fluids travel up through the shallow crust (Davies et al., 2008; Mazzini et al., 2009). The background activity of mud volcanoes ranges from the quiet to vigorous flow of mud and fluids, with the typical intermittent gas bubbles popping up through the saline muddy water; paroxysmal phases may however interrupt this quiescent activity.

Different mechanisms have been advocated to control subsurface sediment mobilisation and the deep plumbing system of mud volcanoes (Van Rensbergen et al., 2003). Mud volcanism has been generally viewed as the surface manifestation of intrusive processes such as mud or shale diapirism, or the development of 'diatremes' (Brown, 1990; Henry et al., 1990; Morley and Guerin, 1996; Kopf, 2002; Morley, 2003a; Fig. 1c). Mud diapirs are subsurface clay and fluid-rich intrusions driven upward by buoyancy forces arising from the bulk density contrast between the overpressured muddy mass and the denser surrounding overburden (Brown, 1990). Diatremes normally develop in response to the rapid flow of pore fluids debouched from a structural or stratigraphic conduit into the base of lower permeability (typically unlithified clay) units, whose sediments become fluidized and entrained in the advecting fluids (Brown, 1990). This process is assisted by the rapid expansion and degassing of the methane (at ca. 1–2 km depth) dissolved in the mud, which produces overpressures and increases the buoyancy and the stress on the surrounding sediments causing their fluidification (Brown, 1990). Other models propose mud volcanoes to be sourced from the depletion of highly fluid-rich source layers at depth (Cooper, 2001; Stewart and Davies, 2006; Davies et al., 2007), with the ascent of the mud–water–gas mix taking place through an intricate plumbing system that includes fluid reservoirs (i.e., networks of mud-filled fractures) interconnected by branched systems of conduits and pipes and networks of anastomosing fault-controlled pathways (Fowler et al., 2000; Cooper, 2001; Dimitrov, 2002; Kopf et al., 2003; Morley, 2003a, b; Planke et al., 2003; Deville et al., 2006; Evans et al., 2008; Mazzini et al., 2009; Roberts et al., 2010). In this process, mud and fluids could be mobilised from the same source layer (e.g., Davies and Stewart, 2005) or the mud removed by fluids originated at deeper stratigraphic levels (e.g., Deville et al., 2006; Davies et al., 2007; Huuse et al., 2010).

Mud volcanoes are frequently located over the crests of anticlines in fold-and-thrust belts (e.g., Jakubov et al., 1971; Higgins and Saunders, 1974; Chigira and Tanaka, 1997; Fowler et al., 2000; Kholodov, 2002b; Planke et al., 2003; Bonini, 2007; Morley, 2007; Fig. 1d), but also at roll-over anticlines associated with listric normal faults (e.g., Graue, 2000). Sealing layers in the fold core may efficiently trap the rising fluids and readily built-up overpressures (Yassir and Bell, 1996). The development of overpressures in sediments is thus a necessary prelude to mud volcanism (Dimitrov, 2002). Other fluid overpressuring mechanisms are related to disequilibrium compaction due to rapid sediment burial, lateral fluid pressure transfer (due to tectonic tilting and differential loading), and diagenetic processes involving mineral transformations, cementation and hydrocarbon generation (Osborne and Swarbrick, 1997; Yardley and Swarbrick, 2000). Though difficult to quantify, tectonic loading provides a pivotal and possibly the most important source for overpressures, as witnessed by the widespread mud volcano occurrence in many active compressional belts worldwide (e.g., Higgins and Saunders, 1974; Yassir and Addis, 2002). Therefore, mud volcanoes clearly represent large-scale evidence of episodic or continuous fluid fluxes from the subsurface dictated by the rise and fall of fluid pressure.
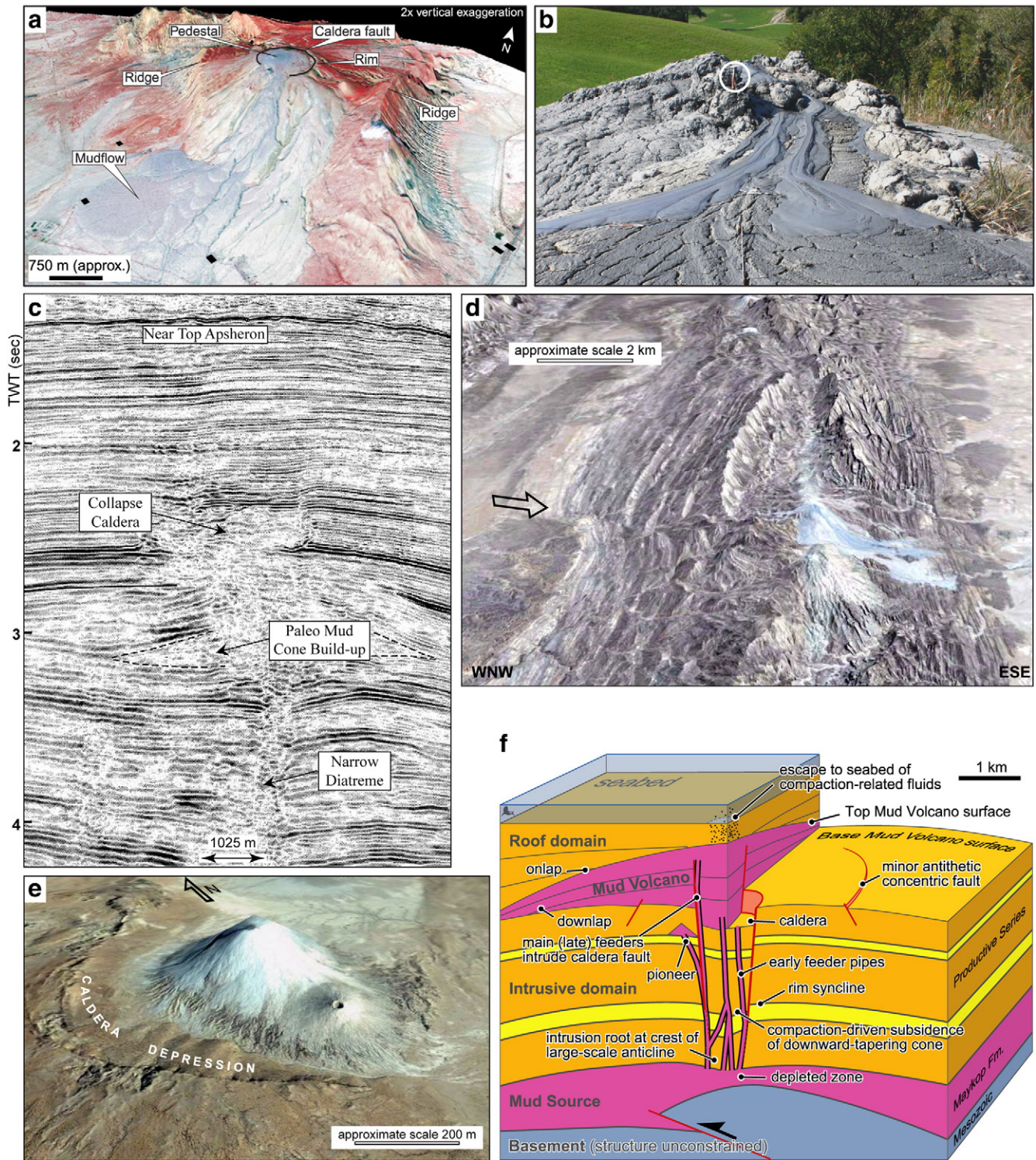
Fig. 1. Morphology and internal characteristics of mud volcano features. (a, b) Two mud volcanoes with different sizes showing similar morphologic features. (a) The ~400 m tall Qaraqus–Dagi mud volcano edifice and caldera in Azerbaijan. (b) A ~2 m tall gryphon at Sassuno, Northern Apennines, Italy (hammer for scale; 7th October 2009). (c) Seismic image illustrating the main features internal to a mud volcano in the Shah Deniz, South Caspian Basin. Mud volcano activity commenced during the late Productive Series (latest Miocene–early Pliocene) and ceased during the Absheron (Early Pleistocene). (d) Coincidence of mud volcanism with thrust anticlines; oblique view (looking from SSW) of mud volcanoes on the Haro Range anticline in Makran (Balochistan) Pakistan (N25°35′53″ E66°06′13″). Note also the coincidence of a mud volcano with the transverse fault indicated by the open arrow. (e) Oblique view of the Chandragup mud volcano (N25°26′44″ E65°51′56″) in eastern Makran, Pakistan. The ~60 m-tall mud volcano rises from a caldera-like depression imitating the setting of genuine volcanic edifices. (f) Three-dimensional model of a typical South Caspian mud volcano system.

Panel a is after Evans et al. (2008), © Copyright 2008 The Geological Society, reprinted by permission of the Geological Society Publishing House. Panel c is after Fowler et al. (2000). Panel f is after Stewart and Davies (2006), AAPG Bulletin, volume 90, Structure and emplacement of mud volcano systems in the South Caspian Basin, AAPG©2006, reprinted by permission of the AAPG whose permission is required for further use. Images in (d) and (e) are extracted from Google Earth®; http://earth.google.it/download-earth.html.

1.2. Aims and outline of the study

This paper investigates the application of the stress orientation concepts established for magmatic features (i.e., elongated calderas, aligned vents and elongated volcanoes) to mud volcanoes (e.g., Bonini, 2008; Bonini and Mazzarini, 2010). The structural controls on mud volcanic processes and subsurface sediment mobilisation exerted by both large-scale structures and outcrop-scale elements represent another target of the work — closely interrelated to the former. After reviewing the magmatic features used as stress indicators and the possible mud volcano analogues, the paper focuses on the mud volcanoes that punctuate the Pede-Apennine margin of the Northern Apennines (Italy), which represents an example of a well-established link between compression and mud volcanism (e.g., Boccaletti et al., 2004). Although mud volcanoes here are relatively small, the plethora of geophysical, structural and geochemical data makes this region particularly fruitful for understanding mud volcano systems.

Stress directions determined through remote sensing in some worldwide regions of mud volcanism have been compared with stress data available in literature. A relevant component of ground-truthing has been added to the analysis of mud volcanoes exposed in Azerbaijan, which represents the most important mud volcanic province on Earth. The results of these applications are promising, and suggest that stress information from mud volcanoes may represent independent or additional means for assessing stress directions. Last but not least, this analysis has paid special attention to the tectonic structures that may identify fluid expulsion and pathways that should have spawned the mud volcano features.

2. Igneous volcanic elements as indicators of tectonic stress orientation

2.1. Vent alignments and volcano elongation

It has been well established that intrusions propagated by hydraulic fracturing commonly form in a plane perpendicular to the least horizontal stress S_h (Stevens, 1911; Anderson, 1951; Odé, 1957; Tsunakawa, 1983; Paquet et al., 2007). This principle has provided the basis for reconstructing the orientation of past and current stress fields (Nakamura, 1969, 1977; Zobak and Zobak, 1980; Delaney et al., 1986). In his pioneer works Nakamura (1969, 1977) inferred that the rows of aligned volcanic vents (i.e. monogenetic cinder cones, domes, volcanic necks, and collapse pits) frequently originate from – and form above – the same subsurface feeder dyke (Fig. 2a, b). Therefore, vent alignments have often been used to infer the direction of the S_h or that of the greatest compressive horizontal stress S_H (Nakamura, 1977; Lutz, 1986; Wadge and Cross, 1988; Takada, 1994; Gudmundsson, 1995, 2005; Tibaldi, 1995; Korme et al., 1997; Paquet et al., 2007). Elongated cinder cones are common in monogenetic vent fields and represent reliable proxies for the determination of subsurface dyke trends (Tibaldi, 1995; Paulsen and Wilson, 2010). On the other hand, factors such as magma-chamber geometry and variations in mechanical properties may lead to abrupt changes in local stress fields, which may have strong effects on the propagation and arrest of dykes (Gudmundsson, 2006). Pre-existing brittle elements (faults and fractures) may influence heavily dyke trajectory, but in general the stress field in the country rock is thought to exert the primary control on dyke orientation (Delaney et al., 1986). Since ideal dykes tend to follow the σ_1-trajectories, the surface vents are expected to align sub-parallel to the direction of the local stress S_H (Odé, 1957; Fig. 2a, b). Alignments of volcanic vents represent an important source of the World Stress Map, which is a standard global compilation of the contemporary tectonic stress orientation (S_H) derived from various types of stress indicators (Heidbach et al., 2008, 2010).

Feeder dykes may also create large elongated volcano edifices (e.g., Breed, 1964) through a prolonged period of volcanic activity

(e.g., Acocella et al., 2008). The elongation of volcanoes and the distribution of flank vents is generally parallel to the strike of the subsurface feeder dyke, which generally intrudes a plane that is on average parallel to the orientation of the S_H axis (Nakamura, 1977; Takahashi, 1994; Tibaldi, 1995; Korme et al., 1997; Adiyaman et al., 1998; Acocella and Neri, 2009; Fig. 2c). The above concepts were applied to a number of natural cases in which the elongation of volcanoes and the alignment of vents and craters were used as a proxy for stress field orientation in the Japanese, Andean and Aleutian arcs (Nakamura, 1969, 1975; Nakamura et al., 1977). In particular, the elongation of many volcanic islands and extension zones in arc volcanoes were found to be essentially parallel to the movement of the plate over which they are located (Tibaldi, 2005; Acocella and Funiciello, 2010).

2.2. Caldera elongation

Classical volcanic calderas develop as a result of some forms of roof collapse following the removal of magma from an underlying magma chamber or reservoir (Anderson, 1936; Smith and Bailey, 1968; Lipman, 1997; Cole et al., 2005; Acocella, 2007). Caldera depressions are often elongated in plan view, and caldera elongation is usually taken to be a reliable indicator of far-field stress orientation. Igneous calderas normally elongate parallel to the direction of the least horizontal compressive stress S_h, and in rift settings the long caldera axes have been used to estimate the direction of regional extension (Bosworth et al., 2003; Casey et al., 2006). Though less common, calderas that have developed in compressional settings are also expected to elongate parallel to the S_h, and to shorten parallel to the S_H (Wallmann et al., 1990; Holohan et al., 2005).

Different models have been proposed to explain the ellipticity (i.e., long axis/short axis) of calderas. In some instances the magma chamber underlying the caldera is envisaged to grow along a discontinuity pre-existing the magma emplacement, and thus the caldera elongation is strongly dependent upon the local structural setting (Acocella, 2007). The growth of the magma chamber may also occur in the direction of the S_h, as the fluid chamber walls change shape due to stress concentration and brittle failure of the wall rock, analogous to the breakouts in a wellbore or tunnel (Bosworth et al., 2000, 2003; Fig. 2d). This theory relies on the principle that there is an originally circular opening in the Earth, or a pipe shaped feeder system that gives rise to circumferential stresses producing the brittle failure of the wall rock in a direction parallel to the S_h (Gudmundsson, 2006).

3. Using mud volcano features as stress indicators

3.1. Similarities between igneous and mud volcanism

The morphologic characteristics of mud volcano edifices show impressive similarities with the igneous counterparts, as do the mudflows originating from the summit of steep-sided cones that mimic genuine lava flows (Fig. 1a, b). Also, mud calderas are morphologically similar to the igneous equivalents, as shown by the Chandragup mud volcano (Pakistan; Fig. 1e) erecting from a subsided depression in the same way as lava domes and volcanic vents rise from topographically depressed calderas. The height of mud volcanoes may reach ~400 m (Jakubov et al., 1971), and large collapse caldera depressions 4 km in width or 10–15 km² (Fowler et al., 2000; Stewart and Davies, 2006). Even larger are the serpentinite mud volcanoes on the Mariana forearc, which may exceed 25 km in diameter and 2 km in height (e.g., Fryer et al., 1999). The dimensions of the largest mud volcanoes are thus comparable to those of igneous polygenic volcanoes.

Other similarities concern the internal structure and eruptive history. In particular, the relatively small magmatic 'monogenic' cones that form over a short time span may be analogous to the gryphons/cones that grow during a single period of activity, while the 'polygenic' volcanoes
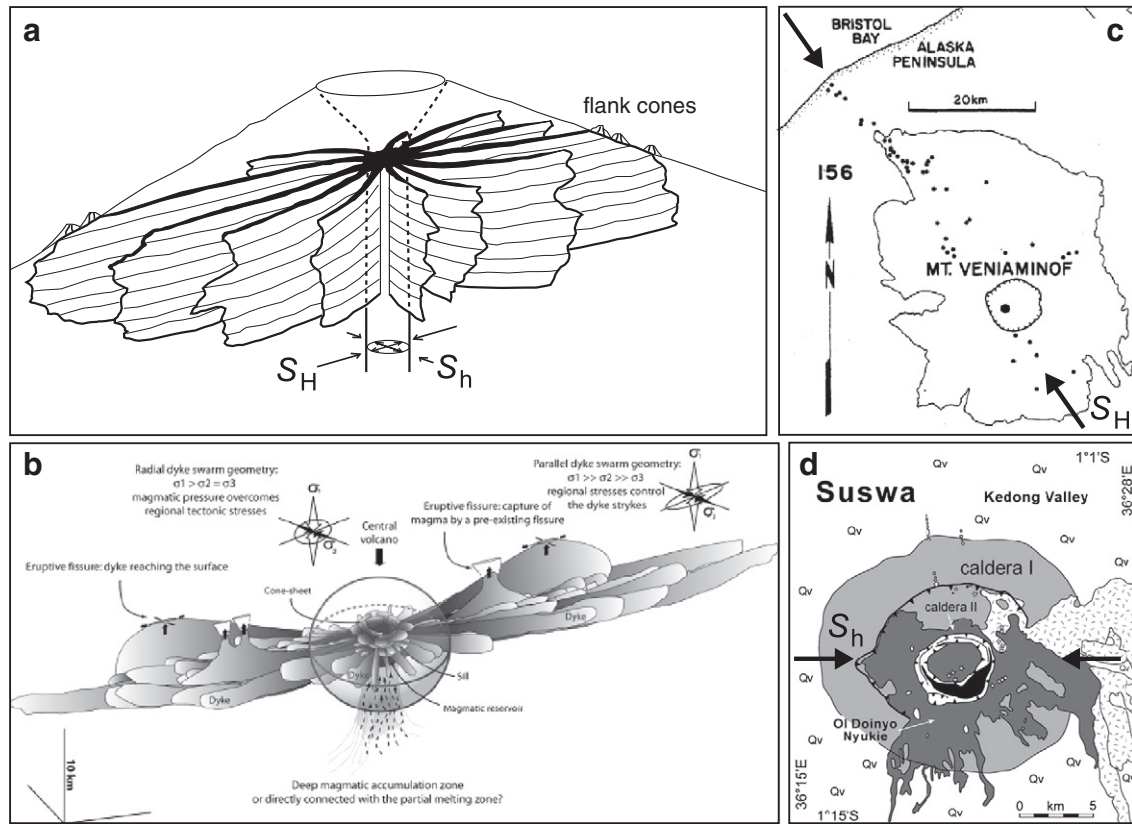
Fig. 2. (a) Idealised cartoon showing radial dykes feeding monogenetic volcanic cones on the flank of a polygenetic volcano deformed under a differential horizontal stress. The flank volcanoes localise along the trend of radial dyke concentration, which corresponds to the direction of the maximum horizontal stress S_H. (b) Schematic 3D representation of a dyke swarm in Iceland. The stress field is almost isotropic near the eruptive centre and dykes show radial distribution; away from the eruptive centre, dykes form essentially in planes sub-perpendicular to the regional extensional stress (i.e., the least horizontal stress S_h). (c) Aligned flank volcanoes (small black dots) on the flank of the elongated Mount Veniaminof volcano, Alaska. The convergent black arrows indicate the estimated maximum horizontal stress S_H. (d) Elongated Suswa caldera in the Kenya rift valley. Caldera I collapse occurred between 240 and 100 ka, while S_h was oriented ca. E–W.
Panel a is redrawn after Nakamura (1977). Panel b is after Paquet et al. (2007). Panel c is after Nakamura (1977). Panel d is after Bosworth et al. (2003).

may be equivalent to the large mud volcanoes that result from discrete extrusive periods and that may remain active over a few million years (e.g., Yusifov and Rabinowitz, 2004; Evans et al., 2006). The models of caldera-forming eruption cycles (Smith and Bailey, 1968) also correlate well to the various phases of activity identified for the Chirag mud volcano in the Caspian Sea (Evans et al., 2008). 3D seismic reflection data has allowed the imaging of the vertical architecture of an idealised mud volcano system composed of a cone-shaped extrusive edifice overlying a caldera depression connected by a feeder system to a deeper source layer (Fig. 1f; Davies and Stewart, 2005; Stewart and Davies, 2006). These characteristics are similar to those hypothesised for the igneous features (Davies and Stewart, 2005), though faults may also dip outward below magmatic calderas. In addition, feeder complexes and the collapse of some Azerbaijan mud volcanoes may imitate the 'stoping process' and 'sector collapse' structures typical of igneous volcanoes (Roberts et al., 2010, 2011a), and the velocity of mud ascent (60–300 km yr^{-1}) is comparable to that of silicate magmas (Kopf and Behrmann, 2000). Last but not least, both magmatic and mud eruptions share the same threshold seismic energy to be triggered off by distant earthquakes (Wang and Manga, 2010).

In conclusion, the above similarities have been interpreted as evidence that mud and magmatic volcano systems share some causal mechanisms (Davies and Stewart, 2005; Evans et al., 2006, 2008; Stewart and Davies, 2006; Bonini, 2008; Kopf, 2008; van Loon, 2010; Roberts et al., 2011a). Even though obvious differences do exist – mud volcanism being almost entirely driven by fluid pressure, and magmatic volcanism driven by pressure in addition to temperature, magma chemistry, volatiles, etc. – the

processes governing both volcano systems may be viewed as dynamically similar. Both magmatic and mud volcanoes are in fact driven by gas escape, and there are several processes and properties shared by these features, including the buoyancy supplied by exsolved gases, and the presence of an in-depth overpressured source (Manga et al., 2009; Wang and Manga, 2010). In this perspective, the stress indicator concepts formerly concerned for the igneous features could also be applied to the same features developed in mud volcanic settings.

3.2. Mud volcanoes as stress direction indicators: principles and methods

3.2.1. Mud vents alignment and volcano elongation

Alignments of active mud volcano vents have been analysed for estimating the present-day stress field in the shallow crust of Azerbaijan (Bonini and Mazzarini, 2010; Roberts et al., 2011b). Even though seismic imaging and field mapping of some mud volcanoes in Azerbaijan suggest pipe-like feeders (Stewart and Davies, 2006; Roberts et al., 2010, 2011b), other examples of exposed fossil feeder systems of mud volcanoes consist of long and narrow mud-filled planar fractures (e.g.,Morley et al., 1998; Morley, 2003b). Mobile shale dykes have also been used to examine paleostress orientations in Brunei (Tingay et al., 2003). Steep mud-filled intrusions have been referred to as hydraulic fractures (e.g., Morley et al., 1998; Morley, 2003ab) and interpreted as potential pathways for the transport of the mud–fluid mix to the surface (Davies et al., 2007). In this sense, a mud–fluid mix would operate like magma dykes and open hydrofractures propagating toward the surface whether fluid pressure (P_f) exceeds both the minimum principal stress

(σ_3) and tensile strength (*T*) of the overburden ($P_f > \sigma_3 + T$; e.g., Sibson, 1998). The level of fluid pressure is generally expressed by the factor $\lambda_v = P_f / \sigma_V$ (Hubbert and Rubey, 1959), where $\sigma_V = \rho gz$ is the vertical lithostatic stress (ρ is the bulk rock density, *g* is the gravity acceleration, and *z* is the depth).

The emplacement of the mud–fluid mix up through these fractures may construct mud ridges or discrete gryphons that may be aligned above a feeder mud dyke not completely reaching the surface, in a similar fashion to magmatic settings (Figs. 3a, 4). In some cases, the mud-filled intrusions may propagate laterally from the main eruptive centre and construct the elongated, large, mud volcanoes (cf. Fig. 2b). The elongation of individual vents closely constrains fissure orientation, and this aspect has thus received great emphasis in the definition and ranking of mono-genetic volcanic vent alignments (Paulsen and Wilson, 2010; Fig. 4a). This procedure has been implemented and adapted to mud volcanism, and the reliability assessment system (A>B>C>D) reported in Table 1 (see Bonini and Mazzarini, 2010). Besides the typical location over the crests of anticlines, mud volcano fields can be attributed to the platform and flank volcano settings typical of the magmatic provinces. The 1.5 km-long vent alignment and the parasitic cones puncturing the flanks of the large mud volcano in the Ormara field (Pakistan) exemplify both settings (Fig. 4c, d).

The elongation direction of individual mud volcanoes is taken as the major axis of the ellipse best approximating the map-view base of the volcanic edifice, with the volcano centre corresponding to its summit (Figs. 3b, 5). The proposed reliability assessment system (A>B>C>D) for mud volcano elongation integrates the volcano shape index (VSI; i.e., long axis/short axis of the best-fit ellipse) with the length of the long volcano axis (LVA), and is reported in Table 1. Note however that the mentioned quality classes of mud vent alignment and volcanoes do not correspond to those used in the World Stress Map.

3.2.2. Mud caldera elongation

Mud volcano calderas and collapse structures (e.g., Prior et al. 1989; Somoza et al. 2003) are referred to voluminous mud withdrawal either from subsurface reservoirs (e.g., Fowler et al., 2000; Deville et al., 2006), or from deep source layers connected to the surface by feeder pipes and dykes (e.g., Stewart and Davies, 2006; Davies et al., 2007). These depressions are thus conceptually similar to the classical volcanic calderas that show clear relationships between loss of volume in the shallow subsurface and caldera collapse (e.g., Cole et al., 2005; Acocella, 2007).

Mud calderas from Azerbaijan and the Northern Apennines often show an elongated plan view shape (Bonini, 2008; Roberts et al., 2011b). Regardless of those exploiting pre-existing fabrics, some mud calderas topping the crest of anticlines are inferred to elongate parallel to the S_h direction (e.g., Bonini, 2008; Fig. 3d). The short axis of these mud volcano depressions is often parallel to the regional S_H (Bonini and Mazzarini, 2010), which causes the caldera to shorten in this direction and to attain its elliptical shape. Mud calderas would thus reflect the shape of the underlying strained fluid chambers (e.g., Roberts et al., 2011b) that become elongated in the S_h direction
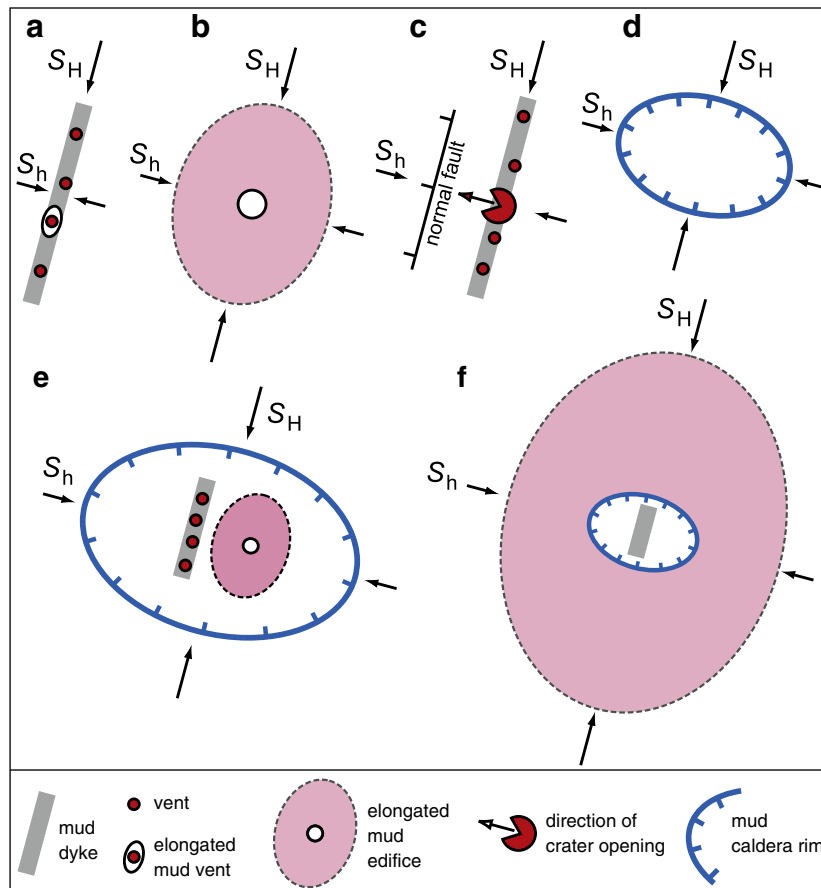
Fig. 3. Cartoons showing the various associations of mud volcano features used as indicators for the orientation of the maximum and minimum horizontal stresses (S_H and S_h, respectively). (a) Vents stemmed from an underlying feeder mud dyke. (b) Elongated mud volcano edifice. (c) Direction of crater opening associated with transverse normal faults (inspired to the extinct Montegibbio mud volcano in the Northern Apennines). (d) Elliptical mud caldera-like depression. (e, f) Theoretical association of mud volcano features. (e) Mud caldera and associated intracaldera elements, such as vent alignments and elongated mud cones/volcanoes. (f) Elongated mud volcano and associated summit caldera. Panel a is after Bonini and Mazzarini (2010).
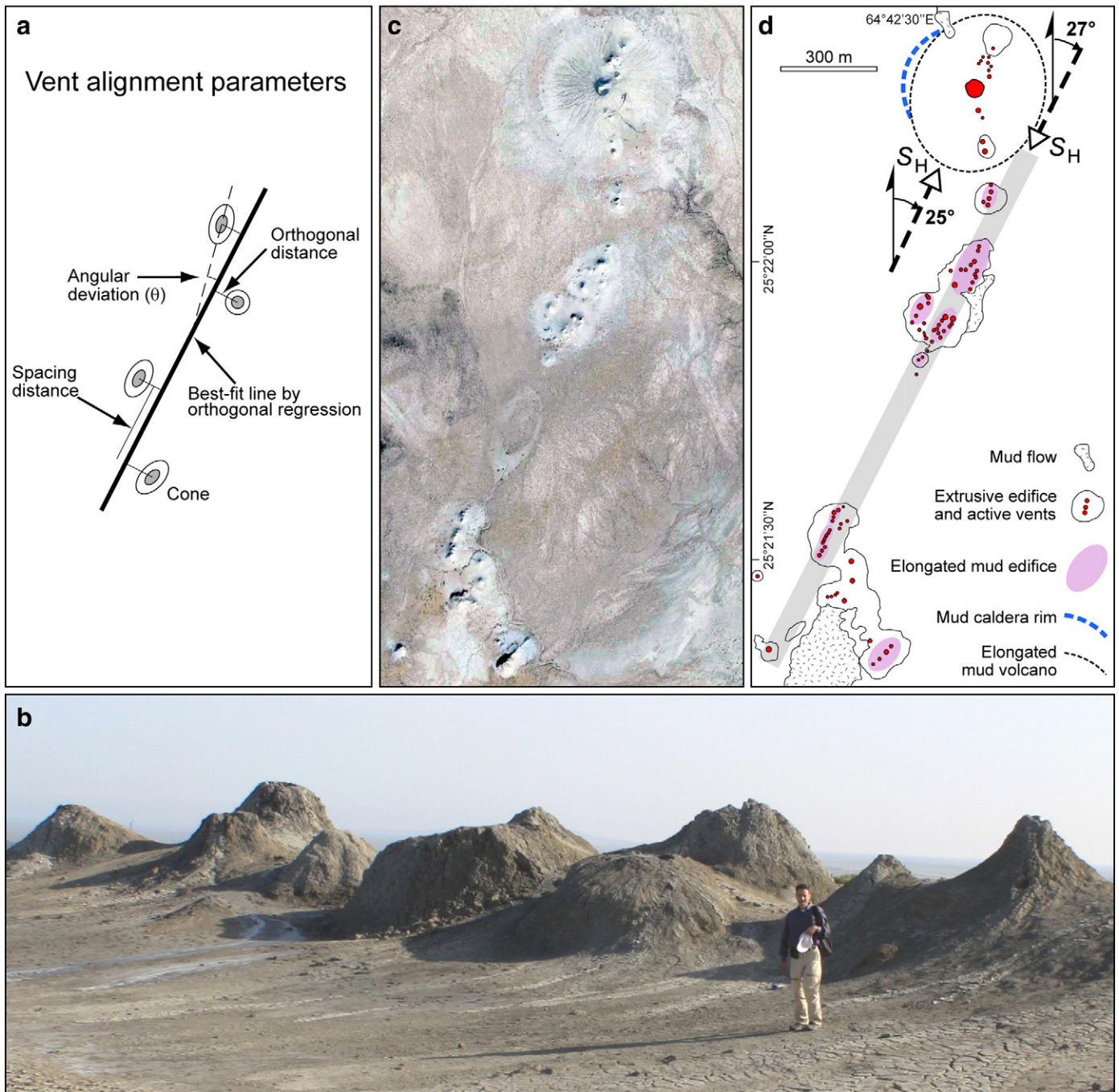
Fig. 4. Morphologic characteristics of vent alignments. (a) Attributes used to characterise and assess volcanic vents alignments, specifically (1) the number of vents composing the alignment, (2) the standard deviation of vent centre points from a best-fit line obtained from linear regression, (3) the number and type of elongated vents, (4) the standard angular deviation of vent long axes from the direction of the best-fit line, and (5) average vent spacing distances. Field examples of aligned vents and gryphons. (b) ~N160°E-trending gryphon alignment at the Dashgil mud volcano, Azerbaijan (N39°59′47″ E49°24′09″; 23rd May 2010). (c, d) Row of (~30) vents in the Ormara mud volcano field (N25°21′46″ E64°42′26″), Makran coast, Pakistan, defining a 1.5 km long and ~N27°E-trending alignment. (c) Satellite image, and (d) interpreted line-drawing of mud volcano features. Note the presence of mud edifices elongating sub-parallel to the main alignment trend. Parasitic gryphons puncture the flanks of the mud volcano settled beside the northern end of this vent alignment. Both volcano elongation and the alignment of parasitic vents are consistent with a ~N25°E direction. The dashed arrows in (d) indicate the direction of the maximum horizontal stress S_H deduced from these mud volcano features.
Panel a is redrawn after Paulsen and Wilson (2010). Panel c is extracted from Google Earth®; http://earth.google.it/download-earth.html.

due to the borehole breakout mechanism (e.g., Bosworth et al., 2000, 2003).

The crestal region of folds may also experience layer-parallel stretching above a neutral surface produced by 'tangential–longitudinal strain folding' (Ramsay, 1967). Subsurface outer-arc normal faults may thus control the shape of mud calderas, which would elongate parallel to a local, shallow, fold axis-parallel S_H (Fig. 6a). Mud calderas have thus been differentiated into those elongating parallel to the S_h, or the S_H. The trend of intracaldera features (i.e., rows of vents, elongated mud volcanoes; Fig. 3e) with respect to the fold axis direction

Table 1

Reliability assessment system (A>B>C>D) for mud volcano stress indicator features (from Bonini and Mazzarini, 2010).

Mud vent alignments

Reliability grade, RG	Number of vents	Average distance of vents from best-fit line (m)	Standard deviation best-fit line distance (m)	Index of vent elongation[a]	Standard angular deviation vent long axes (°)	Average vent spacing distance projected on the best-fit line (m)	Standard deviation of spacing (m)
A	≥7	≤0.01 L	≤0.01 L	No shape data	≤30	≤0.1 L	≤0.1 L
	≥4	≤0.02 L	≤0.02 L	1 cleft cone -or- 1 fissure ridge -or- 2≥1.6 -or- 1≥1.6 and 1≥1.4	≤30	No limit	No limit
B	≥5	≤0.015 L	≤0.015 L	No shape data	No shape data	≤0.1 L[b] or ≤0.12 L[c]	≤0.1 L[b] or ≤0.12 L[c]
	≥3	≤0.02 L	≤0.02 L	1≥1.6 -or- 2≥1.4 -or- 1≥1.5 and 2≥1.2	≤35	No limit	No limit
C	≥4	≤0.02 L	≤0.02 L	No shape data	No shape data	≤0.1 L[b] or ≤0.12 L[c]	≤0.1 L[b] or ≤0.12 L[c]
	≥3	≤0.025 L	≤0.025 L	1≥1.4 -or- 2≥1.2	≤40	No limit	No limit
D	≥3	≤0.02 L	≤0.02 L	No shape data	No shape data	≤0.12 L[b] or ≤0.15 L[c]	≤0.12 L[b] or ≤0.15 L[c]
	≥3	≤0.025 L	≤0.025 L	1≥1.2	>40	No limit	No limit
	≥3	≤0.035 L	≤0.035 L	2≥1.2	>40	No limit	No limit

Volcano elongation

	VSI	LVA (m)
A	≥1.6	≥1000
B	≥1.4	≥1000
	≥1.6	≥500
C	≥1.2	≥1000
	≥1.4	≥500
	≥1.6	≥100
D	≥1.2	≥500
	≥1.3	≥100
	≥1.4	<100

Caldera elongation

	CEI	LDA (m)	Number and rank of intracaldera elements[d] (vent alignments or elongated volcanoes)
A	≥1.4	≥500	≥1 A-ranked
B	≥1.3	≥500	≥1 B-ranked
	≥1.4	≥300	≥1 B-ranked
C	≥1.2	≥500	≥1 C-ranked
	≥1.3	≥300	≥1 C-ranked
	≥1.4	≥100	≥1 C-ranked
D	≥1.2	<100	≥1 D-ranked, or caldera-parallel faults, or fold-axis oblique calderas

L, length of vent alignment.

[a] Volcano/vent elongation (from Paulsen and Wilson, 2010): vents with best-fit ellipse axial ratios <1.2 are classified as circular, ≥1.2 and <1.4 as slightly elongated, ≥1.4 and <1.6 as elongated, ≥1.6 and <1.8 as very elongated, and ≥1.8 as cleft cones.

[b] For vents on the flanks of large volcanoes or topping the crest of anticlines.

[c] For vents within platform fields. VSI, volcano shape index (long axis/short axis); LVA, length of the longer volcano axis; CEI, caldera elongation index (long axis/short axis); and LDA length (m) of the long depression axis.

[d] Orientation of intracaldera mud volcano elements with respect to the long caldera axis: cova, caldera-orthogonal vent alignment; cpva, caldera-parallel vent alignment; coev, caldera-orthogonal elongated volcano; cpev, caldera-parallel elongated volcano; cpf, caldera (and fold-axis)-parallel faults. Relationships between elongated mud calderas and fold anticlines hosting mud volcanism: fpc, fold-axis parallel LDA; forc, fold-orthogonal LDA; fobc, fold-axis oblique LDA (when the angle between the LDA and the fold axis exceeds 20°); unr, calderas unrelated to fold anticlines; und, relations between calderas and fold anticlines undefined. D grade is attributed to mud calderas when the determination is based only on caldera-parallel faults or fold-axis oblique LDA.

may help identifying the different models of caldera elongation (Fig. 6a, b). The long caldera axis may also display some obliquity to the fold trend (Fig. 6c), and mud calderas may elongate orthogonal to the outer-arc faults (Fig. 6d), both cases suggesting autonomy from such faults (e.g., Roberts et al., 2011b). Outer-arc faults are also likely to control the emplacement of linear mud ridges at the core of anticlines (Fig. 6e). A data quality ranking of elongated mud calderas (A>B>C>D) is reported in Table 1; this combines the caldera elongation index (CEI; long axis/short axis of the best-fit ellipse), the length of the longer depression axis (LDA), and the presence of intracaldera elements.

4. A case study from the Northern Apennines (Italy) mud volcanoes

4.1. Regional framework

The Northern Apennines is an ~NE-verging fold-and-thrust belt developed in the framework of the Euro-African convergence. A north-eastward migrating thrust front-foredeep basin system developed in Oligocene–Miocene, during which siliciclastic foredeep sequences were progressively incorporated into the thrust wedge (e.g., Ricci Lucchi, 1986). The Ligurian Units represent allochthonous oceanic remnants of Alpine Tethys, and are uppermost in the
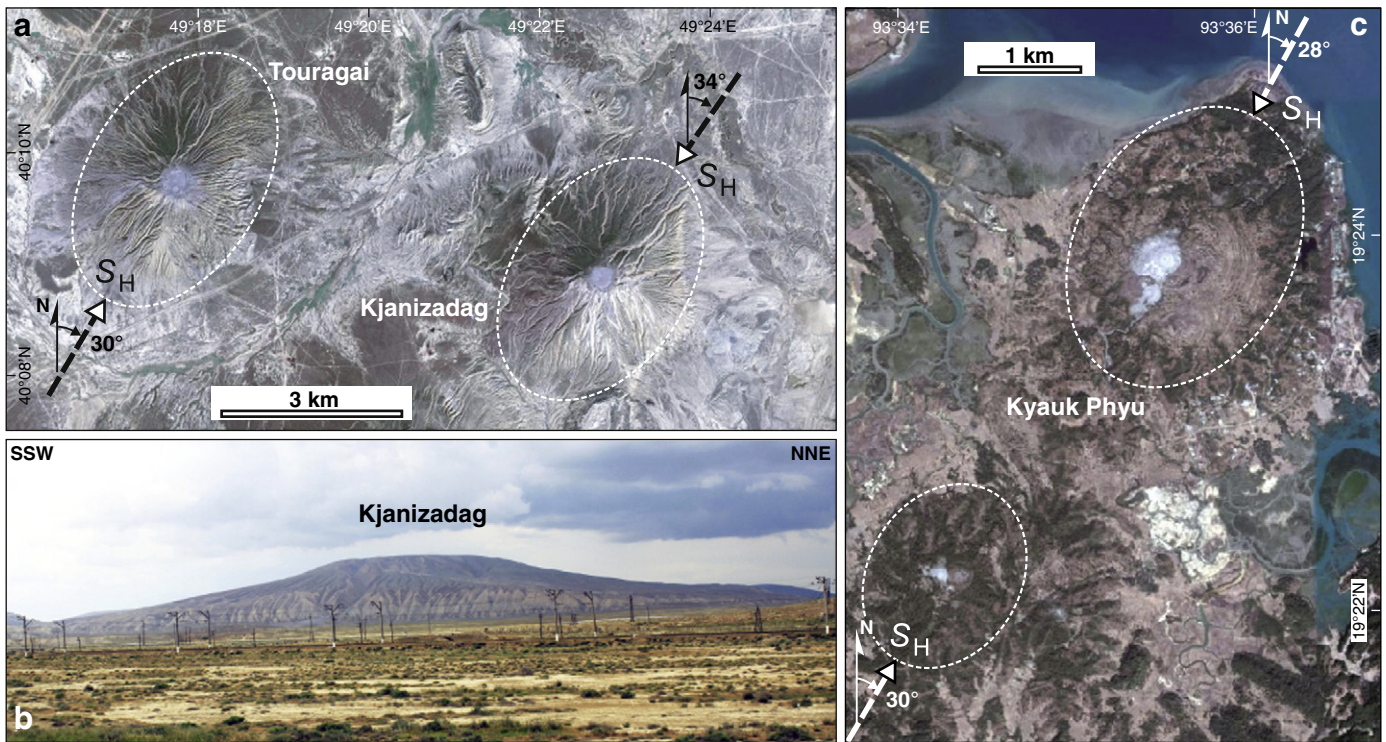
Fig. 5. Morphologic characteristics of elongated mud volcanoes. (a) Touragai (N40°09′48″ E49°17′50″) and Kjanizadag (N40°08′26″ E49°22′50″) mud volcanoes in Azerbaijan Greater Caucasus. (b) Lateral view of the Kjanizadag mud volcano rising more than 300–350 m above the surrounding low relief morphology (25th May 2010). (c) Elongated and aligned Kyauk Phyu mud volcanoes (N19°23′51″ E93°35′29″ and N19°22′11″ E93°34′20″) at the Rámri Island, Burma. The dashed arrows in (a) and (c) indicate the direction of the maximum horizontal stress S_H deduced from the elongated mud volcanoes.
Images in (a) and (c) are extracted from Google Earth®, http://earth.google.it/download-earth.html.

Apennine nappe pile. The Ligurian Units are widely exposed in the Emilia Apennines, while they are limited in the Romagna Apennines where the underlying Marnoso Arenacea foredeep sandstones dominate (Fig. 7a). The Pede-Apennine margin represents the main physiographic element separating an uplifted and exposed accretionary wedge from the topographically flat Po Plain, where the more external thrust fronts are buried beneath a thick sequence of Pliocene–Quaternary sediments (Pieri and Groppi, 1981; Fig. 7a).

Mud volcanoes typically occur on the Pede-Apennine foothills along a belt sub-parallel and adjacent to the Pede-Apennine margin. The latter is marked by a rather continuous NNE-verging and SSW-dipping thrust system referred to hereafter as 'Pede-Apennine thrust' front (PAT) (Boccaletti et al., 1985; Fig. 7a). Historical and instrumental seismicity distribution (Castello et al., 2006) and the dominant reverse earthquake focal solutions (Pondrelli et al., 2006) suggest that frontal thrusts and lateral thrust ramps are potentially seismogenic (Boccaletti et al., 1985, 2004; Selvaggi et al., 2001; Calderoni et al., 2009; Fig. 7a). Geological and geophysical evidence support the ongoing compressional tectonic activity of the PAT, which displaces post-800 ka continental deposits and 125 ka -old alluvial terraces (Ghiselli and Martelli, 1997; Benedetti et al., 2003; Boccaletti et al., 2004). Segments of the PAT have also been identified as individual seismogenic sources associated with some historical events (Basili et al., 2008; DISS Working Group, 2010; Fig. 7a). The PAT is imaged as a steep thrust surfacing at specific sectors along the Emilia Pede-Apennine margin (Benedetti et al., 2003; Boccaletti et al., 2004). The Romagna mountain front on the contrary is associated with an extensive foreland-dipping monocline lifted by NE-dipping backthrusts (Boccaletti et al., 2004).

The mud volcanoes almost invariably occur over the Ligurian Units, presumably taking advantage of the overpressures that this imperme-able barrier is expected to generate (Fig. 7a, b). In contrast, only gaseous (methane) emissions occur in the Romagna Apennines where these

rock units are absent (e.g., Bonini, 2007) (Fig. 7a, c). Methane is sourced from the Marnoso Arenacea and/or deeper, mostly Triassic, rocks (Pieri, 2001), and normally exceeds 90% in the mud volcanoes. The Marnoso Arenacea sandstones provide most of the formation water (Lindquist, 1999), while the Ligurian Units have originated most of the extruded rock fragments (e.g., Kopf, 2002).

4.2. Structural setting of the Pede-Apennine mud volcanoes

Mud volcanoes basically localise over the hangingwall of the PAT, most often above the crest of thrust-related folds. Frequently the PAT lifts and folds the continental Lower and Upper Emilia–Romagna Synthems (0.65–0.45 Ma and 0.45 Ma–Present, respectively) that uncon-formably overlie the marine Pliocene–Early Pleistocene sediments (Regione Emilia–Romagna and ENI — AGIP, 1998; Boccaletti et al., 2004). In some places (around San Polo d'Enza) the PAT mountain front is characterised by prominent faceted spurs, a laterally continuous and sharp basal scarp and strong fluvial hangingwall erosion, which im-part a morphostructural signature typical of active thrusting (Boccaletti et al., 2004). These geological and geomorphic elements demonstrate a post-0.45 Ma and potentially ongoing PAT tectonic activity (see Section 4.1). Mud volcanism is thus intimately linked to the PAT, and is es-sentially connected to the structurally controlled fluid pathways resulting from the deformation of its hangingwall (Bonini, 2007, 2009). The Nirano mud volcano will now be briefly described to exemplify these relations.

The Nirano venting area is located approximately 2 km southwest of the PAT (Fig. 8). The vents are hosted in an elliptical flat depression that coincides with the crest of an anticline folding the Pliocene–Early Pleis-tocene claystones (Regione Emilia-Romagna, 2005; Bonini, 2007). The long depression axis is slightly oblique (ca. 20°) to the anticline trend (Fig. 8). Fractures collected around the mud volcano depression and along the fold trace can be broadly subdivided into a fold-orthogonal
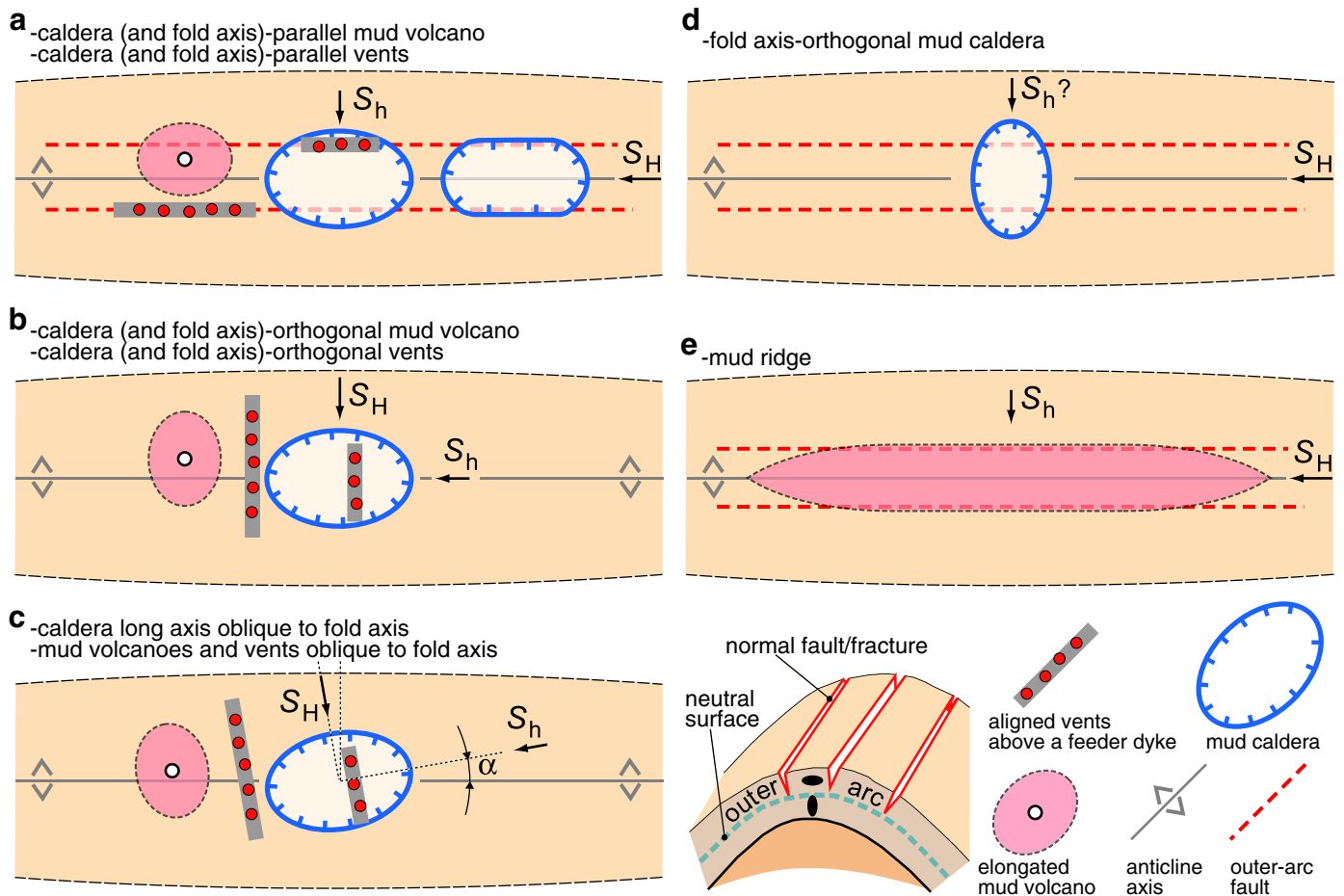
Fig. 6. Idealised geometric relations between stress axes and elongated mud calderas and mud ridges developed atop the fold anticlines. (a) Caldera elongation controlled by fold-axis parallel outer-arc faulting, in which mud calderas elongate parallel to the fold axis and local S_H (see the 3D block diagram at the bottom right-hand side; adapted from Carminati et al. (2010)). (b) Mud caldera elongating parallel to the fold axis and local S_h. (c) Mud caldera elongating obliquely to the fold axis and parallel to the local S_h. (d) Caldera elongating sub-orthogonal to the fold axis and outer-arc normal faults. (e) Linear mud ridge intruded at the core of an anticline. S_H, maximum horizontal stress; S_h, minimum horizontal stress. The fold axis-parallel S_H in (a), (d) and (e) is intended as a shallow and local S_H.
Panel d is inspired from Stewart and Davies (2006). Panels a–c are after Bonini and Mazzarini (2010).

set (cross-fold set or set *ac*) and a fold-parallel set (strike joints or set *bc*) (for details, see Bonini, 2007). Both sets clearly follow the rotation of the anticline axis from ~ESE to ~SE as this fold approaches the ~NE-trending strike-slip fault that delimits the mud volcano field to the southeast (Fig. 8). Mesoscopic faults collected along the trace of this transverse fault suggest dominant left-lateral fault kinematics, compatible with both the apparent PAT offset and the deflection of the fold axis (Fig. 8). Other fluid escape sites in the area localise above a backward fold near the Rio del Petrolio creek.

4.3. Stress indicator features from the Pede-Apennine mud volcanoes

The relationships of mud volcanoes with the stress field (Section 3 and Table 1), and structural elements are illustrated in key areas from Northwest to Southeast. The attributed reliability classes and stress data obtained from other mud volcano fields of the Pede-Apennine margin are reported in Table 2.

4.3.1. Rivalta and Torre

The Rivalta and Torre mud volcano fields occur in elliptical depressions approximately coincident with the axis of an ~WNW–ESE-trending anticline (Fig. 9a). Both depressions are interpreted here as elliptical mud calderas with long axis trending N110°E (Rivalta) and N105°E (Torre).

The Rivalta field is hosted in a sub-tabular mud-filled depression, and active seepage currently occurs as short gryphons and small bubbling pools in its central sector (Fig. 9a). Vents define ~N30°E and ~N110°–120°E alignments, which trend sub-orthogonal and sub-parallel to the fold and depression long axis, respectively. The Torre field depression exhibits comparatively steeper scarps that connect downsection to a gentler zone likely to represent the residual caldera floor (Fig. 9a). Fluid venting occurs in two areas corresponding to the apical part of small creeks entering the amphitheatre (Fig. 9a, b). The vents mostly consist of bubbling mud pots that are aligned in a N10°–15°E direction; very similar vent alignments were reported in Biasutti (1907). An ~10 m-tall sub-conical morphologic high between the two venting areas is suspected to represent a relic mud cone elongating in a N–NNE direction (Fig. 9a). Both the intracaldera vent alignments and the elongated mud cone trend sub-orthogonal to the anticline and depression axes, suggesting S_h-parallel caldera growth (Fig. 9a). Though less constrained, a similar mechanism can be suggested for the Rivalta depression where the major vent alignment also trends sub-orthogonal to the anticline and caldera axes. The Torre and Rivalta depressions would be thus consistent with local S_H directions striking respectively N15°E and N20°E (Table 2). The caldera dimension and elongation, together with the intracaldera elements, allow the attribution of the Rivalta and Torre stress data (S_h) as quality classes D and C, respectively (Table 2).
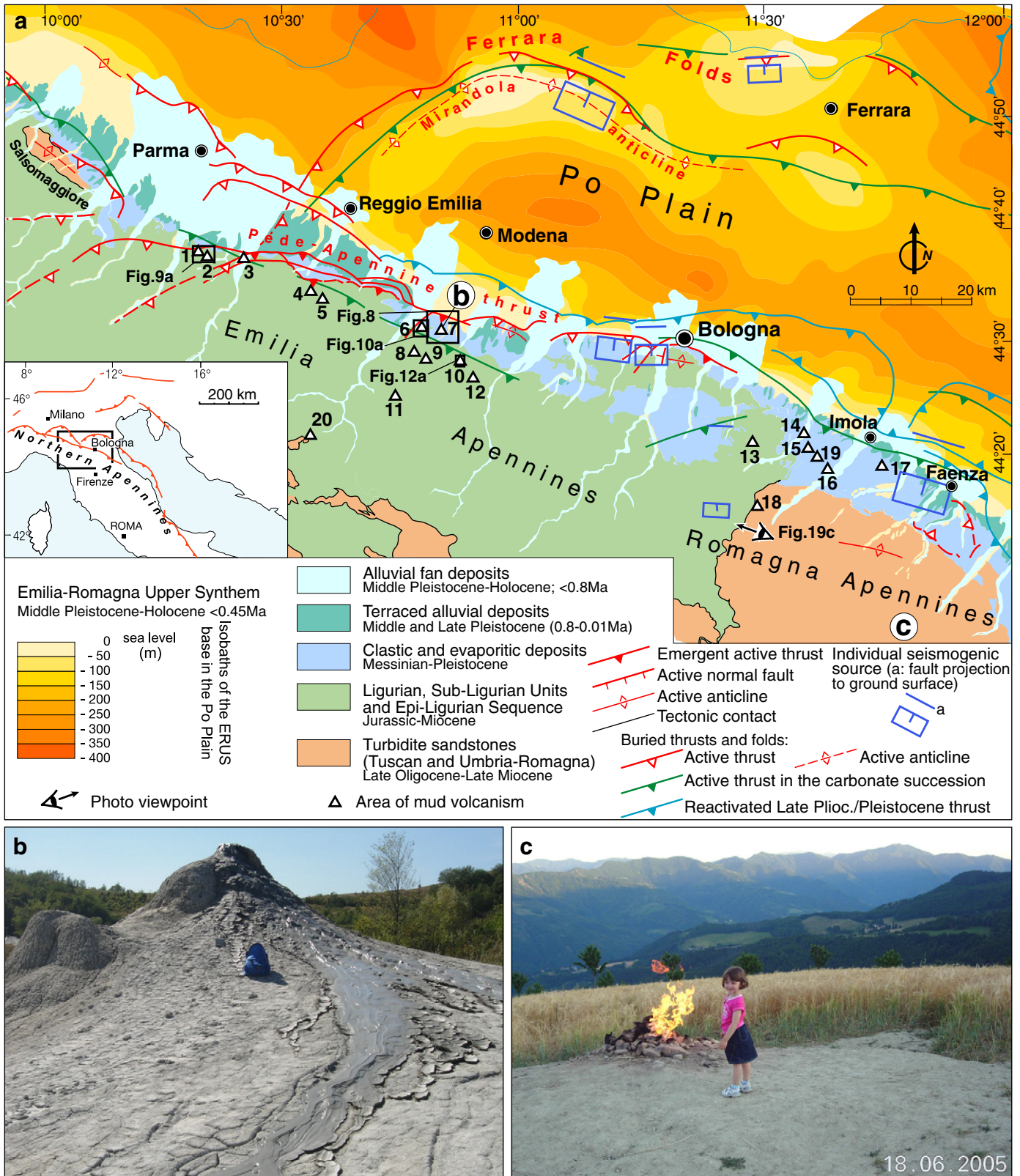
Fig. 7. (a) Geological–structural sketch map of the Emilia–Romagna Apennines; the areas of mud volcanism are shown (modified from Boccaletti et al., 2004). The surface projection of individual seismogenic sources is also reported (from DISS Working Group, 2010). The position of the buried Mirandola anticline is reported from Carminati et al. (2010). (b, c) Main fluid seepage features associated with the surface emission of methane. (b) Mud cone at Nirano, and (c) everlasting burning fire associated with a dry seep at Portico di Romagna (locations in a). Mud volcanoes: 1, Rivalta; 2, Torre; 3, San Polo d'Enza (July 1997); 4, Casola-Querzola; 5, Regnano; 6, Montegibbio; 7, Nirano; 8, Montebaranzone; 9, Centora; 10, Madonna di Puianello; 11, Canalina; 12, Ospitaletto; 13, Dragone di Sassuno; 14, S. Martino in Pedriolo; 15, Sellustra valley; 16, Casalfiumanese; 17, Bergullo; 18, Cà Rubano (Sassoleone); 19, Pedriaga; and 20, Macognano.
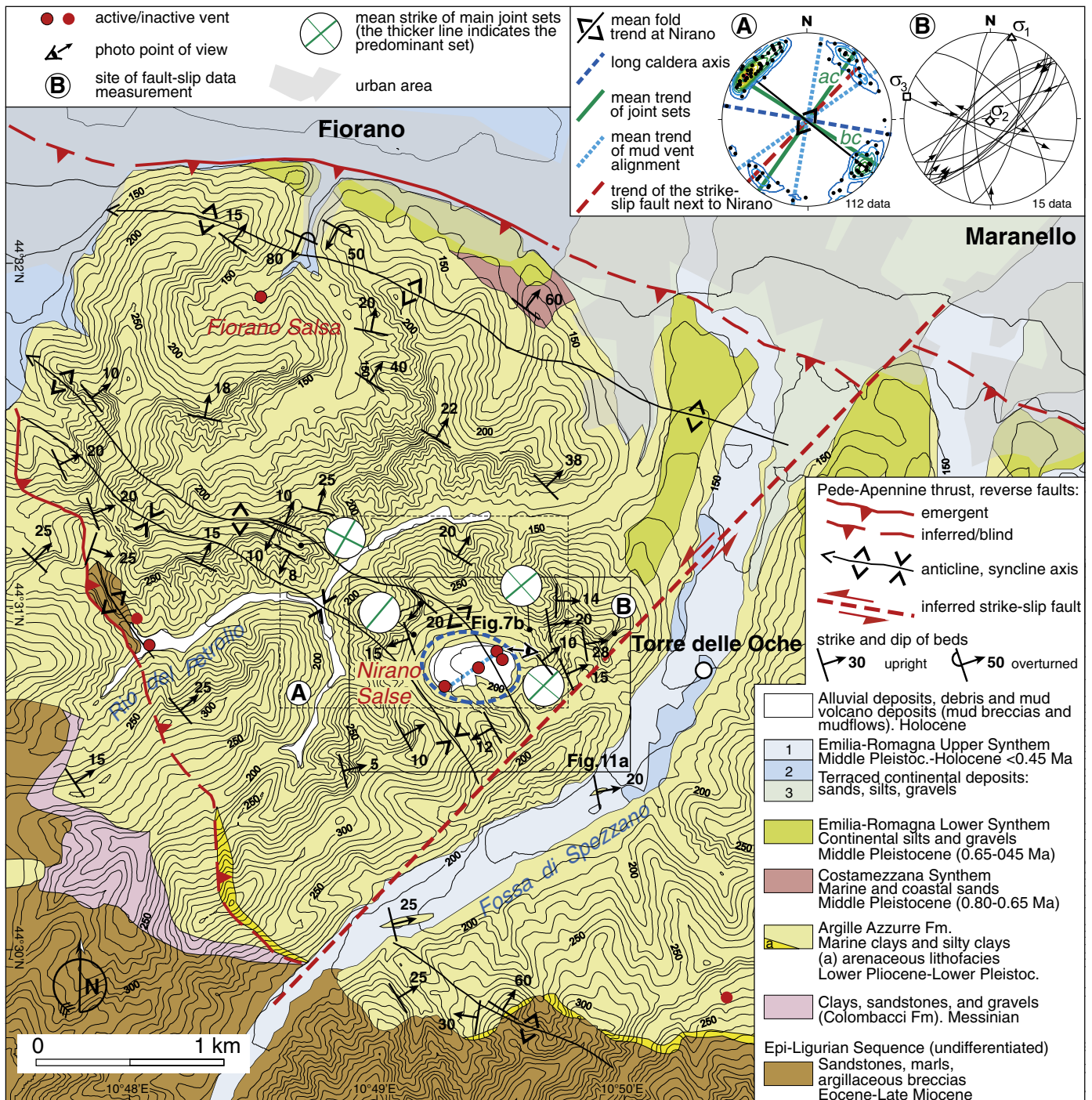
Fig. 8. Geological–structural sketch map of the Nirano mud volcano field and the Pede-Apennine thrust in the Fiorano–Maranello sector (modified from Bonini, 2007) (location in Fig. 7a). Contour lines are 10 m equidistant. Insets show mesoscopic structural elements. A: distribution of joints in relation to the main structural elements around the Nirano field; the black circles indicate the pole to joint planes, and the dashed box indicates the area of joint collection (equal area net, lower hemisphere). B: fault-slip data collected along the NE-trending fault southeast of the Nirano salse (Wulff projection, lower hemisphere); stress inversion of fault-slip data has been performed using the right dihedral method (Angelier and Mechler, 1977).

4.3.2. Montegibbio

The Montegibbio area has been mentioned in several historical chronicles (as *Salsa di Montegibbio* or *Salsa di Sassuolo*) owing to its recurrent explosive activity (e.g. Dé Brignoli di Brunnhoff, 1836). However, the present-day activity is radically reduced, as this is merely represented by small pools with limited gas bubbling. Such pools occur within a NNE-trending moderately elongated depression (Fig. 10a). Though not universally accepted (e.g. Barbieri, 1947), this depression is thought to be linked to massive evacuations of subsurface material. A ~NNE-

trending fault, of undefined kinematics, coincides with the long depression axis, suggesting a fault control on caldera elongation. Other ~NNE-trending transverse fault segments occur on the eastern flank of the Secchia River valley (Fig. 10a). The displacement of stratigraphic boundaries suggests that they are normal faults that likely formed to accommodate the differential flexure of the PAT hangingwall.

The mud volcano that caused the large 1835 eruption (described in detail and mapped by Dé Brignoli di Brunnhoff, 1836; Stöhr, 1867) is now extinct and is positioned over the northern edge of this depression

Table 2
Geometric parameters and stress indicator use of Emilia–Romagna mud volcano features.

Mud volcano	Elongated caldera							LDA trend to anticline axis	Local S az (°)		RG	Aligned vents					Elongated volcano			
	Axis (m)		CEI a/b	LDA az (°)	Intracaldera vent alignment or elongated volcano							Length (m)	Vent numb.	Elong. vents no.	Az (°) − local S_H	RG	LVA (a)		VSI	RG
	Long (a) LDA	Short (b)			No.	Or.[a]	RG		S_H	S_h							Length (m)	Az (°)		
Rivalta N44°37′50″ E10°19′34″	540	370	1.46	110	1	cova	D	fpc		110	D	15	7		30	D				
					1	cpva	D					80	5		120	D				
					1	cpva	D					15	8		110	D				
Torre N44°37′16″ E10°20′15″	350	260	1.35	105	1	cova	B	fpc		105	C	35	6		10	B	120	15	1.52	D
					1	coev	D													
Casola-Querzola N44°34′26″ E10°34′00″												26[b]	3[b]		15[b]	D				
Regnano N44°33′29″ E10°34′33″	150	105	1.43	105	1	cpf	D	fpc	105		D						40	12	1.43	D
					1	coev														
Montegibbio N44°31′07″ E10°46′45″	550	470	1.17	30		–		unr.	–	–		600	4		15	C				
Nirano N44°30′49″ E10°49′25″	500	350	1.43	100	5	cova	C–B	fobc		100	B	20	4	≥1	50	C				
												60	7	≥1	60	B				
												50	6	≥1	7	B				
												40	5		10	C				
												25	3		20	D				
												50	5		18	C				
Centora N44°28′09″ E10°47′41″	380	300	1.27	115		–		und.	–	–										
Montebaranzone N44°29′01″ E10°46′22″	65	50	1.30	98		–		und.	–	–										
Madonna di Puianello																				
a) Possessione N44°27′57″ E10°51′45″	470	340?	1.38	110	2	cova	C	unr.		110	C	24	4		05	C	18	15	1.28	–
												18	5		01	C				
b) Rio delle Sarse N44°27′57″ E10°51′45″												300[c]	4[c]		20[c]	D				
Canalina N44°24′50″ E10°43′40″	30	25	1.20	111	1	cova	D	unr.		111	D	5	3		30	D				
Ospitaletto N44°26′22″ E10°53′03″	40	25	1.60	155	1	cpva	C	und.	155		C	20	5		170	C				
												7	3		110	D				
Macognano N44°21′11.5″ E10°32′58″	15	14	1.07	110		–		und.	–	–										
Sassuno N44°20′09″ E11°27′16″	25	20	1.20	97	1	cova	C	fobc		97	D	10	4		5	C				
Sellustra N44°20′09″ E11°35′03″												2700[b]	4[b]		25[b]	D				
Casalfiumanese N44°18′12″ E11°37′35″												130	4		135	D				

Az, azimuth (0°–180° interval). CEI, caldera elongation index (long axis/short axis); VSI, volcano shape index (long axis/short axis); LDA, long depression axis; and LVA, long volcano axis. RG, reliability grade (A>B>C>D); data quality assessment follows the criterions described in Table 1.

[a] Or, Orientation of mud volcano elements associated with calderas and/or folds.
[b] Data obtained from maps in Biasutti (1907).
[c] Data obtained from maps in Ferrari and Vianello (1985).

(Fig. 10a, b). Dé Brignoli di Brunnhoff (1836) described the crater as a semi-elliptical depression bounded by rims ~15.7 m tall and 8.4 m tall before and after the eruption, respectively. Currently, this relic mud volcano slightly exceeds 10 m in height, and shows a ~WNW-directed

crater opening roughly perpendicular to the strike of the normal faults and the S_H (Figs. 3c, 10c). Moreover, the extinct mud volcano is aligned with both the active bubbling pools and another extinct salsa defining a ~N15°E direction (Table 2). Numerous NNE-trending
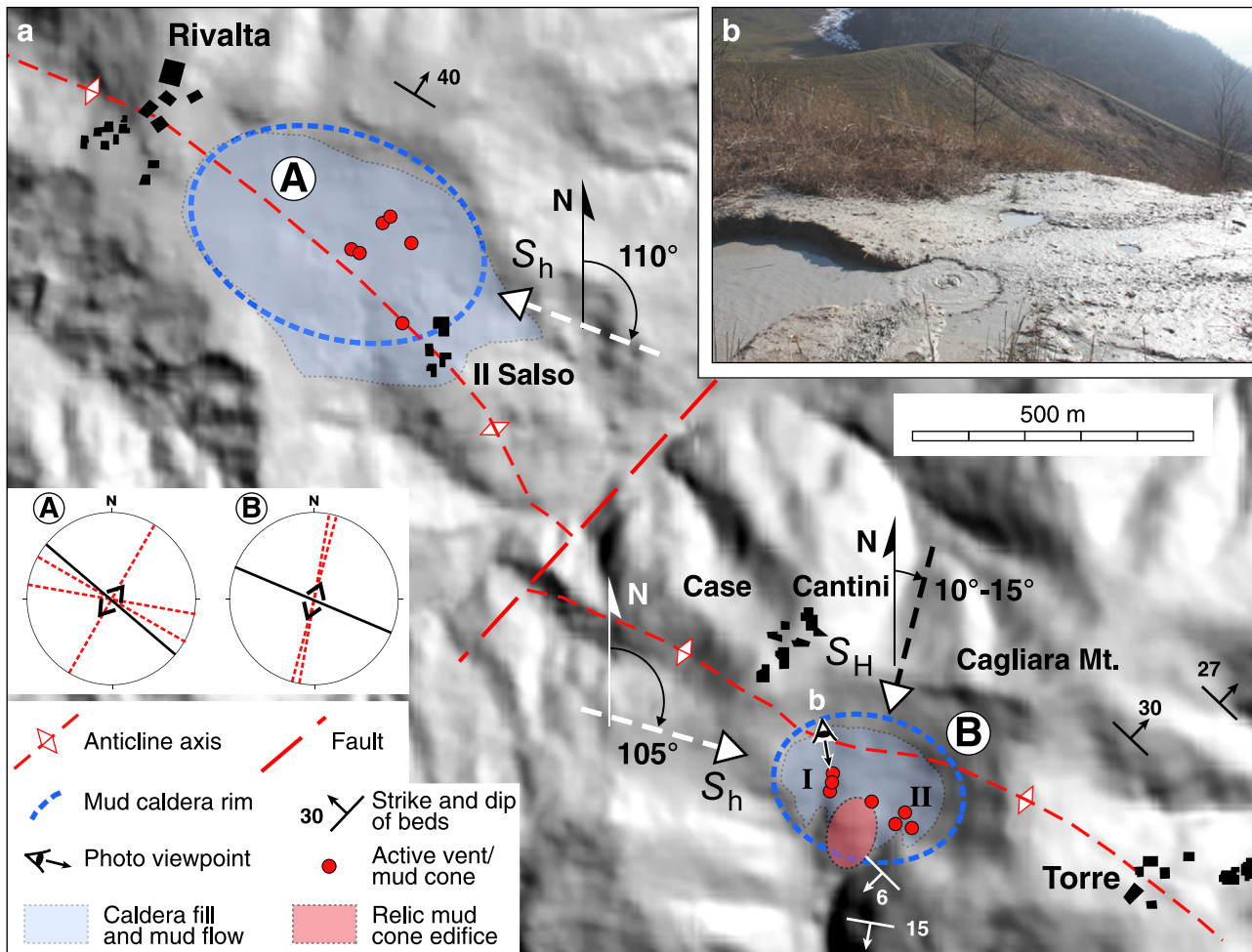
Fig. 9. (a) Rivalta and Torre mud volcano fields, northern Italy. Structural and mud volcano features are reported onto a 5 m-resolution digital terrain model (DTM courtesy of Regione Emilia–Romagna; location in Fig. 7a). The dashed arrows indicate the obtained directions of local S_H and S_h. (b) Active venting at area II of the Torre field (30th January 2009). The stereonets (Wulff net, lower hemisphere) report the intracaldera vents alignments and elongated vents (red dashing), together with the local trend of anticline axis (thick black line).

fractures developed during the 1835 eruption at several hundreds of metres from the mud volcano (Dé Brignoli di Brunnhoff, 1836), and could be associated with the emplacement of the mud-fluid mix along a subsurface feeder dyke (Fig. 10a, b). Other ESE-trending fractures formed near the main crater and developed in the direction of the crater opening (Fig. 10a, b), defining a setting that shows some analogies with dykes originating from igneous volcanoes (e.g., Takada, 1997).

4.3.3. Nirano

Nirano is one of the most spectacular gryphon fields of the Northern Apennines, and is thus protected as natural reserve (*Salse di Nirano*). The vents are hosted in an elliptical flat depression that is flanked by steep scarps in Pliocene–Early Pleistocene marine claystones (Fig. 8). The depression elongates in a N100°E direction and its short ellipse axis trends ~N10°E (Bonini, 2008; Fig. 11a and Table 2). The ongoing fluid emission occurs at a number of gryphons and vents (~30 in March 2009) clustered into four main venting areas (referred to as I to IV) that correspond to larger extrusive edifices slightly exceeding 3 m in height (Fig. 11b, c). The activity of this mud volcano can be essentially regarded as quiet (Bianconi, 1840; Biasutti, 1907), although old chronicles and more recent observations have documented relatively vigorous phases of fluid emission.

Intracaldera vents define an ~ENE alignment that has been commonly traced across the whole caldera, and thus regarded as the dominant set

(average N55°E; e.g. Castaldini et al., 2005; Bonini, 2007). Other vents delineate shorter N–NNE trends that are orthogonal to the ellipse long axis, and thus slightly oblique to the anticline axis traced across the depression (Figs. 8, 11c; Table 2). Both directions are supported by the presence of elongated edifices and mud mounds resulting from coalescent extrusive features (Fig. 11b, c). Yet, the contemporaneous presence of such ~ENE and N–NNE-trending intracaldera alignments cannot be easily explained. One possible explanation is that the ~ENE alignment, which emits the great part of the material, is intruding pre-existing cross-fold (*ac*) joints to which it strikes sub-parallel (plot A in Fig. 8; Bonini, 2007). Instead, the N–NNE-trending set could be linked to caldera-forming stresses, this set being perpendicular to the long caldera axis (plot A in Fig. 8). Long-term vent position has been established from the superposition of the current vent distribution (2009) with older maps, such as those reported in Biasutti (1907) and Mucchi (1968). The results indicate that venting has essentially been occurring in the same spots, with the most relevant difference being the comparatively higher importance of the N–NNE-trending vent alignments in area I during 1906–07 and 1966 (Fig. 11c). Dimensions, eccentricity and rank of the intracaldera vent alignments have allowed the attribution of the Nirano caldera stress data to class B (Table 2). It might be worth noting that the N10°E S_H is coherent with the dominant sinistral kinematics of the NE-trending fault that delimits the Nirano caldera to southeast (Fig. 8).
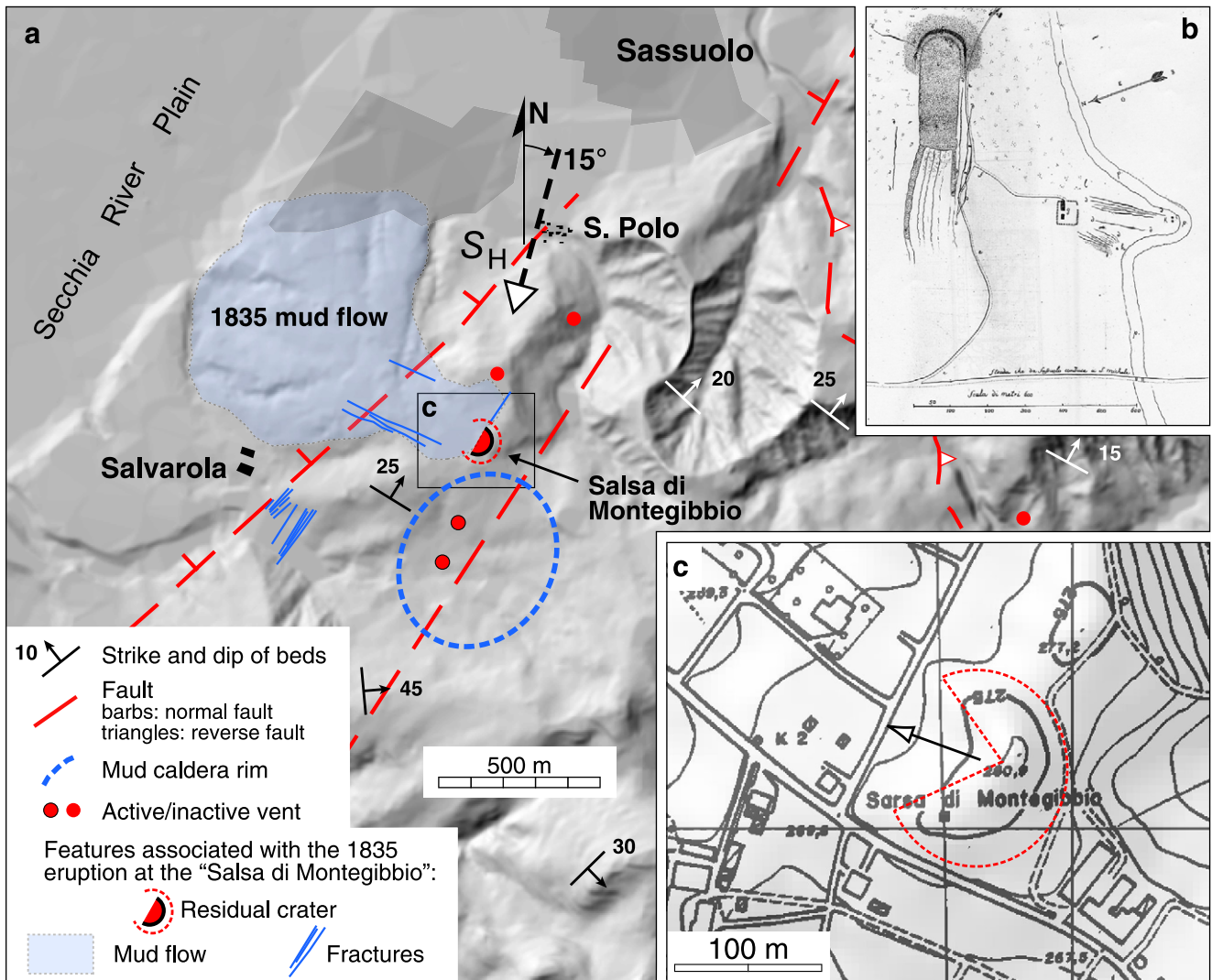
Fig. 10. (a) Montegibbio mud volcano field (relic *Salsa di Montegibbio*), northern Italy. Structural and mud volcano features are reported onto a 5 m-resolution digital terrain model (DTM courtesy of Regione Emilia–Romagna; location in Fig. 7a). The fractures that accompanied the 1835 eruption (blue lines) are taken from Dé Brignoli di Brunnhoff (1836). The dashed arrow indicates the inferred local S_H direction. (b) Original cartoon showing the surface features observed after the 1835 eruption (after Dé Brignoli di Brunnhoff, 1836). (c) Topographic map of the *Salsa di Montegibbio*; the red dashing outlines the mud volcano edifice, and the white arrowhead indicates the direction of crater opening, which is almost perpendicular to the normal fault strike and S_H.

4.3.4. Madonna di Puianello

The Madonna di Puianello vents occur in two main areas, the Casa Possessione and Rio delle Sarse (Fig. 12a). The active venting at Casa Possessione is characterised by gryphons and bubbling mud pools located in a typical flat depression that probably represents another caldera-like feature. This depression is elliptical in shape, but only its southern rim is preserved and clearly identifiable (Fig. 12a, d). A ca. N33°E-trending morphologic crest originating from this depression is tentatively interpreted as a mud ridge (Fig. 12a). The intracaldera vents define N–S to N5°E alignments that are consistent with the geometry of elongated edifice, including a relatively large mud cone with N15°E long axis (Fig. 12b, c; Table 2). Clear N- to NNE-trending vent alignments were also mapped by Biasutti (1907). Small vents punctuate the Rio delle Salse, northward of the depression (Ferrari and Vianello, 1985; Gasperi et al., 1987), and outline a trend around N20°E (Fig. 12a and Table 2). The long axis of the Casa Possessione depression trends ca. N110°E, thus roughly orthogonal to both the intracaldera vents and the suspected mud ridge, as well as to the alignment of vents identified along the Rio delle Sarse (Fig. 12a). This setting, along with the consideration that the Puianello depression is not located over an anticline crest, is interpreted as a case of mud-caldera elongation in the S_h direction.

4.4. Mud volcano stress data and relations with the regional stress field

The orientation of stress axes obtained from the Pede-Apennine mud volcanoes have been reported in Fig. 13a and plotted on a rose diagram in Fig. 14a (data from Table 2). The S_h directions materialised by the caldera long axes are dominantly E–W to ESE orientated. Instead, the S_H directions obtained from vent alignments and the few volcano elongations show a dominant NNE trend (Fig. 13a and Table 2), which is roughly perpendicular to the trend of thrust faults and folds.

These stress directions are in good agreement with those derived from different geophysical information, such as the S_H axes reported in the World Stress Map (WSM) database, earthquake focal mechanism solutions, and well bore breakouts (Fig. 13b). Generally, the S_H trajectories obtained from mud volcanoes are sub-parallel to both the WSM S_H and the earthquake P-axes distributed around the
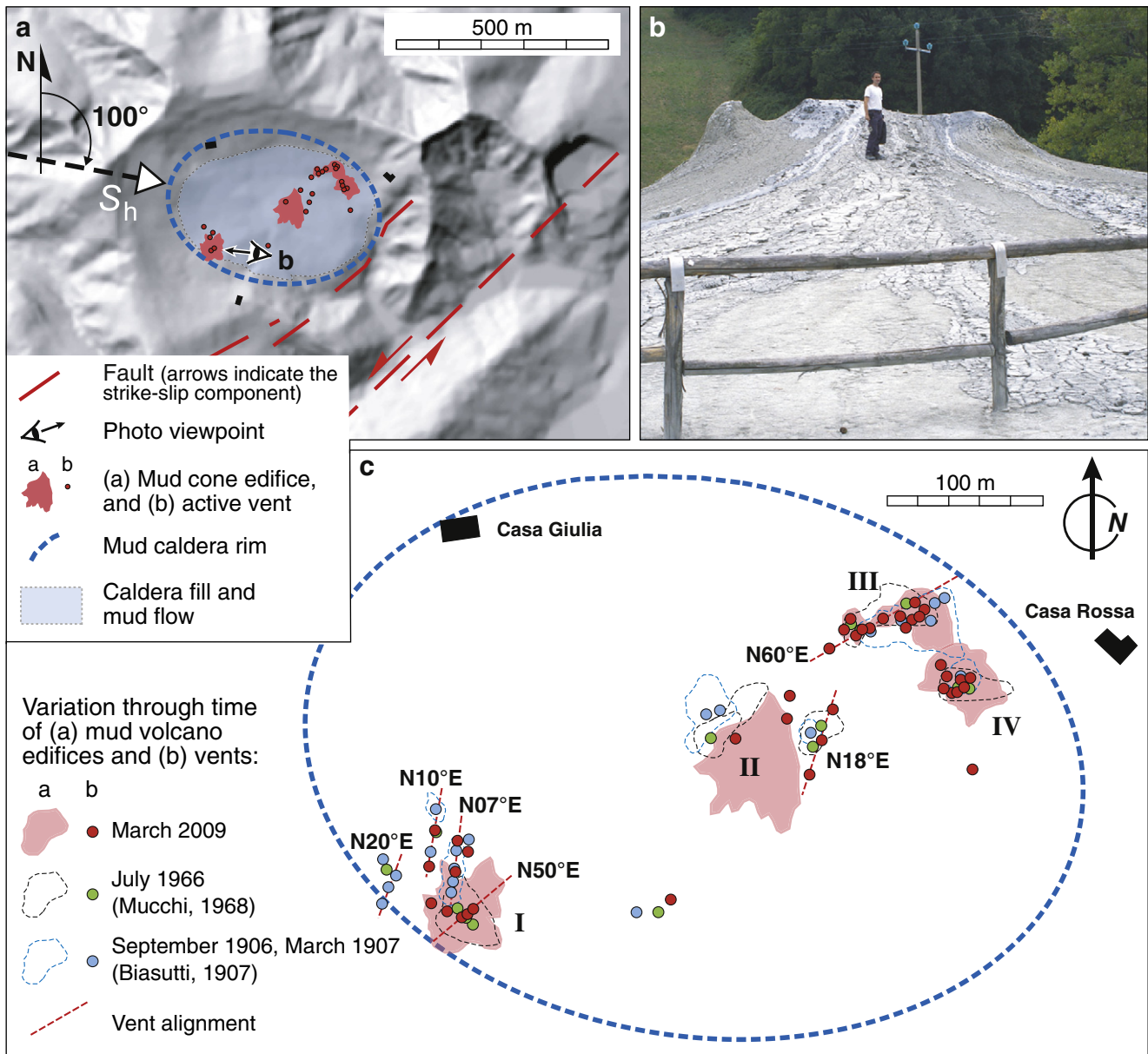
Fig. 11. (a) Nirano mud volcano field, northern Italy. Structural and mud volcano features are reported onto a 5 m-resolution digital terrain model (DTM courtesy of Regione Emilia–Romagna; location in Fig. 8). The dashed arrow indicates the inferred local S_h direction. (b) View of an elongated ~N50°E-trending vent (10th September 2008). (c) Variation through time of the extrusive edifices and vents contained within the elliptical depression; I–IV, main venting areas.

Pede-Apennine margin. This setting is particularly evident around Nirano (no. 7) and Montegibbio (no. 6), where the mud volcano-related stresses reveal consistent N10°E to N15°E S_H axes (cf. Fig. 13a with Fig. 13b). S_H axes trending between N10°E and N15°E have also been determined in the Rivalta (no. 1) and Torre (no. 2) fields, where the N105°E and N110°E-trending S_h axes (identified from the calderas) remarkably match the breakouts and WSM data (cf. Fig. 13a and b). The Rivalta (no. 1) and Torre (no. 2) S_H axes also show a striking correspondence with the N14°E-trending σ_1 axis computed from the earthquakes that hit near these mud volcanoes on 23rd December 2008 (Fig. 13b).

Following Bonini and Mazzarini (2010), a cumulative analysis of the mud volcano stress indicators has been attempted for estimating a mean direction of the regional S_H. This analysis has considered the local S_H directions obtained from (1) vent alignments, (2) volcano elongations, and (3) short caldera axes (Fig. 14b). The distribution of mud volcano stress directions has been obtained by weighting the stress data by the attributed reliability classes (Table 2). A Fisher distribution analysis defines a main cluster in the N8°E–16°E interval, with the main frequency peak striking ~N14°E (Fig. 14c). These results suggest that the N8°E–16°E range could approximately contain the direction of regional S_H. Despite the relatively low number of stress indicator data, this direction interval is in excellent agreement with the orientation of the present-day stresses in the Earth's crust estimated from the WSM data, which indicate a maximum data point concentration in the N10°E–20°E interval (Fig. 14d). The mud volcano-deduced N8°E–16°E S_H interval also matches well the N99°E-trending S_h direction representative of the active stress in the Ferrara thrust folds (Montone and Mariucci, 1999), several tens of kilometres northeast of the mud volcanic belt (Fig. 13b). Notably, a consistent N12°E-trending σ_1 axis has been computed from the very recent (Mw = 5.9, Mw = 5.0, Mw = 4.9; INGV TDMT, 2012) earthquakes that struck this area on 20th May 2012 (Fig. 13b). Finally, the mud volcano stresses are well comparable with the average ~N16°E-trending regional GPS velocity determined in this sector of the Apennines (D'Agostino et al., 2008; Fig. 13b). It is
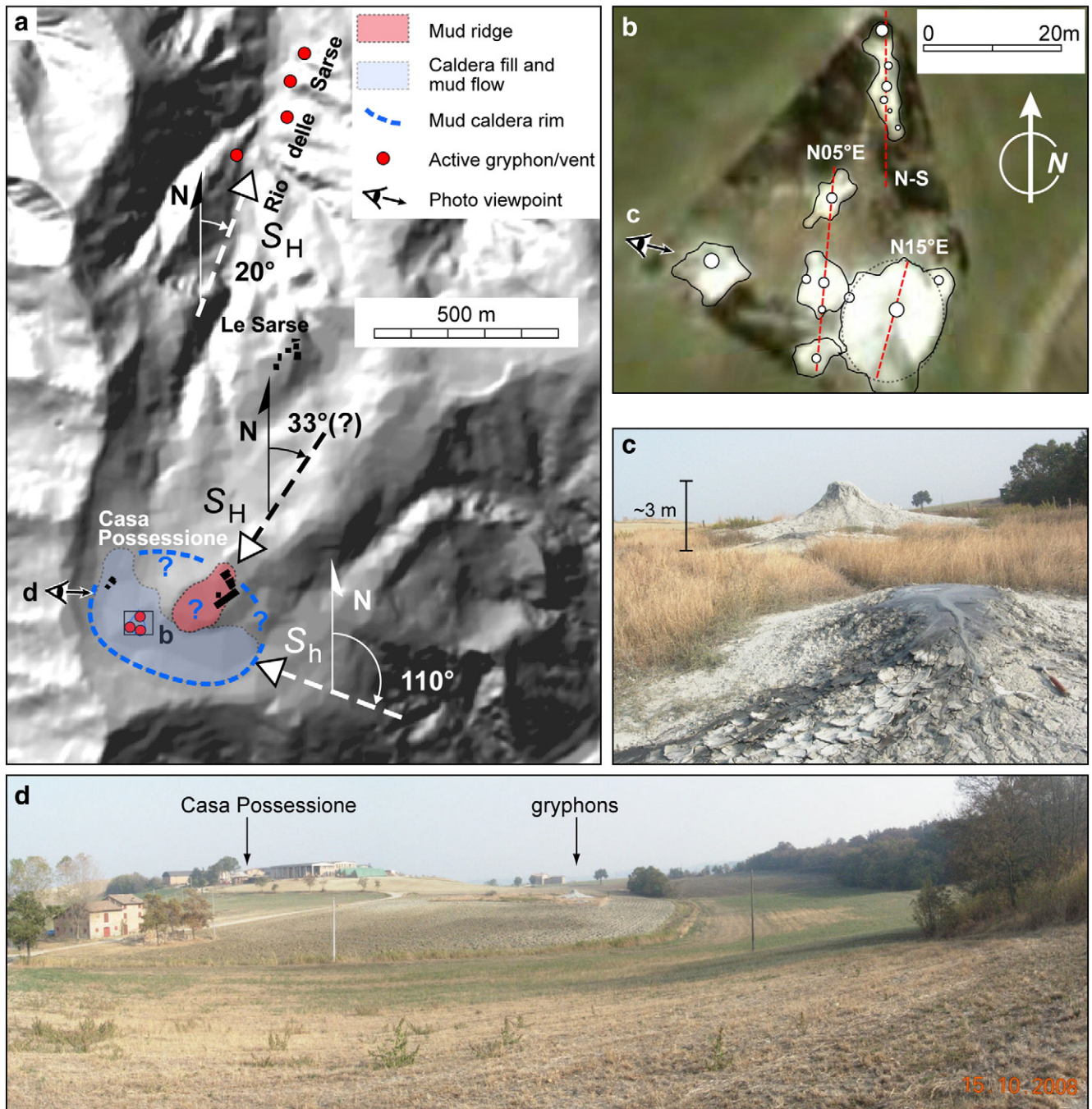
Fig. 12. (a) Mud volcanism at Casa Possessione and Rio delle Sarse (Madonna di Puianello field), northern Italy. Structural and mud volcano features are reported onto a 5 m-resolution digital terrain model (DTM courtesy of Regione Emilia–Romagna; location in Fig. 7a); the small vents along the Rio delle Sarse are taken from Ferrari and Vianello (1985) and Gasperi et al. (1987). The dashed arrows indicate the direction of local S_H and S_h inferred from the mud volcano features. (b) Alignments of vents near Casa Possessione, and (c) view of active gryphons. Note the dark flows indicating the expulsion of bituminous material. (d) Lateral view of the Casa Possessione depression hosting the gryphon field (15th October 2008).
Image in panel b is extracted from Google Earth®; http://earth.google.it/download-earth.html.

concluded that the S_H trend (N8°E–16°E range) estimated from the Pede-Apennine mud volcanoes represents a reliable proxy for the contemporary regional S_H operating in the external area of Northern Apennines, and that the collection of this kind of features over a wide belt may hint reliably for the active stress pattern.

5. Stress indicators from mud volcanoes of Azerbaijan

The potential application of this methodology will now also be discussed for Azerbaijan, which is the best known area of mud volcanism on Earth. There, previous work on stress indicators was determined on the basis of remote sensing studies (Bonini and Mazzarini, 2010; Roberts et al., 2011b). New ground-truthing has been carried out in Azerbaijan to improve the identification of the mud volcano features, and some results of this analysis are presented below. The methodology has also been tested in a number of case histories from well-known areas of mud volcanism worldwide, including Kerch-Taman, Makran, Hokkaido and Sakhalin, and the Indonesian Archipelago; the cases are illustrated in Appendix A, Supplementary data.

STRESSES FROM MUD VOLCANO FEATURES
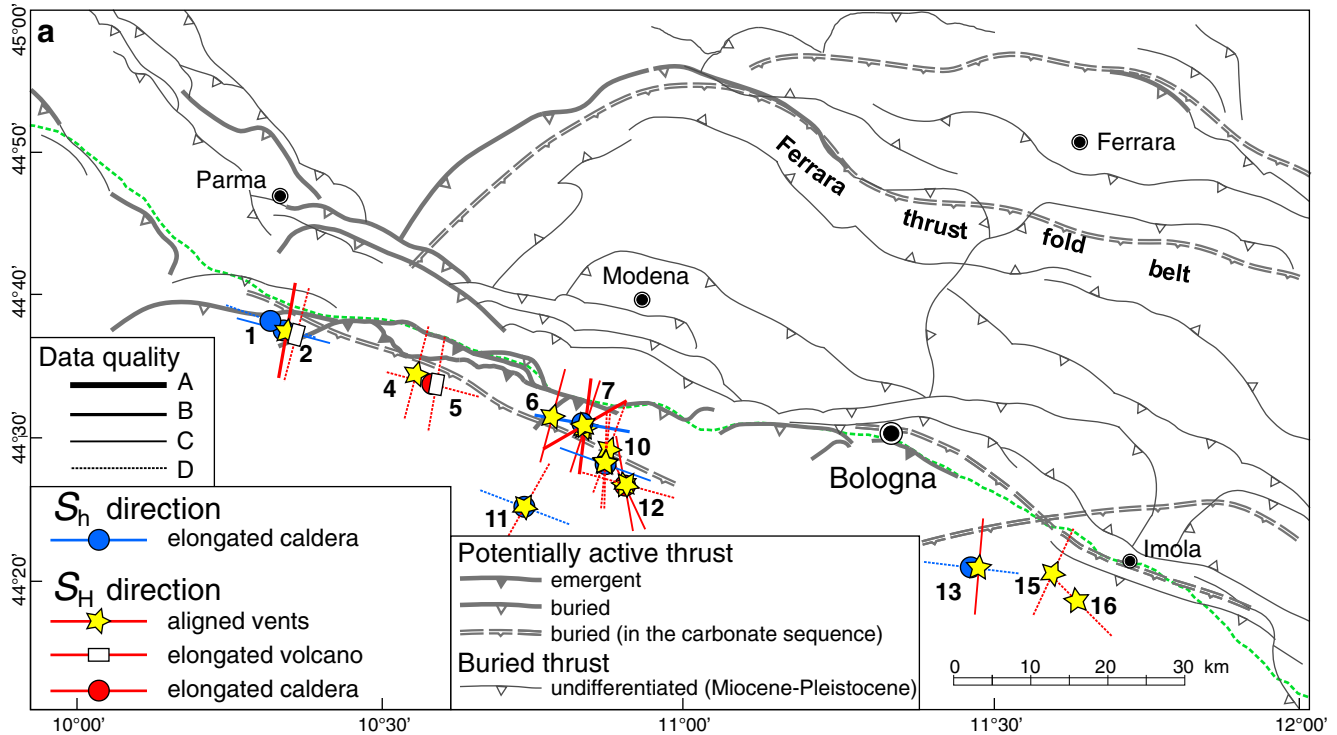
STRESSES FROM GEOPHYSICAL DATA
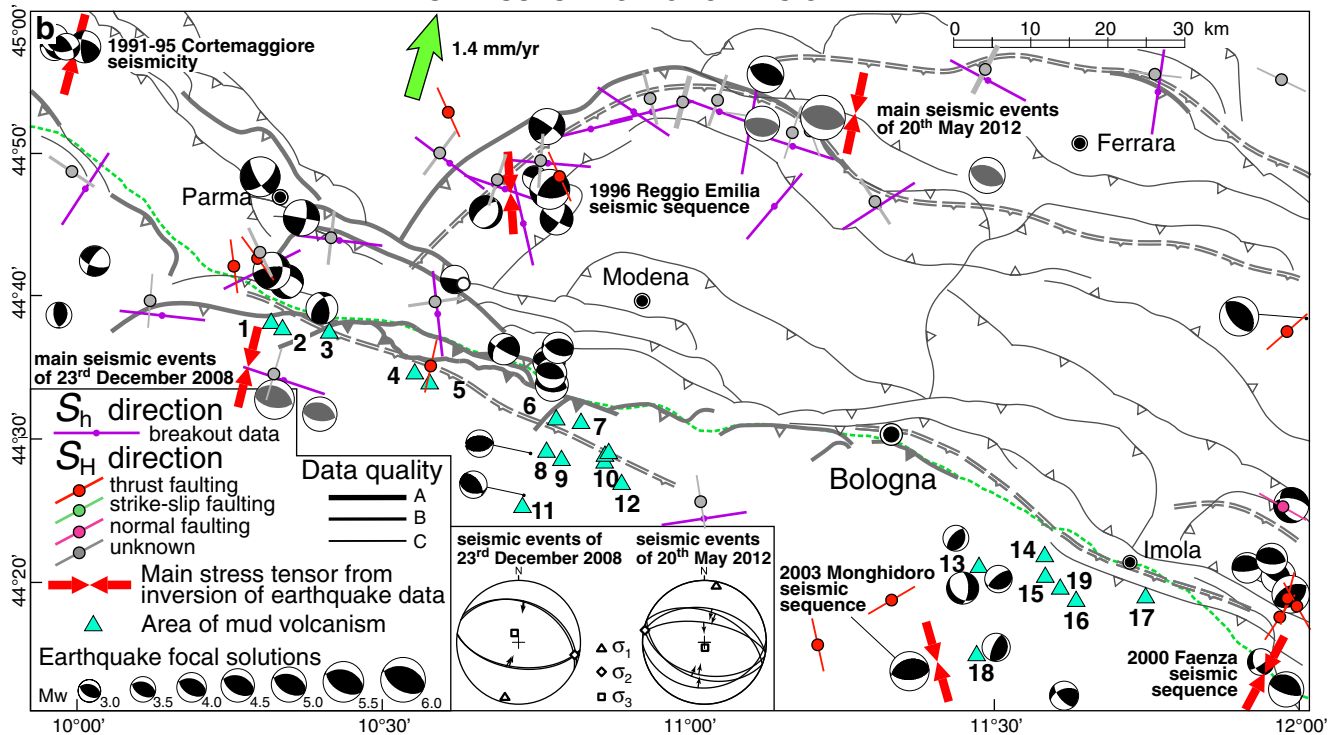
Fig. 13. Comparison between mud volcano and convectional stress indicator features in the Pede-Apennine margin and Po Plain (northern Italy). (a) Direction of minimum and maximum horizontal stresses (S_h and S_H, respectively) obtained from mud volcanoes (data in Table 2). (b) Stress axes obtained from various sources: S_H directions (from the World Stress Map; Heidbach et al., 2008), S_h directions from breakout data (from Montone and Mariucci, 1999; Mariucci and Müller, 2003; Montone et al., 2004), and principal compressive stress axes from inversion of earthquake data (from Boncio and Bracone, 2009). The focal mechanism solutions (black 'beach balls') are from Boccaletti et al. (2004), with the exceptions of those (grey 'beach balls') of 23rd December 2008 (from MedNet INGV, 2009) and 20th May 2012 (from INGV TDMT, 2012). The principal and auxiliary planes of the 2008 and 2012 seismic events have been inverted using the right dihedral method (Angelier and Mechler, 1977). Stress inversion of the Mw = 5.4 and Mw = 4.9 earthquakes of 23rd December 2008 yields σ_1 = 194/11, σ_2 = 103/08, σ_3 = 337/77. Stress inversion of the Mw = 5.9, Mw = 5.0, and Mw = 4.9 earthquakes of 20th May 2012 yields σ_1 = 12/07, σ_2 = 281/02, σ_3 = 174/83. The green arrow is a representative regional velocity relative to Eurasia calculated from the GPS-derived poles (from D'Agostino et al., 2008). The dashed green line indicates the Pede-Apennine margin. Main mud volcano fields: 1, Rivalta; 2, Torre; 3, San Polo d'Enza; 4, Casola–Querzola; 5, Regnano; 6, Montegibbio; 7, Nirano; 8, Montebaranzone; 9, Centora; 10, Madonna di Puianello; 11, Canalina; 12, Ospitaletto; 13, Dragone di Sassuno; 14, S. Martino in Pedriolo; 15, Sellustra valley; 16, Casalfiumanese; 17, Bergullo; 18, Cà Rubano (Sassoleone); and 19, Pedriaga.
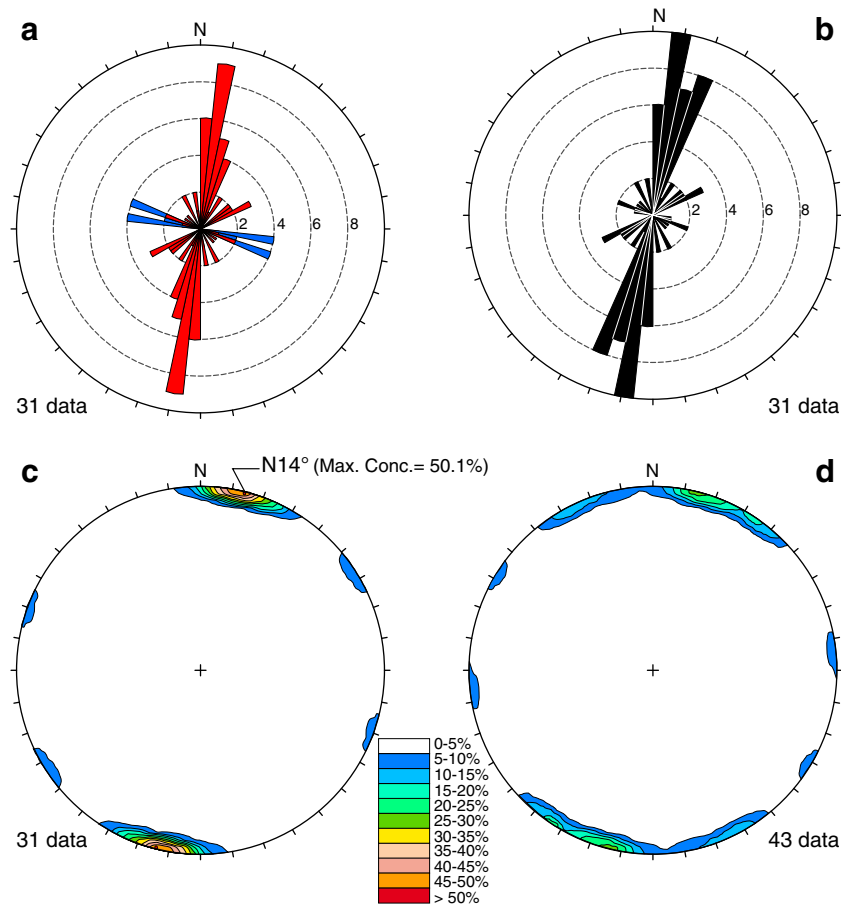
Fig. 14. Statistical analysis of stress indicators obtained from mud volcanoes of the Northern Apennines (data reported in Table 2). (a) Rose diagram of S_h (blue) and S_H (red) azimuths (bin angle 6°). (b) Cumulative rose diagram of local S_H axes, including the short axis of calderas elongated in the S_h direction. The data are statistically weighted by the quality class attribution that considers the following correction coefficients: A = 4, B = 3, C = 2, and D = 1 (reliability grade attribution in Table 2). (c) Contour plot (Fisher distribution; equal area, lower hemisphere) of the stress populations shown in (b), yielding a peak in data point concentration around N14°E. (d) Contour plot (Fisher distribution; equal area, lower hemisphere) of S_H directions reported in the World Stress Map for the Northern Apennines and Po Plain area. The stress data are weighted by the attributed quality classes with the following coefficients: A = 3, B = 2, and C = 1.
Panel d is from Heidbach et al. (2008).

5.1. Geologic setting of Azerbaijan mud volcanoes

Azerbaijan exposes the most impressive examples of onshore mud volcanoes worldwide (Jakubov et al., 1971). Azerbaijan features mostly occur at the south-eastern termination of the S–SSW-verging Greater Caucasus fold-and-thrust belt (Jakubov et al., 1971; Guliyev and Feizullayev, 1997; Alizadeh, 2008) (Fig. 15a). The front of this range is characterised by lines of elongated SW-to-WSW-vergent anticlines that deform the Pliocene–Pleistocene deposits and continue in the submerged Absheron Sill up to onshore west Turkmenistan, on the eastern side of the Caspian Sea (e.g., Allen et al., 2003, 2004; Stewart and Davies, 2006; Fig. 15a). These folds deform the (up to 5 km thick) latest Miocene–early Pliocene 'Productive Series' of fluvial–deltaic sands, and detach in underlying Oligocene–Miocene 'Maykop' shales (Jakubov et al., 1971; Abrams and Narimanov, 1997; Devlin et al., 1999; Stewart and Davies, 2006).

Mud volcanoes are associated with hydrocarbon traps and typically puncture the crests of anticlines (Jakubov et al., 1971; Guliyev and Feizullayev, 1997; Fowler et al., 2000; Cooper, 2001; Planke et al., 2003; Stewart and Davies, 2006; Fig. 15a). The abundant mud volcanism is likely to have resulted from the combination of different factors, such as (1) very fast (post-4–5 Ma) sedimentation rates, (2) tectonic compression, and (3) hydrocarbon maturation and degassing of the rapidly buried Maykop organic-rich sediments (Guliyev and Feizullayev, 1997; Fowler

et al., 2000; Yusifov and Rabinowitz, 2004). The Maykop Series is the most important regional source rock for hydrocarbons (Jones and Simmons, 1997) and the mud volcano systems (Inan et al., 1997).

5.2. Mud volcano stress indicators with some field examples

The distribution of local maximum horizontal stress directions (S_H) obtained from Azerbaijan mud volcanoes are shown in Fig. 15b and reported in Table A1 of Supplementary Material (for details, see Bonini and Mazzarini, 2010). The stress indicator azimuths reveal clear clusters in volcano elongation, vent alignment, caldera and summit caldera elongation (Fig. 15c). The cumulative analysis of S_H axes yields a main preferential orientation in the interval N20°–40°E (Fig. 15d) with a main frequency peak trending around N30°E, and a secondary peak striking ca. N110°E (Fig. 15e). This statistical distribution is basically similar to that obtained from the World Stress Map S_H axes (Heidbach et al., 2008) situated on the onshore Greater Caucasus (cf. Fig. 15e with 15f). The ~N30°E peak – which trends orthogonal to the Greater Caucasus range (Fig. 15a) – can be thus considered a reliable proxy for the regional S_H orientation. The other ~N110°E-trending secondary cluster has been identified in the distribution of both mud volcano and World Stress Map S_H axes (cf. Fig. 15e with 15f). This peak direction is sub-parallel to the mean trend of fold axes, and it is most likely related to the localised fold-axis parallel outer-arc extension faults (see Fig. 6a).
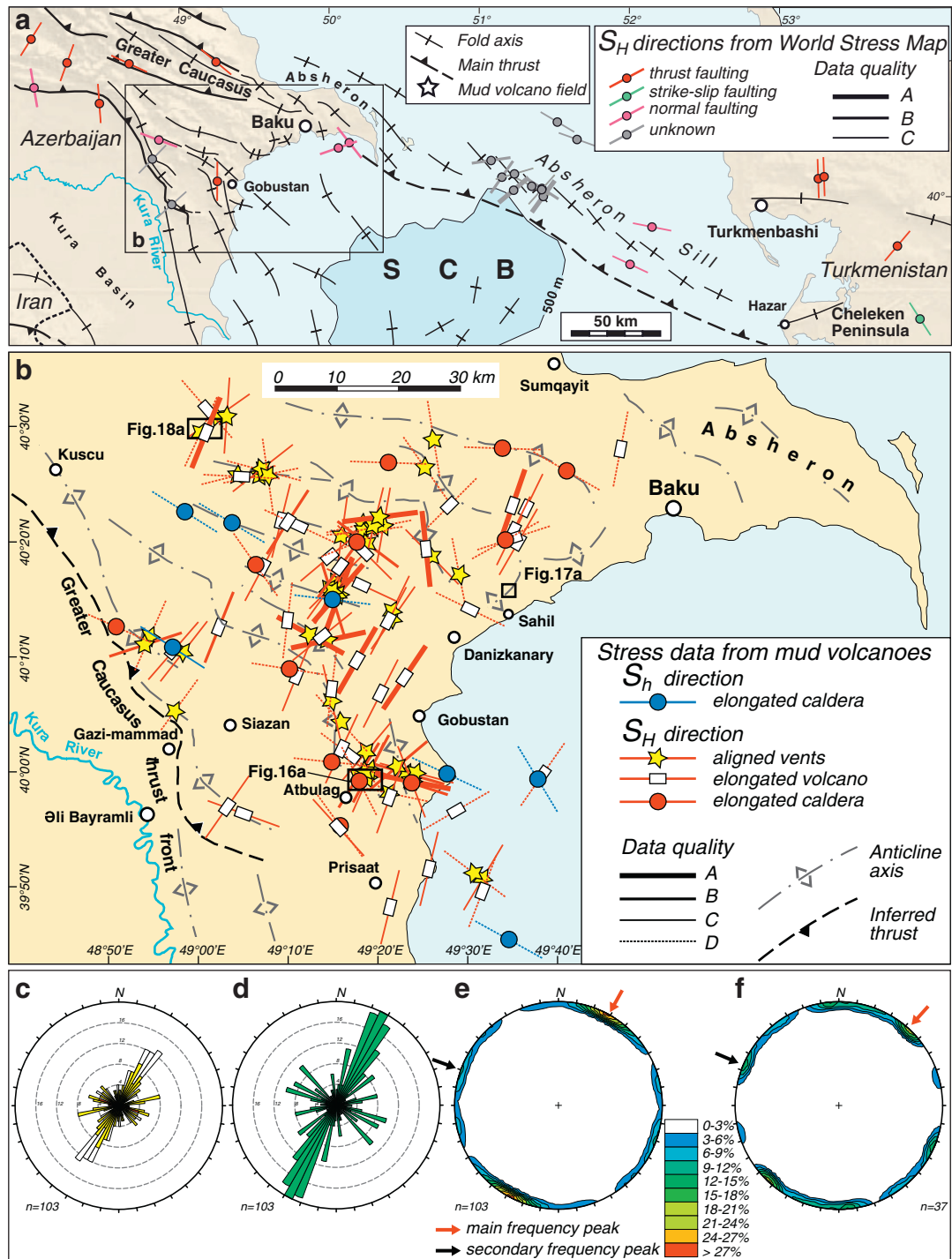
Fig. 15. (a) Tectonic sketch map of the Caspian Basin area. The S_H directions are extracted from the World Stress Map (Heidbach et al., 2008). SCB, South Caspian Basin. (b) Local S_H and S_h directions inferred from the mud volcanoes of Azerbaijan. The fold axes around the Absheron area are from Allen et al. (2003). (c–f) Statistical analysis of mud volcano stress indicators. (c) Rose diagram showing frequency distribution azimuths (bin size 5°) of local S_H axes: white, elongated volcanoes; yellow, vent alignments; red, elongated calderas. (d) Cumulative S_H direction rose diagram (bin angle 5°) of local maximum horizontal stress S_H axes shown in (c). (e) Contour plot (Fisher distribution; lower hemisphere, equal area) of S_H axes reported in (d). (f) Contour plot (Fisher distribution) of S_H axes determined on the Greater Caucasus and Kura Basin (i.e., around the onshore mud volcanoes) (from World Stress Map; Heidbach et al., 2008).
Panel a is adapted from Kholodov (2002b) and Allen et al. (2004). Data in panel b is from Bonini and Mazzarini (2010). Panels c–f are after Bonini and Mazzarini (2010).

Some of the elements identified as stress indicators from the remote sensing analysis have been successively ground-truthed and new ones have been determined. Fieldwork and mapping has focused on the morphology of minor extrusive features (i.e., alignments of gryphons and salses) and tectonic structures (faults or fractures) that are difficult to determine on satellite imagery. In general the surveyed elements have confirmed the results of the remote sensing analysis, and have provided new

evidence regarding the relations between stress, structural elements, and mud volcanoes. More specifically, ground-truthing has documented the presence of fold axis-parallel joints, which were previously suggested to affect fold hinges and to control mud volcanism (Bonini and Mazzarini, 2010; Roberts et al., 2011b). Fieldwork has substantiated the occurrence of vent alignments trending sub-orthogonal to the anticlines over which they are situated, but also the possible coexistence

with vent alignments trending sub-parallel to the same anticlinal axis (Bonini and Mazzarini, 2010; Roberts et al., 2011b). Few cases exemplify these settings.

5.2.1. Dominant fold-orthogonal vent alignments plus 'crestal' calderas (Ayran Tekan field)

The Ayran Tekan mud volcano field is situated over a main anticlinal ridge striking sub-parallel to the Greater Caucasus front (Fig. 15b).

This anticline folds Early Pliocene (Productive Series) to Early Pleistocene (Absheron) deposits and is composed of a zigzag pattern of ~NW–SE- and ~N–S-trending segments (Alizadeh, 2008). The Ayran Tekan field consists of various mud volcanic elements situated along the anticlinal crest (Fig. 16a). Rows of gryphons and small vents define alignments that trend mostly orthogonally to the local trend of fold axis (i.e., alignments labelled 1, 2 and 3 in Fig. 16b), but a fold-axis parallel alignment (alignment 4) has also been identified in the same spot (Fig. 16b–d). A
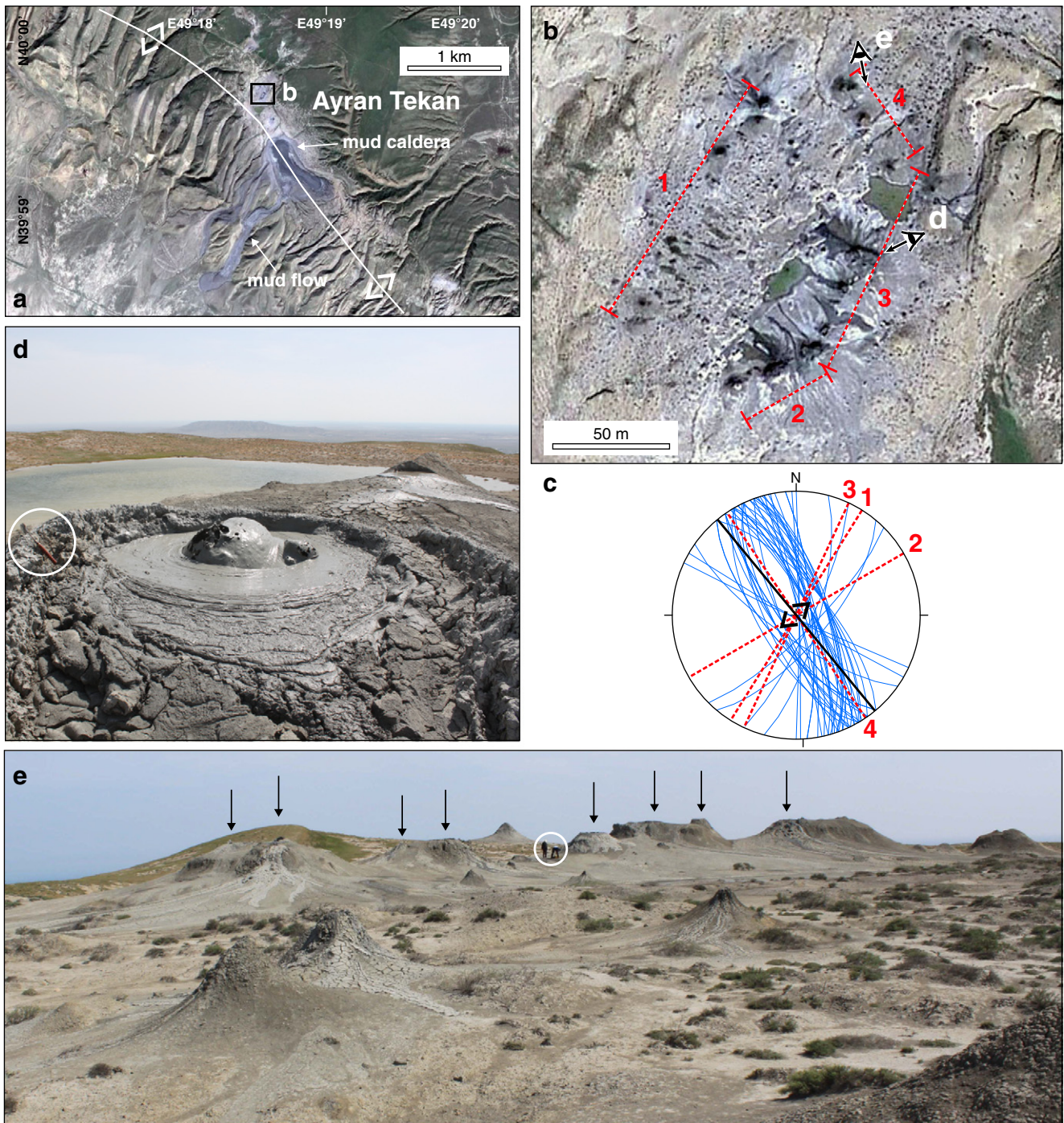
Fig. 16. (a) Ayran Tekan mud volcano field, Azerbaijan. This mud volcano occurs over the crest of a fold anticline north–northeast of Atbulag. (b) Alignments of vents labelled 1 to 4 (red dashing). (c) Stereonet (Wulff net, lower hemisphere) illustrating the trend of vent alignments, the local direction of fold axis (thick black line), and faults and fractures (pale blue cyclographic lines) collected at the rims of the caldera shown in (a). Note the caldera faults (and alignment 4) striking sub-parallel to the fold axis, and alignments 1–3 trending at high-angle to this axis. (d) Typical gas bubble popping up a crater topping an elongated gryphon of alignment 3; hammer (encircled) for scale. (e) View of the Ayran Tekan gryphon field; the black arrows outline vent alignment 3 (23rd May 2010); persons for scale.
Images in (a) and (b) are extracted from Google Earth®; http://earth.google.it/download-earth.html).

caldera is situated along the fold crest a few hundreds of metres to the southeast of the vent alignments (Fig. 16a). The caldera extrudes two mud breccia flows exceeding 1 km in length, and extends downwards to the foot of the anticline forelimb. This depression elongates sub-parallel to the fold axis and shows rectilinear rims defined by fold-parallel faults exposing scarps up to 5–6 m high measured along the outer edge of the caldera (Fig. 16c). These findings apparently support the previous attribution of caldera evolution to outer-arc fault control (Bonini and Mazzarini, 2010).

5.2.2. Dominant fold-parallel vent alignments and outer-arc normal faults (Akhtarma–Karadag field)

The occurrence of outer-arc normal faults has been documented in many localities. For instance, the Akhtarma–Karadag mud volcano field near Sahil (Caspian coast) is composed of some mud volcano features

affecting the crest of an anticline that locally strikes ca. ENE and folds Early Pliocene (Productive Series) to Early Pleistocene (Absheron) sediments (Alizadeh, 2008; Fig. 17a). Here, normal faults deform the fold crest, and have been previously referred to as an 'incipient sector collapse' structure (Roberts et al., 2011a, b). The faults can be grouped into two oppositely-dipping fault sets defining a sort of crestal graben that closely follows the trend of the anticline axis (Fig. 17a, b). The normal faults display an apparent vertical separation of the ground up to ~2 m, and are characterised by relatively fresh and steep scarps that suggest recent formation (Fig. 17c). Such normal faults are similar to those displacing the crest of growing anticlines (e.g., Morley, 2007), and are seemingly the product of outer-arc extension and collapse of the fold crest.

The abundant mud volcanism is mainly related to decametre scale vent populations that align not only in the same orientation as the local anticline axis, but also along with the fold-parallel faults. Therefore,
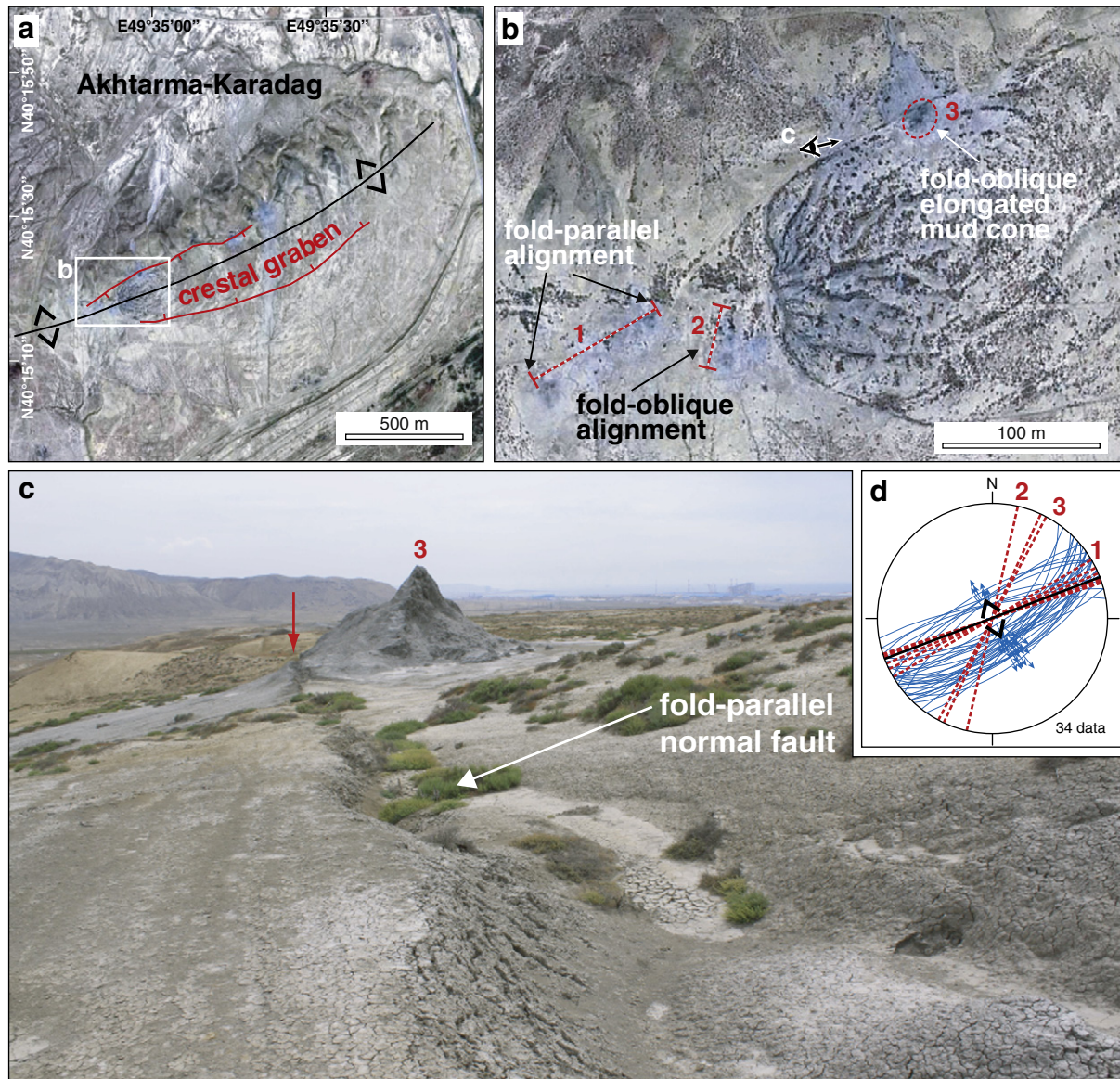
Fig. 17. Akhtarma–Karadag mud volcano field, Sahil, Azerbaijan Caspian coast. (a) Satellite image showing normal faults (red) affecting the crest of the anticline over which the mud volcano is located. (b) Detail of (a). (c) Normal fault displacing the flank of the ~6–7 m-tall elongated mud cone 3. The normal fault is attributed to the extension of the anticline outer-arc and exhibits a vertical scarp up to 1.5–2 m high (25th May 2010) (photo viewpoint in b). (d) Stereonet (Wulff net, lower hemisphere) reporting the fault planes (pale blue cyclographic lines), vents alignments and elongated vents (red dashing) collected over the fold crest, together with the fold axis trend (thick black line). Note that a number of vent alignments and elongated vents trend oblique to the fold axis.
Images in (a) and (b) are extracted from Google Earth®; http://earth.google.it/download-earth.html.

the outer-arc normal faults are most likely structurally controlling the fold-parallel vent alignments (Fig. 17b, d). However, it is notable that some vent alignments and elongated vents internal to the graben conform to the NNE-trending regional S_H (Fig. 17b, d).

5.2.3. Fold-orthogonal alignments at mud volcano summit craters (Shikhzairli volcano)

Gryphons and salses frequently form linear alignments sub-orthogonal to the axes of anticlines. The Shikhzairli mud volcano, which lies in the foothills of the Greater Caucasus, provides an example in this direction. This volcano is a large edifice displaying a clear elongation, with its long axis reaching approximately 1400 m in length (Fig. 18b; Table A1). The Shikhzairli mud volcano is situated over an antiform structure that folds sediments ranging in age from Eocene to Late Pliocene (Alizadeh, 2008); notably, the long axis of this volcano is sub-orthogonal to the axis of this antiform (Fig. 18a, b, d). The summit of the volcano is a nearly-flat sub-circular area (at ca. 640 m elevation) that is characterised by a gryphon field with the peculiar presence (May 2010) of elements that intermittently outburst and shriek manifesting the ongoing rapid ascent of pressurised fluids and gases (Fig. 18c). The gryphons situated in the summit crater define a number of alignments sub-parallel to the long-axis of the main volcanic edifice, implying that they strike sub-orthogonal to the antiform axis (Fig. 18c–f). The gryphon alignments are likely to manifest the subsurface feeder fractures that assisted the reiterated eruptions this volcano experienced during the two last centuries (e.g., Aliyev et al., 2002).

6. Structural controls on mud volcanism in fold-and-thrust belts

Overpressure in sediments and mud volcanism may be controlled by a variety of tectonic elements and structural mechanisms acting over a range of time scales, and at various length scales. In addition, mud volcanism may distribute over large portions of fold-and-thrust belts, or remain localised at discrete large-scale structures. Secondary brittle structural elements represent other features able to control the rising of the mud-fluid mix at the core of anticlines, as seen in the Northern Apennines and the Azerbaijan Greater Caucasus. These tectonic elements are closely linked to the stress field, and are also inferred to exert some control on the paroxysmal events the mud volcano systems may experience. These issues are discussed in separate sections below.
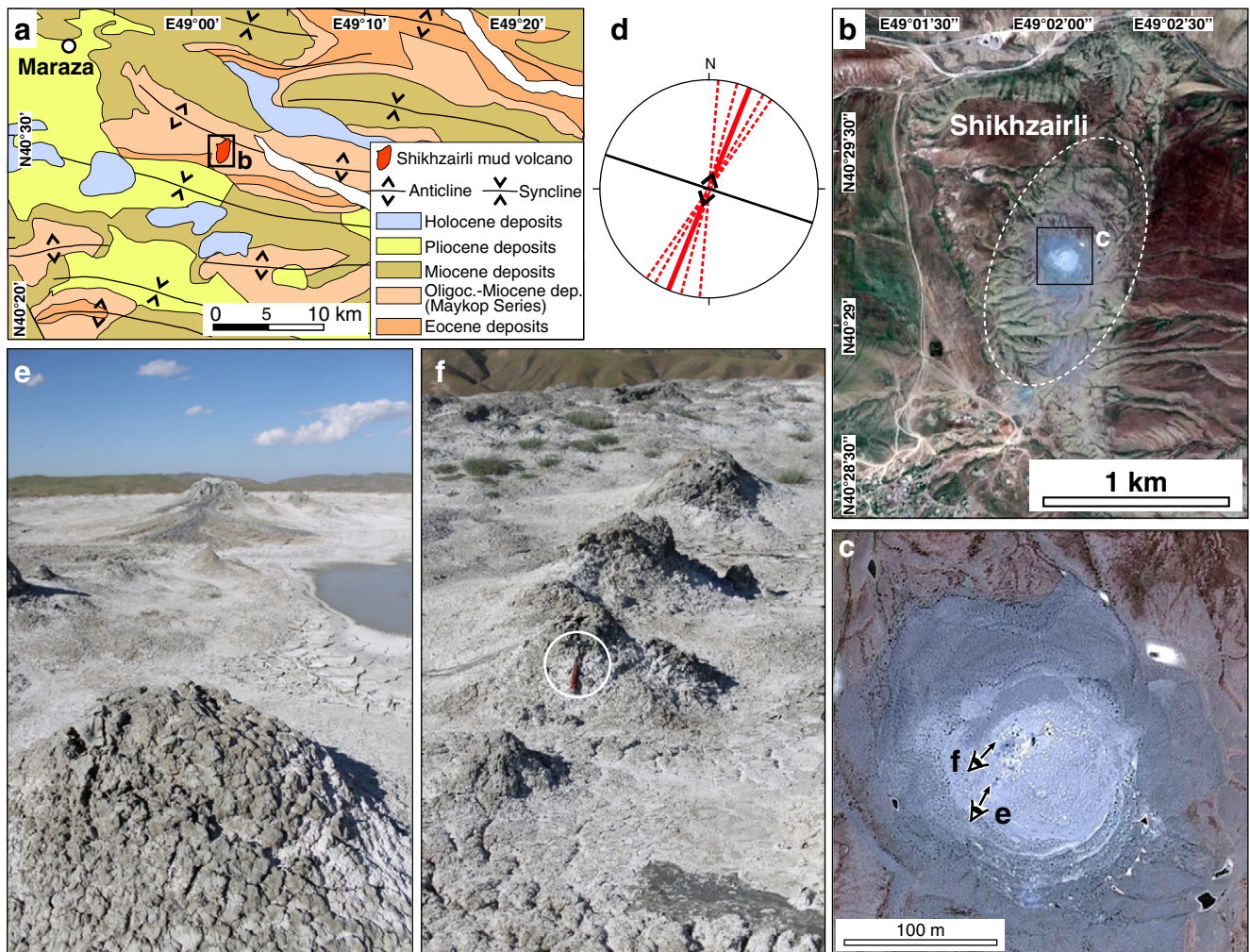
Fig. 18. Shikhzairli mud volcano, Azerbaijan. (a) Geological map showing the volcano settled near the axis of a ca. ESE-trending anticline. (b) Satellite image showing the elongated Shikhzagirli mud volcano. (c) Detail of the summit crater. (d) Stereonet (Wulff net, lower hemisphere) reporting the long axis of the Shikhzagirli mud volcano edifice (thick red line), the vent alignments measured on the crater (red dashing), and the fold axis trend (solid black line). (e, f) Details of gryphon/vent alignments on the summit crater (photo viewpoints in c; 26th May 2010).
Panel a is modified from Alizadeh (2008). Images (b) and (c) are extracted from Google Earth®; http://earth.google.it/download-earth.html.

6.1. Relations between mud volcanism and tectonic structures

6.1.1. Coincidence of mud volcanism with thrust anticlines

A conceptual 3D mechanical model showing the conditions that favour the occurrence of mud volcanism at the crests of anticlines (Fig. 1d) is illustrated in Fig. 19 by reference to the Northern Apennines, but the concepts may also hint at other cases. The model relates the fluid pressure conditions, the rheological layering and the brittle infrastructures in the fold core (Fig. 19a). The alternation of low-permeability and permeable layers in the Northern Apennines stratigraphy highlights
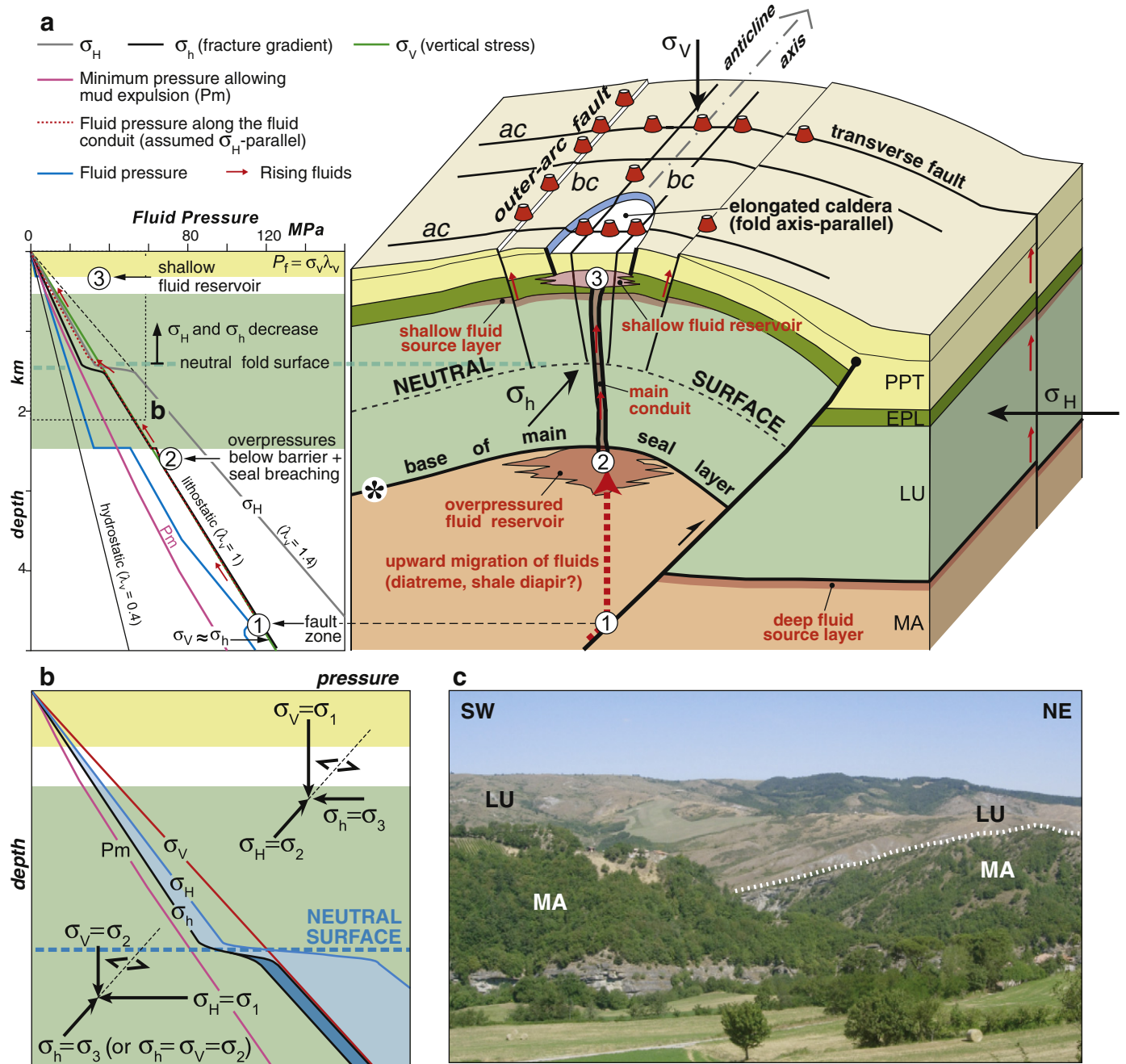
Fig. 19. Conceptual relationships between brittle structures, fluid pressure and mud volcanism at the core of a thrust fold inspired to the Northern Apennines setting. (a) Schematic block diagram showing the principal stress axes and the main fracture sets, together with the inferred variation of fluid pressure (P_f) with depth. The minimum pressure ($Pm = \rho_{mud}gz$) allowing mud expulsion has been computed considering the variation of mud density with depth ($\rho_{mud} = 1$–2000 kg m^{-3} in the 0–5 km depth range) reported in Brown (1990). To allow fluid–mud extrusion, the fluid pressure must exceed Pm throughout the steep conduit. The fluid pressure profiles have considered an average rock density of 2550 kg m^{-3}, and a σ_H increasing with depth at a rate of 35 MPa/km (e.g., Calderoni et al., 2009). The encircled numbers indicate schematic fluid pressure states along an ideal vertical section through the fold: (1) bottom of the main fluid conduit or diatreme, and pressurised (2) deep and (3) shallow fluid reservoirs. MA, Marnoso Arenacea sandstones; LU, Ligurian units; EPL, Epi-Ligurian sequence; and PPT, Pliocene–Pleistocene claystones. (b) Schematic pressure–depth diagram (box in a) and stress states showing the inferred variation of σ_H and σ_h (pale blue area) above and below the neutral surface. A strike-slip stress state ($\sigma_h < \sigma_v$) is assumed below the neutral surface (e.g., Carminati et al., 2010). The dark blue area schematically indicates the inferred range of the σ_h, which may locally reach the lithostatic stress; σ_H-parallel, vertical feeder hydrofractures may thus develop (see text for details). (c) Low-angle tectonic contact superposing the Ligurian Units (LU) over the Marnoso Arenacea (MA). The contact is well exposed in the transition zone between the Emilia and Romagna Apennines (Sillaro Valley between Piancaldoli and Giugnola; location in Fig. 7a), and shows in outcrop what is inferred to be an important hydraulic interface at depth (indicated with the asterisk in a).
Panel a is adapted from Deville et al. (2006) and Bonini (2007).

the presence of different fluid pressure compartments, with the main fluid reservoirs expected to develop in the core of the thrust folds beneath the main sealing layers (Fig. 19c).

The tops of subsurface shale intrusions coring thrust anticlines (e.g., Duerto and McClay, 2002; Grando and McClay, 2007) may represent regions of localised overpressures (similar to the tops of any hydraulically conductive fault) that could favour the formation of leakage structures such as pipes and dykes (e.g., Mourgues et al., 2011). Unloading of the anticline cores operated by erosion during exhumation would progressively reduce the overburden load acting on the fold hinge and increase the potential for the mud–water–gas mix to travel up-through anticlinal cores.

The increase in rock permeability caused by the joints that normally accompany the development of anticlines (e.g., Stearns, 1968; Hancock, 1985; Engelder et al., 1997; Fischer and Wilkerson, 2000) would also significantly contribute to the localization of mud volcanism at folds. The development of typical mud volcano alignments and mud ridges along anticlinal crests is likely to take advantage of tensile failures on the outer arc and upper parts of the fold anticline (e.g., Bonini, 2007; Roberts et al., 2011a, 2011b). Stretching of the anticline outer-arc implies a transition of σ_H and σ_h to values lower than the vertical lithostatic stress σ_V, a mechanism that reduces the pore pressure required for fracturing (Fig. 19b). However, other fold-related joint sets may focus the surface fluid flow, such as cross-fold (*ac*) joints (e.g., Cooper, 1992), or other joints that are neither parallel nor perpendicular to the fold axis (Fischer and Wilkerson, 2000).

6.1.2. Spatial distribution of mud volcanoes in fold-and-thrust belts

The action of compressive stresses is common and determinant for driving mud volcanism, yet this may show obvious and remarkable differences in spatial distribution and products. The prolific mud volcanism of Azerbaijan is strictly associated with hydrocarbon maturation and the presence of the Maykop shales, which also provide a regional décollement that has spatially distributed the lines of detachment folds. Mud volcanoes predominantly occur along or near the crests of these anticlines, and for this reason mud volcanism is more or less evenly distributed over the Azerbaijan Greater Caucasus (Fig. 15b). Mud volcanism in the Kerch–Taman peninsulas (Appendix A1, Supplementary data) presents characteristics essentially equivalent to those of Azerbaijan. On the other hand, mud volcanoes of the Northern Apennines are essentially restricted to a relatively narrow belt running over the hangingwall of the Pede-Apennine thrust (Fig. 7a).

Such a contrasting mud volcano distribution (cf. Fig. 7a and Fig. 15b) may define two end-members possibly identified in other fold-and-thrust belts and accretionary prisms. Basal décollements of accretionary prisms distribute the internal deformation over wide areas, and the general coincidence of mud volcanoes at thrust-related folds yields these settings to represent a general case of distributed mud volcanism. These characteristics are well-known thanks to the 'classic' Barbados (Henry et al., 1990; Deville et al., 2010) and Mediterranean Ridge (Kopf et al., 2001), but these are common to other cases, for instance sectors of the Gulf of Cadiz (Somoza et al., 2003; Van Rensbergen et al., 2005). Similar structural patterns have been identified in the submerged and exposed Makran accretionary prism (Appendix A2, Supplementary data). Conversely, mud volcanism localises over the hangingwall of the Central Sakhalin fault and thus represents a case of regional-scale discrete fault control (Appendix A3, Supplementary data).

6.1.3. The Pede-Apennine thrust as an example of discrete structural control

The plethora of geophysical and structural data from the Pede-Apennine thrust (PAT) makes it particularly fruitful to understand the processes governing a large-scale structural control on mud volcanism. Interpreted seismic profiles have generally imaged the PAT as a steep

fault dipping SSW in the 50–60° range, and extending at least up to ~10 km depth (Pieri and Groppi, 1981; Pieri, 1983; Castellarin et al., 1985; Bertello et al., 2008). Reshear along high-angle faults requires high fluid pressure (P_f), which must exceed supralithostatic magnitudes ($P_f > \sigma_V$, or $\lambda_v > 1$) whether the fault enters the severe misorientation field defined by the frictional lockup angle $\theta_r = \tan^{-1}(1/\mu_s)$ (Sibson, 1985). The PAT thus approaches the frictional lockup expected at $\theta_r \approx 59°$ for reverse faults having friction coefficient $\mu_s = 0.6$ (Sibson and Xie, 1998).

It is well established that in compressional settings fault loading can occur by increasing the σ_1 and/or increasing fluid pressure, but other factors may favour or inhibit reshear along the PAT, namely the coefficient of friction of intact and anisotropic rock (μ_i and μ_s, respectively), and the cohesive strength of intact and fault rock (c_i and c_s, respectively). These concepts can be illustrated through a simple mechanical analysis of the Mohr diagram considering a reactivation angle $\theta_r = 50°$. For a cohesionless fault plane ($c_s = 0$), the critical conditions for reshear can be defined when the half circle touches the Mohr envelop for intact rock and contemporaneously it is in the proper position for reshear (i.e., $2\theta_r = 100°$). This situation is explicated by the half circle I for $c_i = 20$ MPa (Fig. 20a). In this case, a coefficient of fluid pressure $\lambda_v \approx 0.74$ is estimated as an approximate lower limit (together with a maximum differential stress of ≈ 280 MPa) for reshear. Higher fluid pressure favours the reactivation of the PAT, whereas for lower fluid pressure the Mohr circles touches the fault failure curve before reaching the reshear condition (see circle II), and new thrust faults ensue (Fig. 20a). For weaker cohesion ($c_i = 10$ MPa), higher fluid pressure levels and lower differential stresses are necessary for reactivation. Circle III indicates the lower boundary conditions for reactivation ($\lambda_v > ~0.89$ and $\sigma_1 - \sigma_3 < ~125$ MPa; Fig. 20b). The boundary conditions are also extremely sensitive to the cohesion of the fault rock c_s, as an increase of this parameter shifts the system toward very high fluid pressure regimes (e.g. Sibson and Xie, 1998; Streit and Cox, 2001). For $c_s = 5$ MPa reshear requires near lithostatic overpressure ($\lambda_v \to 1$) and very small differential stresses (ca. 40 MPa) (see circle IV in Fig. 20b). Higher cohesive strengths require more extreme conditions with supralithostatic overpressures ($\lambda_v > 1$).

Despite the intrinsic difficulty of determining all the various interacting parameters, this analysis highlights the importance of fluid overpressures in the fault reactivation process. In agreement with these results, high fluid pressure factors ($\lambda_v \approx 0.86$) and differential stress of the order of 100 MPa have been estimated (at 10 km depth) in the Pede-Apennine margin near Faenza (Calderoni et al., 2009). Boncio and Bracone (2009) reached similar conclusions and estimated fluid factors $\lambda_v \geq 0.7$ for fault dip angles $\geq 49°$. The geometry of the PAT thus exerts an obvious influence on the fluid pressure regime and ultimately on mud volcanism. In particular, the presence of a steep fault coupled with the occurrence of an impermeable barrier (i.e., the Ligurian Units) and active shortening favour the entrapment of fluids at the highest overpressure (Sibson, 2004, 2007). On one hand, the achievement of strong overpressures represents a condition necessary for explaining the ongoing slippage along the steep PAT (see Section 4.1). On the other hand, the overpressures are consistent with mud volcano occurrence providing independent evidence of fluid leakage from subsurface pressurised reservoirs. Therefore, compressive tectonic loading and fluid overpressures may establish a positive feedback loop that is likely to be important for the PAT movement and the transfer of deep fluids to the surface.

Similar relations can be envisaged for the Central Sakhalin fault (see Appendix A3, Supplementary data), which is an active reverse fault (Bulgakov et al., 2002) characterised both by a steeply-dipping plane and mud volcanism on its hangingwall. Transverse geological sections image this as a 30°-to-45°-dipping reverse fault (Mel'nikov et al., 2008), which may dip as much as 55° along the major Tym–Poronay active fault segment (Kozhurin, 2004).

Reshear conditions along the Pede-Apennine thrust (PAT)
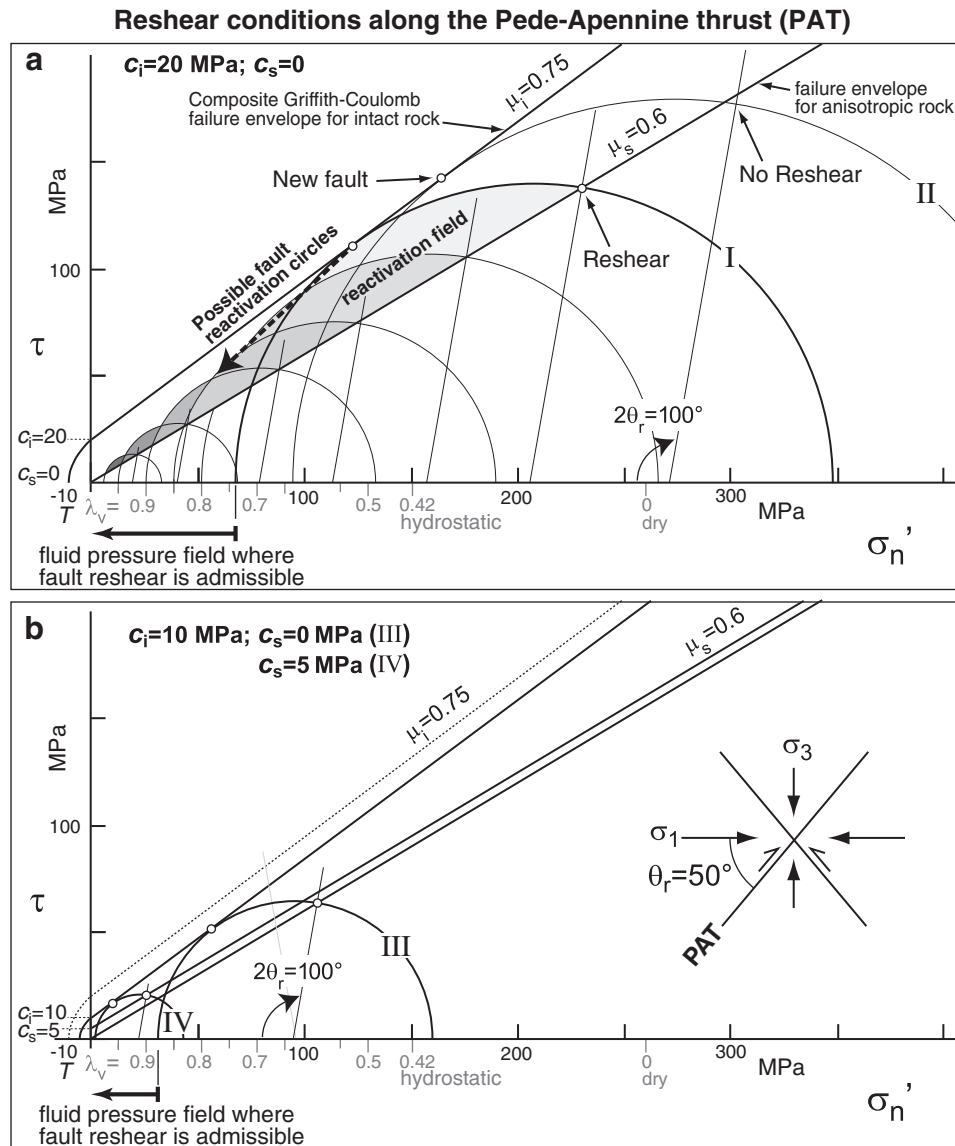
Fig. 20. Reactivation of the steep Pede-Apennine thrust (PAT) and its relationships with stress and pore fluid pressure conditions. The considered parameters are: depth $z = 10$ km, $\mu_s = 0.6$, rock density $\rho = 2650$ kg m^{-3}, and reactivation angle $\theta_r = 50°$; it is also assumed that the σ_2 axis lies near the strike of the PAT, and that this fault is moving with an essentially dip-slip kinematics. (a) Half circle I indicates the critical conditions – in terms of maximum differential stress and minimum fluid pressure – necessary for reshear along a 50°-dipping cohesionless ($c_s = 0$) fault plane (representing the PAT) for a cohesion of intact rock (c_i) of 20 MPa. (b) Half circle III represents the same conditions of circle I but with $c_i = 10$ MPa. Higher fluid pressure levels are necessary in case of fault planes with cohesive strength ($c_s > 0$); half circle IV shows the case with $c_s = 5$ MPa.

6.2. Brittle fluid pathways and the stress field

6.2.1. Surface fluid discharge along planar brittle structural elements

Vertical fluid migration from depth occurs up through steep, sub-planar hydrofractures and mud dykes (Brown and Westbrook, 1988; Morley et al., 1998; Tingay et al., 2003) as well as along sub-circular pipes (Roberts et al., 2010) whereby fluid conduit pressure exceeds the tensile strength and σ_h of the rock (i.e., the fracture gradient) and sub-vertical fracture networks may be generated (Morley, 2003a; Fig. 19a). The common association of elevated pore fluid pressure and elevated minimum horizontal stress σ_h (pore pressure/stress coupling) plays a major role in rock failure (e.g., Hillis, 2003; Tingay et al., 2009). Normally these relations are applied to sedimentary and passive margin basins undergoing normal faulting regimes (i.e., $\sigma_V = \sigma_1$; $\sigma_H = \sigma_2$; $\sigma_h = \sigma_3$) (Hillis, 2003; Tingay et al., 2003; Cobbold and Rodrigues, 2007; Mourgues et al., 2011; Fig. 21a).

The development of vertical hydrofractures during compressional tectonic loading (i.e., $\sigma_H = \sigma_1$; $\sigma_h = \sigma_2$; $\sigma_V = \sigma_3$) is more difficult to explain given the common understanding that mode 1 fracture planes contain the σ_1 and σ_2 directions and open orthogonal to the σ_3 direction. Classic theories predict this stress state to produce horizontal hydraulic fractures – unfavourably oriented for the vertical transport of the fluid–mud mix – whether fluid pressure exceeds the lithostatic load (e.g., Secor, 1965; Jaeger and Cook, 1969; Sibson, 2004). Besides, the existence of basin scale σ_H/P_f coupling (σ_H increasing with fluid pressure in a similar fashion to σ_h; Mandl and Harkness, 1987; Yassir and Rogers, 1993) in thrust faulting would favour the development of larger differential stresses and preclude the development of hydraulic fracturing (Fig. 21b).

On the other hand, mud volcanoes are typical manifestations of thrust settings and their existence raises the issue of which stress state may produce the vertical dykes imaged in seismic sections or observed as fossil examples in the field (e.g., Brown and Westbrook,

1988; Morley, 2003b) when σ_3 is predicted to be vertical. Therefore, if our understanding that feeder systems are formed by sub-vertical mode 1 hydrofractures is correct, this implies the existence of some mechanisms redistributing and reorienting the local stress state in the locus where these elements initiate at depth. The consideration of a Mohr space suggests that the σ_h (σ_2) should reduce to magnitudes lower than the σ_V (σ_3) in order for new vertical tensile hydraulic fractures to develop.

Along-depth stress changes have been documented in the active Mirandola anticline of the buried Ferrara folds (Fig. 7a), and are also likely to occur in other regions characterised by thrust faulting (Carminati et al., 2010). In particular, the stress field reconstructed from breakouts has revealed a transition from shallow normal faulting (<1.2–1.3 km depth), to strike slip faulting at intermediate depths (3–4 km), to genuine thrust faulting at deeper depths (Carminati et al., 2010). The establishment of local strike-slip states (i.e., $\sigma_h < \sigma_V$) implies that new σ_H-parallel vertical (feeder) hydrofractures may form at intermediate depths in the cores of anticlines. This setting may be conceptually similar to the vertical feeder magma dykes forming orthogonally to the σ_2 to allow volcanism under a thrust faulting regime (Tibaldi, 2005).

We noted earlier that pre-existing favourably oriented fractures may also represent preferential sites for intrusion. The fluid pressure necessary for emplacing the mud–fluid mix into these sub-planar elements depends on the orientation of the exploitable plane with respect to the stress field, and the fracture tensile strength. Assuming a general case in which the folds strike sub-orthogonally to regional σ_H, the fold-axis orthogonal planes (cross-fold ac joints, transverse faults, tear faults, etc.) would be the most favourable for acting as fluid conduits

(see Figs. 1d, 19a). In sectors of the Pede-Apennine–Po Plain region, the σ_h may be less than (Carminati et al., 2010) or approximately equal to the lithostatic stress acting at intermediate depths (Mariucci and Müller, 2003); σ_V can thus be taken as an upper bound for the fluid pressure necessary for dilating existing (ac) planes in the σ_h direction (Fig. 19a). The ~35 MPa/km depth increase of the σ_1 (Calderoni et al., 2009) suggests that supralithostatic values ($\lambda_v \approx 1.4$) are instead needed to intrude fold-parallel (bc) fractures opening in the σ_H direction. Relatively low overpressures are likely to be necessary if the bc fractures are related to shallow outer-arc faults due to the establishment of an extensional state above the neutral surface (Fig. 19b). The along-depth zonation of stresses in anticlines may thus represent a condition favourable for surface fluid discharge. On one hand, outer-arc faults may intercept shallow fluid reservoirs; on the other hand, the establishment of a strike-slip stress state may allow the formation of new σ_H-parallel vertical hydrofractures, or the exploitation of existing fabrics (Fig. 19a, b).

Besides tangential longitudinal strain folding, other mechanisms have been hypothesised to explain along-depth stress changes in active anticlines of the study area, such as differential sediment compaction and mechanical decoupling along faults (Carminati and Vadacca, 2010). Under certain conditions, seepage forces generated by pressure gradients due to fluid flow through a porous medium may also supposedly play a role in the process. In general, seepage forces (F_s) can be viewed as the drag applied by the fluid flow to the particles (Mourgues and Cobbold, 2003). F_s act in the flow direction and, according to Darcy's Law, may generate lateral variations in fluid overpressure gradients that may modify the effective stresses (Mourgues and Cobbold, 2003; Rozhko et al., 2007). In the event of vertical overpressure gradients, seepage forces may act in opposition to gravity and generate apparent weight loss in a rock column (Mourgues and Cobbold, 2003). Longitudinal or transverse sub-horizontal F_s components may potentially arise in sedimentary basins as a consequence of elevated lateral overpressure gradients. The sub-horizontal F_s components may affect the σ/P_f coupling and theoretically modify the values and orientations of effective stresses (e.g., Mourgues et al., 2011. If the main F_s component acts in the direction of the σ_h, it may locally decrease the σ_h and produce local conditions with $\sigma_h < \sigma_V$ that may eventually favour the creation of vertical, σ_H-parallel, hydrofractures (Fig. 21b). Seepage forces, if suitably oriented and sufficiently large, could also supposedly produce a local flip between σ_H and σ_h, and generate planar hydrofractures perpendicular to the regional σ_H. On this basis, elevated lateral overpressure gradient variations would serve as nucleation sites where steep feeder fluid dykes may initiate owing to transient stress inversions. Stress permutations have also been reported for volcanic areas undergoing extension. In particular, intrusion of dykes along a vertical trend can cause an increase of the least principal stress and ultimately a flip of principal stresses (Parsons and Thompson, 1991). This process could also operate in mud volcano systems, where the inflation of mud dykes exploiting the weak tensile strength of pre-existing fabrics would produce stress magnitude variations. The latter may eventually promote the permutation of the principal stress axes and the formation of variably oriented faults and fractures.

Fig. 21. (a) Mohr diagram showing the role of fluid overpressures on the development of vertical tensile fractures in a sedimentary basin with vertical principal maximum stress (and uniaxial conditions). Vertical hydrofractures may initiate in case of high fluid overpressure distributed at basin scale (λ_{basin}) coupled with a focused overpressured zone (λ_{loc}) that may affect the pressure/stress coupling (after Mourgues et al., 2011). (b) Hypothetical conditions favouring the development of (σ_H-parallel) vertical hydrofeatures in thrust fault regimes. The σ/P_f coupling largely favours shear failure and inhibits the development of hydraulic fractures. Vertical hydrofractures may however form whether localised seepage forces develop and decrease the σ_h to values lower than the vertical stress.

6.2.2. Active tectonic stress and structural controls on mud volcano eruptions

Magmatic and mud eruptions are modulated by factors internal and external to the volcano. Eruptive phases of magmatic volcanoes typically occur when internal overpressure exceeds the critical value at which the tensile deviatoric stresses are sufficient to allow a dyke to form and magma to propagate up to the surface (Manga and Brodsky, 2006). Probabilistic reasons suggest that only a little fraction of eruptions will be triggered off by external events such as distant earthquakes (Manga and Brodsky, 2006). Yet, some brittle elements accompanying mud eruptions may form in response to stresses external to the volcano system.

The 1835 explosive eruption of the Montegibbio mud volcano was accompanied by the development of ~NNE-trending fissures approximately parallel to the regional S_H (see Fig. 10a, b and Section 4.3.2). No regional earthquakes occurred in the days or weeks prior to the eruption, suggesting that the eruption was mainly primed by internal fluid overpressures exceeding a critical level. Nevertheless, the supposed parallelism of fractures with the regional active stress suggests some tectonic control on the development of these structures.

A similar case may be inferred for the 11th August 2008 eruption of the Santa Barbara mud volcano at Caltanissetta in Sicily, Italy (Fig. 22a). This eruption was not preceded by significant earthquakes, and consisted of the violent eruption of mud that was spewed several metres (ca. 30–40 m) up into the air. The area around the main vent had developed numerous fractures and cracks leaking methane and displacing the ground coevally with the paroxysmal event (INGV, 2008a; Regione Siciliana, 2008; Madonia et al., 2011;

Fig. 22b). Some fractures showed directions radial to the mud volcano, while the major fractures (up to 1 km long) developed at some distance from the main venting area and trended ~NW to NNW. Methane emission defined flux peaks that occurred along a narrow NNW–SSE-oriented zone (INGV, 2008b) striking sub-parallel to the major fractures (Fig. 22b). Both the high gas flux zone and the fractures are remarkably parallel to the sub-horizontal NNW–SSE-trending σ_1 axis derived from stress inversion of earthquake focal solutions of the region around Caltanissetta (Sgroi et al., 2012), which is also parallel to the regional S_H associated with the Africa–Eurasia Plate convergence (e.g., Catalano et al., 2008). On the basis of this striking parallelism, the preferred interpretation is that this paroxysmal event was controlled by fractures (or dykes) forming in a direction roughly parallel to the regional compression direction.

The Lokbatan mud volcano in Azerbaijan experienced several eruptions (Kadirov et al., 2005; Fig. 22c). These were often characterised by the violent release of methane and its ignition occasionally produced

Fig. 22. Structural controls on mud volcano eruptions. (a) Eruption of the mud volcano near Caltanisetta (Maccalube Terrapelata; N37°2948″ E14°0526″) in Sicily, Italy, on 11th August 2008. (b) Geomorphic/structural features observed shortly after the paroxysmal event and methane flux measurements. (c) Skyline of the Lokbatan mud volcano (N40°18′17″ E49°42′32″) in Azerbaijan during dormant period (25th May 2010), approximately three months after the last eruption. (d) Explosive eruption of the Lokbatan volcano on 25th October 2001; photo by Phil Hardy — from BBC NEWS 29th October 2001, Clare Doyle in Baku. (e) The Lokbatan volcano is situated over an anticline (black line), and is affected by normal faults and fissures (red lines) forming a crestal graben sub-parallel the anticline axis.
Photo in panel a is from Regione Siciliana (2008). Panel b after Regione Siciliana (2008) and INGV (2008a b). Panel e is satellite image extracted from Google Earth®; http://earth.google.it/download-earth.html)

sky-scraping flares, such as for the impressive 2001 eruption whose initial flame was around 100 m in diameter and approximately 400 m high (Mukhtarov et al., 2003; Fig. 22d). The mud volcano edifice is affected by a graben collapse structure striking sub-parallel to the anticline axis over which the volcano is situated (Planke et al., 2003; Roberts et al., 2011a; Fig. 22e). Displacement of graben faults and collapse of the western volcano flank occurred during the 2001eruption, a setting referred to as 'mud volcano sector collapses' by Roberts et al. (2011a). This setting may also suggest that outer-arc extension has accomplished this process, and that the graben axis indicates a shallow S_H trending at a high angle to the regional S_H (Fig. 22e). The outer-arc faults would thus represent shallow structural controls on the eruption of the deep-sourced gas.

In conclusion, although the paroxysmal events outlined above were essentially dictated by internal dynamics, the present-day stresses (regional or local) are expected to have exerted some control on the development of the brittle elements through which the subsurface pressurised material was transported upward during the eruptions.

7. Concluding remarks

Understanding the development of structural channelways and the mechanisms through which subsurface fluids and 'greenhouse' gases (i.e., methane) are released in the atmosphere involves implications that may be of paramount importance for the environmental equilibrium on Earth. In the same way, determining whether magmatic and mud volcanoes share some dynamic similarities is of importance beyond satisfying the 'frivolous' search for connections between such different, yet analogous geological phenomena. Thereof, the structural controls on subsurface fluid expulsion in fold-and-thrust belts and the potential use of mud volcanoes as stress indicators have represented the two main targets of this study. These aspects have been investigated at the Pede-Apennine margin of the Northern Apennines, and in worldwide areas of mud volcanism, such as the Azerbaijan Greater Caucasus and other fold-and-thrust belts. The analysis of geological–geophysical data suggests that the discharge of subsurface fluids typically focuses at various typologies of steep brittle structures often associated with anticlines. Vertical zonation of stresses in the cores of folds may represent a pivotal control on the development of feeder fracture sets and ultimately mud emplacement. Stress indicators from mud volcanoes yield promising results, generally showing consistent orientation with respect to the stress field in the upper crust known from classic methods (i.e., earthquake focal mechanism solutions and well bore breakouts). It is therefore proposed that mud volcanoes may provide an independent means and an additional tool for assessing stress directions in the shallow crust, and these data can be profitably employed (1) where other data is unavailable, (2) for inaccessible settings (i.e., underwater or the surface of planets), or (3) simply as supplementary datum to implement existing stress datasets.

Acknowledgements

Appendix A. Supplementary data

Supplementary data to this article can be found online at http://dx.doi.org/10.1016/j.earscirev.2012.09.002.

References

Abrams, M.A., Narimanov, A.A., 1997. Geochemical evaluation of hydrocarbons and their potential sources in the western South Caspian depression, Republic of Azerbaijan. Marine and Petroleum Geology 14, 451–468.

Acocella, V., 2007. Understanding caldera structure and development: an overview of analogue models compared to natural calderas. Earth-Science Reviews 85, 125–160.

Acocella, V., Funiciello, F., 2010. Kinematic setting and structural control of arc volcanism. Earth and Planetary Science Letters 289, 43–53.

Acocella, V., Neri, M., 2009. Dike propagation in volcanic edifices: overview and possible developments. Tectonophysics 471, 67–77.

Acocella, V., Yoshida, T., Yamada, R., Funiciello, F., 2008. Structural control on late Miocene to Quaternary volcanism in the NE Honshu arc, Japan. Tectonics 27, TC5008 http://dx.doi.org/10.1029/2008TC002296.

Adiyaman, O., Chorowicz, J., Kose, O., 1998. Relationships between volcanic patterns and neotectonics in Eastern Anatolia from analysis of satellite images and DEM. Journal of Volcanology and Geothermal Research 85, 17–32.

Aliyev, A.A., Guliyev, I.S., Belov, S., 2002. Catalogue of Recorded Eruptions of Mud Volcanoes of Azerbaijan for Period of Years 1810–2001. Baku Institute of Geology of the Azerbaijan National Academy of Sciences, Nafta Press, Baku, Azerbaijan . 88 pp.

Alizadeh, A.A. (Ed.), 2008. Geological Map of Azerbaijan Republic, Scale 1:500,000, with Explanatory Notes. Baki Kartoqrafiya Fabriki.

Allen, M.B., Vincent, S.J., Alsop, G.I., Ismail-zadehc, A., Flecker, R., 2003. Late Cenozoic deformation in the South Caspian region: effects of a rigid basement block within a collision zone. Tectonophysics 366, 223–239.

Allen, M., Jackson, J., Walker, R., 2004. Late Cenozoic reorganization of the Arabia–Eurasia collision and the comparison of short-term and long-term deformation rates. Tectonics 23, TC2008.

Anderson, E.M., 1936. The dynamics of the formation of cone-sheets, ring-dykes, and caldron-subsidences. Proceedings Royal Society of Edinburgh 56, 128–157.

Anderson, E.M., 1951. The Dynamics of Faulting and Dyke Formation with Applications to Britain, 2nd ed. Oliver and Boyd, White Plains, N.Y . 206 pp.

Angelier, J., Mechler, P., 1977. Sur une méthode graphique de recherché des contraintes principales également utilisable en tectonique et en séismologie: la méthode des dièdres droits. Bulletin de la Société Géologique de France 19, 1309–1318.

Barbieri, G., 1947. Nuove osservazioni sulle salse emiliane. Rivista Geografica Italiana 54, 172–185.

Basili, R., Valensise, G., Vannoli, P., Burrato, P., Fracassi, U., Mariano, S., Tiberti, M.M., Boschi, E., 2008. The Database of Individual Seismogenic Sources (DISS), version 3: summarizing 20 years of research on Italy's earthquake geology. Tectonophysics 453, 20–43.

Benedetti, L.C., Tapponnier, P., Gaudemer, Y., Manighetti, I., Van der Woerd, J., 2003. Geomorphic evidence for an emergent active thrust along the edge of the Po Plain: the Broni–Stradella fault. Journal of Geophysical Research 108, 2238 http://dx.doi.org/10.1029/2001JB001546.

Bertello, F., Fantoni, R., Franciosi, F., 2008. Exploration Country Focus: Italy. Search and Discovery Article #10165, Posted 16 October 2008. available at: http://www.searchanddiscovery.net/documents/2008/08158bertello/index.htm.

Bianconi, G., 1840. Storia naturale dei terreni ardenti, dei vulcani fangosi, delle sorgenti infiammabili, dei pozzi idropinici e di altri fenomeni geologici operati dal gas idrogene. Tipografia Iacopo Marsigli, Bologna . 215 pp.

Biasutti, R., 1907. Materiali per lo studio delle salse — Le salse dell'Appennino Settentrionale. Memoirs Geography 2, 101–255 (published as supplement to the Rivista Geografica Italiana by Giotto Dainelli).

Boccaletti, M., Coli, M., Eva, C., Ferrari, G., Giglia, G., Lazzarotto, A., Merlanti, F., Nicolich, R., Papani, G., Postpischl, D., 1985. Considerations on the seismotectonics of the northern Apennines. Tectonophysics 117, 7–38.

Boccaletti, M., Bonini, M., Corti, G., Gasperini, P.,Martelli, L., Piccardi, L., Tanini, C., Vannucci, G., 2004. Seismotectonic Map of the Emilia–Romagna Region, Scale 1:250,000, with Explanatory Notes, S.EL.CA, Società Elaborazioni Cartografiche, Florence, Italy.

Boncio, P., Bracone, V., 2009. Active stress from earthquake focal mechanisms along the Padan–Adriatic side of the Northern Apennines (Italy), with considerations on stress magnitudes and pore-fluid pressures. Tectonophysics 476, 180–194.

Bonini, M., 2007. Interrelations of mud volcanism, fluid venting, and thrust-anticline folding: examples from the external northern Apennines (Emilia–Romagna, Italy). Journal of Geophysical Research 112, B08413 http://dx.doi.org/10.1029/2006JB004859.

Bonini, M., 2008. Elliptical mud volcano caldera as stress indicator in an active compressional setting (Nirano, Pede-Apennine margin, northern Italy). Geology 36, 131–134 doi:10.1130/G24158A.1.

Bonini, M., 2009. Mud volcano eruptions and earthquakes in the Northern Apennines and Sicily, Italy. Tectonophysics 474, 723–735.

Bonini, M., Mazzarini, F., 2010. Mud volcanoes as potential indicators of regional stress and pressurized layer depth. Tectonophysics 494, 32–47.

Bosworth, W., Strecker, M., Burke, K., 2000. Magma chamber elongation as an indicator of intraplate stress field orientation: "borehole breakout mechanism" and examples from the Late Pleistocene to Recent Kenya Rift Valley. In: Jessell, M.W., Urai, J.L. (Eds.), Stress, Strain and Structure, A Volume in Honor of W. D. Means. J. Virtual Explorer 2. available at http://www.virtualexplorer.com.au/VEjournal/Volume2.

Bosworth, W., Burke, K., Strecker, M., 2003. Effect of stress fields on magma chamber stability and the formation of collapse calderas. Tectonics 22, 1042 http://dx.doi.org/10.1029/2002TC001369.

Breed, W.J., 1964. Morphology and lineation of cinder cones in the San Franciscan volcanic field. Museum of Northern Arizona Bulletin 40, 65–71.

Brown, K.M., 1990. The nature and hydrological significance of mud diapirism and diatremes for accretionary systems. Journal of Geophysical Research 95, 8969–8982.

Brown, K., Westbrook, G.K., 1988. Mud diapirism and subcretion in the Barbados Ridge accretionary complex: the role of fluids in accretionary processes. Tectonics 7, 613–640.

Bulgakov, R.F., Ivashchenko, A.I., Kim Chun Un, A.I., Sergeev, K.F., Streltsov, M.I., Kozhurin, A.I., Besstrashnov, V.M., Strom, A.L., Suzuki, Y., Tsutsumi, H., Watanabe, M., Ueki, T., Shimamoto, T., Okumura, K., Goto, H., Kariya, Y., 2002. Active faults in northeastern Sakhalin. Geotectonics 36 (3), 227–240.

Calderoni, G., Di Giovambattista, R., Burrato, P., Ventura, G., 2009. A seismic sequence from Northern Apennines (Italy) provides new insight on the role of fluids in the active tectonics of accretionary wedges. Earth and Planetary Science Letters 281, 99–109.

Carminati, E., Vadacca, L., 2010. Two- and three-dimensional numerical simulations of the stress field at the thrust front of the Northern Apennines, Italy. Journal of Geophysical Research 115, B12425 http://dx.doi.org/10.1029/2010JB007870.

Carminati, E., Scrocca, D., Doglioni, C., 2010. Compaction-induced stress variations with depth in an active anticline: Northern Apennines, Italy. Journal of Geophysical Research 115, B02401 http://dx.doi.org/10.1029/2009JB006395.

Casey, M., Ebinger, C., Keir, D., Gloaguen, R., Mohamed, F., 2006. Strain accommodation in transitional rifts: extension by magma intrusion and faulting in Ethiopian rift magmatic segments. In: Yirgu, G., Ebinger, C.J., Maguire, P.K.H. (Eds.), The Afar Volcanic Province Within the East African Rift System: Geological Society, London, Special Publications, 259, pp. 143–163.

Castaldini, D., Valdati, J., Ilies, D.C., Chiriac, C., with contributions by Bertogna, I., 2005. Geo-Tourist map of the natural Reserve of Salse di Nirano (Modena Apennines, Northern Italy). Il Quaternario 18, 245–255.

Castellarin, A., Eva, C., Giglia, G., Vai, G.B., 1985. Analisi strutturale del Fronte Appenninico Padano. Giornale di Geologia 47, 47–75.

Castello, B., Selvaggi, G., Chiarabba, C., Amato, A., 2006. CSI Catalogo della sismicità italiana 1981–2002, versione 1.1. INGV-CNT, Roma . http://www.ingv.it/CSI/.

Catalano, S., De Guidi, G., Romagnoli, G., Torrisi, S., Tortorici, G., Tortorici, L., 2008. The migration of plate boundaries in SE Sicily: influence on the large-scale kinematic model of the African promontory in southern Italy. Tectonophysics 449, 41–62.

Chigira, M., Tanaka, K., 1997. Structural features and the history of mud volcanoes in southern Hokkaido, northern Japan. Journal of Geological Society of Japan 103, 781–791.

Cobbold, P.R., Rodrigues, N., 2007. Seepage forces, important factors in the formation of horizontal hydraulic fractures and bedding-parallel fibrous veins ('beef' and 'cone-in-cone'). Geofluids 7, 313–322.

Cole, J.W., Milner, D.M., Spinks, K.D., 2005. Calderas and caldera structures: a review. Earth-Science Reviews 69, 1–26.

Cooper, M., 1992. The analysis of fracture systems in subsurface thrust structures from the foothills of the Canadian Rockies. In: McClay, K.R. (Ed.), Thrust Tectonics. Chapman and Hall, London, pp. 391–405.

Cooper, C., 2001. Mud volcanoes of Azerbaijan visualized using 3D seismic depth cubes: the importance of overpressured fluid and gas instead of non-existent diapirs (abs.). Proceedings of the European Association of Geoscientists and Engineers, Conference on 'Subsurface Sediment Mobilisation', Gent, Belgium, September 2001, p. 71.

D'Agostino, N., Avallone, A., Cheloni, D., D'Anastasio, E., Mantenuto, S., Selvaggi, G., 2008. Active tectonics of the Adriatic region from GPS and earthquake slip vectors. Journal of Geophysical Research 113, B12413 http://dx.doi.org/10.1029/2008JB005860.

Davies, R.J., Stewart, S.A., 2005. Emplacement of giant mud volcanoes in the South Caspian Basin: 3D seismic reflection imaging of their root zones. Journal of the Geological Society of London 162, 1–4.

Davies, R.J., Swarbrick, R.E., Evans, R.J., Huuse, M., 2007. Birth of a mud volcano: East Java, 29 May 2006. Geological Society of America Today 17, 4–9.

Davies, R.J., Brumm, M., Manga, M., Rubiandini, R., Swarbrick, R., Tingay, M., 2008. The East Java mud volcano (2006 to present): an earthquake or drilling trigger? Earth and Planetary Science Letters 272, 627–638 http://dx.doi.org/10.1016/j.epsl.2008.05.029.

Dé Brignoli di Brunnhoff, G., 1836. Relazione accademica dell'ultima eruzione accaduta nel vulcanetto aereo così detta Salsa di Sassuolo nel modenese e considerazioni geognostiche intorno alle salse e alle loro cause. Tipografia Torreggiani & Compagno, Reggio . 64 pp.

Delaney, T., Pollard, D.D., Ziony, J.I., McKee, E.H., 1986. Field relations between dikes and joints: emplacement processes and paleostress analysis. Journal of Geophysical Research 91, 4920–4938.

Deville, E., Guerlais, S.-H., Callec, Y., Griboulard, R., Huyghe, P., Lallemant, S., Mascle, A., Noble, M., Schmitz, J., Caramba working group, 2006. Liquefied vs stratified sediment mobilization processes: insight from the South of the Barbados accretionary prism. Tectonophysics 428, 33–47.

Deville, E., Guerlais, S.-H., Lallemant, S., Schneider, F., 2010. Fluid dynamics and subsurface sediment mobilization processes: an overview from Southeast Caribbean. Basin Research 22, 361–379.

Devlin, W., Cogswell, J., Gaskins, G., Isaksen, G., Pitcher, D., Puls, D., Stanley, K., Wall, G., 1999. South Caspian Basin: young, cool, and full of promise. Geological Society of America Today 9 (7), 1–9.

Dimitrov, L.I., 2002. Mud volcanoes—the most important pathway for degassing deeply buried sediments. Earth-Science Reviews 59, 49–76.

DISS Working Group, 2010. Database of Individual Seismogenic Sources (DISS), Version 3.1.1: A Compilation of Potential Sources for Earthquakes Larger than M 5.5 in Italy and Surrounding Areas. http://diss.rm.ingv.it/diss/ © INGV 2010 – Istituto Nazionale di Geofisica e Vulcanologia – All rights reserved.

Duerto, L., McClay, K., 2002. 3D geometry and evolution of shale diapirs in the Eastern Venezuelan Basin. AAPG Search and Discovery article #10026, at: http://www.searchanddiscovery.net/documents/duerto/index.htm.

Engelder, T., Gross, M.R., Pinkerton, P., 1997. Joint development in clastic rocks of the Elk Basin anticline, Montana–Wyoming. In: Hoak, T., Klawitter, A., Blomquist, P. (Eds.), Fractured Reservoirs: Characterization and Modeling. Rocky Mountain Association of Geologists, Guidebook, Denver, Colorado, pp. 1–18.

Evans, R.J., Davies, R.J., Stewart, S.A., 2006. Internal structure and eruptive history of a kilometre-scale mud volcano system, South Caspian Sea. Basin Research 19, 153–163.

Evans, R.J., Stewart, S.A., Davies, R.J., 2008. The structure and formation of mud volcano summit calderas. Journal of the Geological Society of London 165, 769–780.

Ferrari, C., Vianello, G., 1985. Guida escursionistica. Le Salse dell'Emilia–Romagna. Regione Emilia–Romagna. Grafiche Zanini, Bologna, pp. 85–127.

Feyzullayev, A.A., Lerche, I., 2009. Occurrence and nature of overpressure in the sedimentary section of the South Caspian Basin, Azerbaijan. Energy Exploration & Exploitation 27 (5), 345–366.

Fischer, M.P., Wilkerson, M.S., 2000. Predicting the orientation of joints from fold shape: results of pseudo-three-dimensional modeling and curvature analysis. Geology 28, 15–18.

Fowler, S.R., Mildenhall, J., Zalova, S., Riley, G., Elsley, G., Desplanques, A., Guliyev, F., 2000. Mud volcanoes and structural development on Shah Deniz. Journal of Petroleum Science and Engineering 28, 189–206.

Fryer, P., Wheat, C.G., Mottl, M.J., 1999. Mariana Blueschist mud volcanism: implications for conditions within the subduction zone. Geology 27, 103–106.

Gasperi, G., Cremaschi, M., Mantovani Uguzzoni, M.P., Cardarelli, A., Cattani, M., Labate, D., 1987. Evoluzione plio-quaternaria del margine appenninico modenese e dell'antistante pianura. Note illustrative alla Carta Geologica (with geological map by Gasperi, G, scale 1:25,000). Memorie Società Geologica Italiana 39, 375–431.

Ghiselli, F., Martelli, L., 1997. Evoluzione dei campi di stress lungo il margine appenninico-padano dal Pleistocene medio all'Attuale: analisi strutturale dei depositi pleistocenici affioranti tra Castell'Arquato (Piacenza) e Rimini. Il Quaternario 10, 439–444.

Grando, G., McClay, K., 2007. Morphotectonics domains and structural styles in the Makran accretionary prism, offshore Iran. Sedimentary Geology 196, 157–179.

Graue, K., 2000. Mud volcanoes in deepwater Nigeria. Marine and Petroleum Geology 17, 959–974.

Gudmundsson, A., 1995. Infrastructure and mechanics of volcanic systems in Iceland. Journal of Volcanology and Geothermal Research 64, 1–22.

Gudmundsson, A., 2005. The effects of layering and local stresses in composite volcanoes on dyke emplacement and volcanic hazards. Comptes Rendus Geosciences 337, 1216–1222.

Gudmundsson, A., 2006. How local stresses control magma-chamber ruptures, dyke injections, and eruptions in composite volcanoes. Earth-Science Reviews 79, 1–31.

Guliyev, I.S., Feizullayev, A.A., 1997. All About Mud Volcanoes. Baku Institute of Geology of the Azerbaijan National Academy of Sciences, Nafta Press, Baku, Azerbaijan . 52 pp.

Hancock, P.L., 1985. Brittle microtectonics: principles and practice. Journal of Structural Geology 7, 437–457.

Heidbach, O., Tingay, M., Barth, A., Reinecker, J., Kurfeß, D., Müller, B., 2008. The World Stress Map Database Release 2008. available online at www.world-stress-map.org doi:10.1594/GFZ.WSM.Rel2008, 2008.

Heidbach, O., Tingay, M., Barth, A., Reinecker, J., Kurfeß, D., Müller, B., 2010. Global crustal stress pattern based on the World Stress Map database release 2008. Tectonophysics 482, 3–15.

Henry, P., Le Pichon, X.L., Lallemant, S., Foucher, J.-P., Westbrook, G., Hobart, M., 1990. Mud volcano field seaward of the Barbados Accretionary Complex: a deep-towed side scan sonar survey. Journal of Geophysical Research 95, 8917–8929.

Higgins, G.E., Saunders, J.B., 1974. Mud volcanoes — their nature and origin. In: Jung, P., Bolli, H.M., Panchaud, R., Saunders, J.B., Schaefer, H., Wiedenmayer, F. (Eds.), Contributions to the Geology and Paleobiology of the Caribbean and Adjacent Areas: Verhandlungen der Naturforschenden Gesellschaft von Basel, 84, pp. 101–152 (1).

Hillis, R.R., 2003. Pore pressure/stress coupling and its implications for rock failure. In: Van Rensbergen, P., Hillis, R.R., Maltman, A.J., Morley, C.K. (Eds.), Subsurface Sediment Mobilization: Geological Society, London, Special Publications, 216, pp. 359–368.

Holohan, E.P., Troll, V.R., Walter, T.R., Munn, S., McDonell, S., Shipton, Z.K., 2005. Elliptical calderas in active tectonic settings: an experimental approach. Journal of Volcanology and Geothermal Research 114, 119–136.

Hovland, M., Hill, A., Stokes, D., 1997. The structure and geomorphology of the Dashgil mud volcano, Azerbaijan. Geomorphology 21, 1–15.

Hubbert, M.K., Rubey, W.W., 1959. Role of fluid pressure in mechanics of overthrust faulting. Geological Society of America Bulletin 70, 115–166.

Huuse, M., Jackson, C.A.-L., Van Rensbergen, P., Davies, R.J., Flemings, P.B., Dixon, R.J., 2010. Subsurface sediment remobilization and fluid flow in sedimentary basins: an overview. Basin Research 22, 342–360.

Inan, S., Yalcin, M.N., Guliev, I.S., Kuliev, K., Feizullayev, A.A., 1997. Deep petroleum occurrences in the lower Kura depression, south Caspian Basin, Azerbaijan: an organic geochemical and basin modelling study. Marine and Petroleum Geology 14, 731–762.

INGV, 2008a. Comunicato sull'eruzione di fango in C.da Terrapelata-Santa Barbara (Cl) 11 Agosto 2008 — Aggiornamento del 16 Agosto. Istituto Nazionale di Geofisica e Vulcanologia, Sezione di Palermo . (available at http://www.pa.ingv.it/).

INGV, 2008b. Comunicato sull'eruzione di fango in C.da Terrapelata-Santa Barbara (Cl) — Aggiornamento del 22 Agosto. Istituto Nazionale di Geofisica e Vulcanologia, Sezione di Palermo . (availble at http://www.pa.ingv.it/).

INGV TDMT, 2012. Time Domain Moment Tensors. available at http://cnt.rm.ingv.it/tdmt.html.

Jaeger, J.C., Cook, N.G.W., 1969. Fundamentals of Rock Mechanics. Barnes and Nobles, New York . 513 pp.

Jakubov, A.A., Ali-Zade, A.A., Zeinalov, M.M., 1971. Mud Volcanoes of the Azerbaijan SSR. Atlas (in Russian), Azerbaijan Academy of Sciences, Baku.

Jones, R.W., Simmons, M.D., 1997. A review of the stratigraphy of eastern Paratethys (Oligocene–Holocene), with particular emphasis on the Black Sea. In: Robinson, A. (Ed.), Regional and Petroleum Geology of the Black Sea and Surrounding Regions: AAPG Memoir, 68, pp. 39–52.

Kadirov, F.A., Lerche, I., Guliyev, I.S., Kadyrov, A.G., Feyzullayev, A.A., Mukhtarov, A.Sh., 2005. Deep structure model and dynamics of mud volcanoes, southwest Absheron Peninsula (Azerbaijan). Energy Exploration & Exploitation 23, 307–332.

Kholodov, V.N., 2002a. Mud volcanoes, their distribution regularities and genesis: communication 1. Mud volcanic provinces and morphology of mud volcanoes. Lithology and Mineral Resources 37, 197–209.

Kholodov, V.N., 2002b. Mud volcanoes: distribution regularities and genesis (Communication 2. Geological–geochemical peculiarities and formation model). Lithology and Mineral Resources 37, 293–309.

Kopf, A.J., 2002. Significance of mud volcanism. Reviews of Geophysics 40 (2), 1005.

Kopf, A.J., 2003. Global methane emission through mud volcanoes and its past and present impact on the Earth's climate. International Journal of Earth Sciences (Geol Rundsch) 92, 806–816.

Kopf, A.J., 2008. Making calderas from mud. Nature Geoscience 1, 500–501.

Kopf, A., Behrmann, J.H., 2000. Extrusion dynamics of mud volcanoes on the Mediterranean Ridge accretionary complex. In: Vendeville, B., Mart, Y., Vigneresse, J.-L. (Eds.), Salt, Shale and Igneous Diapirs in and Around Europe: Geological Society, London, Special Publications, 174, pp. 169–204.

Kopf, A., Klaeschen, D., Mascle, J., 2001. Extreme efficiency of mud volcanism in dewatering accretionary prisms. Earth and Planetary Science Letters 189, 295–313.

Kopf, A., Deyhle, A., Lavrushin, V.Y., Polyak, B.G., Gieskes, J.M., Buachidze, G.I., Wallmann, K., Eisenhauer, A., 2003. Isotopic evidence (He, B, C) for deep fluid and mud mobilization from mud volcanoes in the Caucasus continental collision zone. International Journal of Earth Sciences (Geol Rundsch) 92, 407–425 http://dx.doi.org/10.1007/s00531-003-0326-y.

Korme, T., Chorowicz, B., Collet, B., Bonavia, F.F., 1997. Volcanic vents rooted on extension fractures and their geodynamic implications in the Ethiopian Rift. Journal of Volcanology and Geothermal Research 79, 205–222.

Kozhurin, A.I., 2004. Active faulting at the Eurasian, North American and Pacific plates junction. Tectonophysics 380, 273–285.

Kvenvolden, K.A., Rogers, B.W., 2005. Gaia's breath — global methane exhalations. Marine and Petroleum Geology 22, 579–590.

Lindquist, S.J., 1999. Petroleum systems of the Po Basin Province of Northern Italy and the Northern Adriatic Sea: Porto Garibaldi (Biogenic), Meride/Riva di Solto (Thermal), and Marnoso Arenacea (Thermal). USGS Open-File Report 99-50-M.

Lipman, P.W., 1997. Subsidence of ash-flow calderas: relation to caldera size and magma-chamber geometry. Bulletin of Volcanology 59, 198–218.

Lutz, T.M., 1986. An analysis of the orientation of large scale crustal structures: a statistical approach based on areal distribution of pointlike features. Journal of Geophysical Research 91, 421–434.

Madonia, P., Grassa, F., Cangemi, M., Musumeci, C., 2011. Geomorphological and geochemical characterization of the 11 August 2008 mud volcano eruption at S. Barbara village (Sicily, Italy) and its possible relationship with seismic activity. Natural Hazards and Earth System Sciences 11, 1545–1557.

Mandl, G., Harkness, R.M., 1987. Hydrocarbon migration by hydraulic fracturing. In: Jones, M.E., Preston, R.M.F. (Eds.), Deformation of Sediments and Sedimentary Rocks: Geological Society, London, Special Publications, 29, pp. 39–53.

Manga, M., Brodsky, E.E., 2006. Seismic triggering of eruptions in the far field: volcanoes and geysers. Annual Review of Earth and Planetary Sciences 34, 263–291.

Manga, M., Brumm, M., Rudolph, M.L., 2009. Earthquake triggering of mud volcanoes. Marine and Petroleum Geology 26, 1785–1798.

Mariucci, M.T., Müller, B., 2003. The tectonic regime in Italy inferred from borehole breakout data. Tectonophysics 361, 21–35.

Mazzini, A. (Ed.), 2009. Mud volcanism: Processes and Implications: Marine and Petroleum Geology, pp. 1677–1896. 26, pp.

Mazzini, A., Svensen, H., Planke, S., Guliyev, I., Akhmanov, G.G., Fallik, T., Banks, D., 2009. When mud volcanoes sleep: insight from seep geochemistry at the Dashgil mud volcano, Azerbaijan. Marine and Petroleum Geology 26, 1704–1715.

MedNet INGV, 2009. Earthquake Catalogue. available at http://mednet.rm.ingv.it/quick_rcmt.php.

Mel'nikov, O.A., Ershov, V.V., Ung, Kim Choon, Se, Sen Rak, 2008. Dynamics of the gryphon activity of gas–water lithoclastic (mud) volcanoes and their relation to the natural seismicity as exemplified by Yuzhno-Sakhalinsk Volcano (Sakhalin Island). Russian Journal of Pacific Geology 2, 397–411.

Milkov, A.V., 2000. Worldwide distribution of submarine mud volcanoes and associated gas hydrates. Marine Geology 167, 29–42.

Milkov, A.V., 2004. Global estimates of hydrate-bound gas in marine sediments: how much is really out there? Earth-Science Reviews 66, 83–197.

Montone, P., Mariucci, M.T., 1999. Active stress along the NE external margin of the Apennines: the Ferrara arc, northern Italy. Journal of Geodynamics 17, 140–154.

Montone, P., Mariucci, M.T., Pondrelli, S., Amato, A., 2004. An improved stress map for Italy and surrounding regions (central Mediterranean). Journal of Geophysical Research 109, B10410 http://dx.doi.org/10.1029/2003JB002703.

Morley, C.K., 2003a. Mobile shale related deformation in large deltas developed on passive and active margins. In: Van Rensbergen, P., Hillis, R.R., Maltman, A.J., Morley, C.K. (Eds.), Subsurface Sediment Mobilization: Geological Society, London, Special Publications, 216, pp. 335–357.

Morley, C.K., 2003b. Outcrop examples of mudstone intrusions from the Jerudong anticline, Brunei Darussalam and inferences for hydrocarbon reservoirs. In: Van Rensbergen, P., Hillis, R.R., Maltman, A.J., Morley, C.K. (Eds.), Subsurface Sediment Mobilization: Geological Society, London, Special Publications, 216, pp. 381–394.

Morley, C.K., 2007. Development of crestal normal faults associated with deepwater fold growth. Journal of Structural Geology 29, 1148–1163.

Morley, C.K., Guerin, G., 1996. Comparison of gravity-driven deformation styles and behaviour associated with mobile shales and salt. Tectonics 15, 1154–1170.

Morley, C.K., Crevello, P., Ahmad, Z.H., 1998. Shale tectonics and deformation associated with active diapirism: the Jerudong Anticline, Brunei Darussalam. Journal of the Geological Society of London 155, 475–490.

Mourgues, R., Cobbold, P.R., 2003. Some tectonic consequences of fluid overpressures and seepage forces as demonstrated by sandbox modelling. Tectonophysics 376, 75–97.

Mourgues, R., Gressier, J.B., Bodet, L., Bureau, D., Gay, A., 2011. "Basin scale" versus "localized" pore pressure/stress coupling — implications for trap integrity evaluation. Marine and Petroleum Geology 28, 1111–1121.

Mucchi, A.M., 1968. Le salse del Modenese e del Reggiano. L'Universo 48, 421–436.

Mukhtarov, A.Sh., Kadirov, F.A., Guliyev, I.S., Feyzullayev, A.A., Lerche, I., 2003. Temperature evolution in the Lokbatan mud volcano crater (Azerbaijan) after the eruption of 25 October 2001. Energy Exploration & Exploitation 21, 187–207.

Nakamura, K., 1969. Arrangement of parasitic cones as a possible key to regional stress field. Bulletin of Volcanological Society of Japan 14, 8–20.

Nakamura, K., 1975. Volcano structure and possible mechanical correlation between volcanic eruptions and earthquakes. Bulletin of Volcanological Society of Japan 20, 229–240.

Nakamura, K., 1977. Volcanoes as possible indicators of tectonic stress orientation—principle and proposal. Journal of Volcanology and Geothermal Research 2, 1–16.

Nakamura, K., Jacob, K.H., Davies, J.N., 1977. Volcanoes as possible indicators of tectonic stress orientation—Aleutians and Alaska. Pure and Applied Geophysics 115, 87–112.

Odé, H., 1957. Mechanical analysis of the dike pattern of the Spanish Peaks area, Colorado. Geological Society of America Bulletin 68, 567–576.

Osborne, M.J., Swarbrick, R.E., 1997. Mechanisms for generating overpressure in sedimentary basins: a reevaluation. AAPG Bulletin 81, 1023–1041.

Paquet, F., Dauteuil, O., Hallot, E., Moreau, F., 2007. Tectonics and magma dynamics coupling in a dyke swarm of Iceland. Journal of Structural Geology 29, 1477–1493.

Parsons, T., Thompson, G.A., 1991. The role of magma overpressure in suppressing earthquakes and topography: worldwide examples. Science 253, 1399–1402.

Paulsen, T.S., Wilson, T.J., 2010. New criteria for systematic mapping and reliability assessment of monogenetic volcanic vent alignments and elongate volcanic vents for crustal stress analyses. Tectonophysics 482, 16–28.

Pieri, M., 1983. Three seismic profiles through the Po Plain. In: Bally, A.W. (Ed.), Seismic Expression of Structural Styles. : Studies in Geology Series #15, Vol. 3. The American Association of Petroleum Geologists, Tulsa, Oklahoma, USA. 3.4.1-8–3.4.1-26.

Pieri, M., 2001. Italian petroleum geology. In: Vai, G.B., Martini, I.P. (Eds.), Anatomy of an Orogen: The Apennines and Adjacent Mediterranean Basins. Kluwer Academic Publisher, pp. 533–550.

Pieri, M., Groppi, G., 1981. Subsurface Geological Structure of the Po Plain, Italy. Consiglio Nazionale delle Ricerche, Rome . Pubbl. 414.

Planke, S., Svensen, H., Hovland, M., Banks, D.A., Jamtveit, B., 2003. Mud and fluid migration in active mud volcanoes in Azerbaijan. Geo-Marine Letters 23, 258–268.

Pondrelli, S., Salimbeni, S., Ekström, G., Morelli, A., Gasperini, P., Vannucci, G., 2006. The Italian CMT dataset from 1977 to the present. Physics of the Earth and Planetary Interiors 159, 286–303.

Prior, D.B., Doyle, E.H., Kaluza, M.J., 1989. Evidence for sediment eruption on deep sea floor, Gulf of Mexico. Science 243, 517–519.

Ramsay, J.G., 1967. Folding and Fracturing of Rocks. McGraw Hill, New York, NY, USA.

Regione Emilia–Romagna, ENI — AGIP, 1998. Riserve idriche sotterranee della Regione Emilia–Romagna. S.EL.CA, Firenze, Italy, p. 119 pp.

Regione Emilia-Romagna, 2005. Carta geologica d'Italia, Sheet 219, Sassuolo, Scale 1:50,000, with Explanatory Notes. Soc. Elaborazioni Cartogr, Florence, Italy.

Regione Siciliana, 2008. Emergenza "Maccalube" dell'11 Agosto 2008 nel Comune di Caltanissetta. Descrizione dell'evento e dei danni. Regione Siciliana, Presidenza, Dipartimento della Protezione Civile, Servizio di Caltanissetta, Settembre 2008, p. 30. report avallae at: http://www.regione.sicilia.it/presidenza/protezionecivile/documenti/documenti.asp.

Ricci Lucchi, F., 1986. The Oligocene to Recent foreland basins of the Northern Apennines. In: Allen, P.A., Homewood, P. (Eds.), Foreland Basins: International Association of Sedimentologists Special Publication, 8, pp. 105–139.

Roberts, K.S., Davies, R.J., Stewart, S.A., 2010. Structure of exhumed mud volcano feeder complexes, Azerbaijan. Basin Research 22, 439–451.

Roberts, K.S., Stewart, S.A., Davies, R.J., Evans, R.J., 2011a. Sector collapse of mud volcanoes, Azerbaijan. Journal of the Geological Society 168, 49–60.

Roberts, K.S., Davies, R.J., Stewart, S.A., Tingay, M., 2011b. Structural controls on mud volcano vent distributions: examples from Azerbaijan and Lusi, east Java. Journal of the Geological Society 168, 1013–1030.

Rozhko, A.Y., Podladchikov, Y.Y., Renard, F., 2007. Failure patterns caused by localized rise in pore-fluid overpressure and effective strength of rocks. Geophysical Research Letters 34, L22304 http://dx.doi.org/10.1029/2007GL031696.

Secor, D.T., 1965. Role of fluid pressure in jointing. American Journal of Science 263, 633–646.

Selvaggi, G., Ferulano, F., Di Bona, M., Frepoli, A., Azzara, R., Basili, A., Chiarabba, C., Ciaccio, M.G., Di Luccio, F., Lucente, F.P., Margheriti, L., Nostro, C., 2001. The Mw 5.4 Reggio Emilia 1996 earthquake: active compressional tectonics in the Po Plain, Italy. Geophysical Journal International 144, 1–13.

Sgroi, T., de Nardis, R., Lavecchia, G., 2012. Crustal structure and seismotectonics of central Sicily (southern Italy): new constraints from instrumental seismicity. Geophysical Journal International 189, 1237–1252.

Sibson, R.H., 1985. A note on fault reactivation. Journal of Structural Geology 7, 751–754.

Sibson, R.H., 1998. Brittle failure mode plots for compressional and extensional tectonic regimes. Journal of Structural Geology 20, 655–660.

Sibson, R.H., 2004. Controls on maximum fluid overpressure defining conditions for mesozonal mineralization. Journal of Structural Geology 26, 1127–1136.

Sibson, R.H., 2007. An episode of fault-valve behaviour during compressional inversion? — The 2004 MJ6.8 Mid-Niigata Prefecture, Japan, earthquake sequence. Earth and Planetary Science Letters 257, 188–199.

Sibson, R.H., Xie, G., 1998. Dip range for intracontinental reverse fault ruptures: truth not stranger than friction? Bulletin of the Seismological Society of America 88, 1014–1022.

Smith, R.L., Bailey, R.A., 1968. Resurgent cauldrons. Geological Society of American Memoirs 116, 613–662.

Somoza, L., D|iaz-del-Río, V., León, R., Ivanov, M., Fernández-Puga, M.C., Gardner, J.M., Somoza, L., D|iaz-del-Río, V., León, R., Ivanov, M., Fernández-Puga, M.C., Gardner, J.M., Hernández-Molina, F.J., Pinheiro, L.M., Rodero, J., Lobato, A., Maestro, A., Vázquez, J.T., Medialdea, T., Fernández-Salas, L.M., 2003. Seabed morphology and hydrocarbon seepage in the Gulf of Cádiz mud volcano area: acoustic imagery, multibeam and ultra-high resolution seismic data. Marine Geology 195, 153–176.

Stearns, D.W., 1968. Certain aspects of fractures in naturally deformed rocks. In: Riecker, R.E. (Ed.), Rock Mechanics Seminar. Terrestrial Sciences Laboratory, Bedford, pp. 97–118.

Stevens, B., 1911. The laws of intrusion. American Institute of Mineral Engineering Bulletin 49, 1–23.

Stewart, S.A., Davies, R.J., 2006. Structure and emplacement of mud volcano systems in the South Caspian Basin. AAPG Bulletin 90, 771–786.

Stöhr, E., 1867. Schiarimenti intorno alla carta delle Salse e delle località oleifere di Monte Gibio. Annuario della Società dei Naturalisti in Modena 2, 169–178.

Streit, J.E., Cox, S.F., 2001. Fluid pressures at hypocenters of moderate to large earthquakes. Journal of Geophysical Research 106, 2235–2243.

Takada, A., 1994. Development of a subvolcanic structure by the interaction of liquid-filled cracks. Journal of Volcanology and Geothermal Research 62, 207–224.

Takada, A., 1997. Cyclic flank-vent and central-vent eruption patterns. Bulletin of Volcanology 58, 539–556.

Takahashi, M., 1994. Structure of polygenetic volcano and its relation to crustal stress field: 2. P-type, O-type volcano. Bulletin of Volcanological Society of Japan 4, 207–218.

Tibaldi, A., 1995. Morphology of pyroclastic cones and tectonics. Journal of Geophysical Research 100, 24,521–24,535.

Tibaldi, A., 2005. Volcanism in compressional tectonic settings: is it possible? Geophysical Research Letters 32, L06309 http://dx.doi.org/10.1029/2004GL021798.

Tingay, M.R.P., Hillis, R.R., Morley, C.K., Swarbrick, R.E., Okpere, E.C., et al., 2003. Pore pressure/stress coupling in Brunei Darussalam — implications for shale injection. In: Van Rensbergen, P. (Ed.), Subsurface Sediment Mobilization: Geological Society, London, Special Publications, 216, pp. 369–379.

Tingay, M.R.P., Hillis, R., Morley, C., Swarbrick, R., Okpere, E., 2009. Present-day stress and neotectonics of Brunei: implications for petroleum exploration and production. AAPG Bulletin 93, 75–100.

Tsunakawa, H., 1983. Simnple two-dimensional model of propagation of magma-filled cracks. Journal of Volcanology and Geothermal Research 16, 335–342.

van Loon, (Tom) A.J., 2010. Sedimentary volcanoes: overview and implications for the definition of a volcano on Earth. In: Cañón-Tapia, E., Szakács, A. (Eds.), What is a Volcano? : The Geological Society of America Special Paper, 470, pp. 31–41. doi: 10.1130/2010.2470(03).

Van Rensbergen, P., Hillis, R.R., Maltman, A.J., Morley, C.K., 2003. Subsurface sediment mobilization: introduction. Geological Society, London, Special Publications 216, 1–8.

Van Rensbergen, P., Depreiter, D., Pannemans, B., Moerkerke, G., Van Rooij, D., Marsset, B., Akhmanov, G., Blinova, V., Ivanov, M., Rachidi, M., Magalhaes, V., Pinheiro, L., Cunha, M., Henriet, J.-P., 2005. The El Arraiche mud volcano field at the Moroccan Atlantic slope, Gulf of Cadiz. Marine Geology 219, 1–17.

Wadge, G., Cross, A., 1988. Quantitative methods for detecting aligned points: an application to the volcanic vents of the Michoacan–Guanajutato volcanic field, Mexico. Geology 16, 815–818.

Wallmann, P.C., Pollard, D.D., Hildreth, W., Eichelberger, J.C., 1990. New structural limits on magma chamber locations at the Valley of Ten Thousand Smokes, Katmai National Park, Alaska. Geology 18, 1240–1243.

Wang, C.-Y., Manga, M., 2010. Hydrologic responses to earthquakes and a general metric. Geofluids 10, 206–216.

Yardley, G.S., Swarbrick, R.E., 2000. Lateral transfer: a source of additional overpressure? Marine and Petroleum Geology 17, 523–537.

Yassir, N.A., Addis, M.A., 2002. Relationships between pore pressure and stress in different tectonic settings. In: Huffman, A.R., Bowers, G.L. (Eds.), Pressure Regimes in Sedimentary Basins and Their Prediction: AAPG Memoir, 76, pp. 79–88.

Yassir, N.A., Bell, J.S., 1996. Abnormally high fluid pressure and associated porosities and stress regimes in sedimentary basins. SPE Formation Evaluation 48, 5–10.

Yassir, N.A., Rogers, A.L., 1993. Overpressures, fluid flow and stress regimes in the Jeanne d'Arc Basin, Canada. International Journal of Rock Mechanics and Mining Science 30, 1209–1213.

Yusifov, M., Rabinowitz, P.D., 2004. Classification of mud volcanoes in the South Caspian Basin, offshore Azerbaijan. Marine and Petroleum Geology 21, 965–975.

Zobak, M.L., Zobak, M., 1980. State of stress in the conterminous United States. Journal of Geophysical Research 85, 6113–6156.